CHARACTERIZATION OF THE HYDROSTRATIGRAPHIC UNITS OF THE SODWANA AREA USING THE ELECTRICAL RESISTIVITY METHOD

BY

NWEZE AUGUSTINE

STUDENT NUMBER: 201100900

SUBMITTED TO

THE FACULTY OF SCIENCE AND AGRICULTURE

IN PARTIAL FULFILLMENT OF THE REQUIREMENT FOR THE DEGREE OF

MASTER OF SCIENCE

IN THE DEPARTMENT OF HYDROLOGY, UNIVERSITY OF ZULULAND, KWADLANGEZWA

Supervisor:

Professor J. J. Simonis

Co-Supervisors:

Professor B. Kelbe

Mark Schapers

DECLARATION

I declare that the work in this dissertation was conducted in the Department of Hydrology at the University of Zululand, KwaDlangezwa. This is the original copy handed in by the author and has never been published by anyone else for the award of any Degree in any Institution.

……..

Nweze Augustine

ACKNOWLEDGEMENTS

I am grateful to the Almighty God for His everlasting grace.

I acknowledge the efforts of Professor J. Simonis, Professor B. Kelbe and Mark Schapers for making this study what it is. I am also grateful to them for their guidance and support. I also thank all the lecturers in the Department of Hydrology, University of Zululand. My thanks go to my family and friends for their support and encouragement.

ABSTRACT

This study was aimed at defining the geological facies of the Sodwana area. It formed part of a bigger project designed to investigate the linkages between the hydrological and ecological drivers of the Mgobolezeni Catchment, Sodwana. Monitoring boreholes were drilled by the Department of Water Affairs (DWA) at several locations in the study area for the purpose of monitoring groundwater changes in the Catchment. There was a need to interpolate the geology and groundwater conditions between the monitoring boreholes. This research provided the geological conditions between the monitoring boreholes using the electrical resistivity geophysical method. The Geotron (G41) resistivity meter was used to conduct the survey.

Vertical electrical sounding (VES) were conducted initially in close proximity to DWS monitoring boreholes for calibration purposes. The VES data were plotted and interpreted using IPI2win computer software.

Hydrostratigraphic models were developed for all VES locations in close proximity to monitoring boreholes. These models were used for interpolation of the geology between the boreholes. A total of 20 VES were conducting in the study area. 16 VES results showed 5-layer models while 4 VES results showed 4-layer models. The top layer showed very high resistivity values (> 2000Ωm) and was interpreted as dry sand (Kwambonambi Formation). The second layer showed a resistivity range of 200Ωm – 2000Ωm. In some locations, the second layer showed a resistivity range of 120Ωm - 200Ωm and was interpreted as the shallow aquifer in the Kwambonambi Formation. The third layer showed a resistivity range of 50Ωm - 120Ωm and was interpreted as the low transmissivity Kosi Bay/Isipingo Formations. The fourth layer had a resistivity range of 10Ωm - 50Ωm and was interpreted as the deeper aquifer unit of the Uloa Formation. The basement Cretaceous rock formed the fifth layer that showed a clear increase and higher resistivity values than that of the overlying fourth layer. Transmissivity values observed from the pumping tests conducted on the calibration boreholes were combined with VES results to define the transmissivity of the inferred deeper aquifer in between boreholes.

The thicknesses of the geoelectric layers obtained from VES results showed a good relationship with corresponding geologic units in borehole logs. The varying apparent resistivity values and lithological information enabled the demarcation of the geoelectric units into hydrostratigraphic units. VES results also showed that the surface of the Cretaceous unit is deeper in the eastern side of the study area than in the western side, showing that the Cretaceous unit dips towards the east. The modelled transmissivity also showed a good statistical relationship (R^2 = 0.99)

with the observed transmissivity. Therefore the VES method used for this study successfully achieved the aim of this study

TABLE OF CONTENTS

List of Figures

List of Tables

List of Abbreviations

DWS	Department of Water and Sanitation
ER	Electrical Resistivity
VES	Vertical Electrical Sounding
AMSL	Above Mean Sea Level
BMSL	Below Mean Sea Level
MA	Million Years Ago

CHAPTER ONE

1 INTRODUCTION

1.1 Introduction

The Sodwana area forms part of the Coastal Plain of north-eastern KwaZulu-Natal Province, South Africa. The Plain is characterised by sediments deposited during the Cenozoic period. This group of sediments extends from north-eastern KwaZulu-Natal to the Mozambican Coastal Plain and are grouped together as the Maputaland Formation (Porat and Botha, 2008). Erosion and deposition during periods of regression and transgression reworked the Maputaland Formation and this resulted in variability of the geohydrological characteristics of the Formations as described by Worthington (1978), Miller (2001) and, Thornhill and Vuuren (2009).

The Sodwana area is considered as the catchment area for Lake Mgobolezeni which is one of the freshwater lakes that occur in the area. The nature of the sediments of the area makes it a good groundwater reservoir. It contains some wetlands that are important because of their ecological biodiversity and also for maintenance of the ecosystem (Grundling *et al*, 2013). The increasing population, tourism and agricultural activities can result in over abstraction of groundwater and also put stress on the wetlands. The University of Zululand and Nelson Mandela Metropolitan University have been conducting a research project which was designed to study the linkages between the hydrological and ecological drivers of the Mgobolezeni Catchment in the Sodwana area (Kelbe et al, 2013). This study mapped the geological conditions of the Mgobolezeni Catchment to support the geohydrological investigation of the groundwater dynamics using numerical methods.

Geohydrological studies over the years have been mostly dependent on data or information obtained from boreholes. The amount and accuracy of information obtainable from boreholes is limited due to the availability of information that is often restricted to specific project areas, and because of the high cost of drilling over large unexplored areas. Detailed groundwater study requires an adequate and accurate understanding of the subsurface geology. Geological information such as grain size, composition and texture of the soil play an important role in the field of hydrogeology and can provide needed information for groundwater models (Saad *et al*, 2012).

The application of geophysical techniques such as electrical resistivity (ER) has enhanced groundwater studies to serve as a connection between geology and hydrogeology. Electrical resistivity prospecting is applied in groundwater studies to better map the subsurface facies of geological units and also compare solute transport properties in mapping freshwater and salt water regimes (Worthington, 1978). Lithological properties of a geological unit such as grain size, texture and composition determine the primary porosity, permeability, and hydraulic conductivity of such a unit. Similarly, the electrical conductivity of a geological unit is a function of the grain size, composition and texture (Meads *et al*, 2003). The electrical resistivity method can therefore link geology and hydrogeology in groundwater studies and can be useful for the investigation of some parameters required for groundwater modelling (Herckenrath, 2012 and Bredehoeft, 2005). In unconsolidated sediments such as in the Sodwana area, sediments that were formed under different sedimentary processes over time exhibit different lithological properties and therefore have the potential to be differentiated using the electrical resistivity method.

Groundwater models are representations of reality which require definitive analysis of many parameters such as the geological framework for proper development (Wang and Anderson, 1995). A conceptual groundwater model is the theoretical framework for developing numerical models that predict groundwater flow using parameters that must be determined and verified in the field. The accuracy of a model depends on how the predictions and the verified parameters correlate (Bredehoeft, 2005 and Boonstra and de Ridder, 1981). The electrical resistivity method is one of the tools that can be used for measuring these parameters. An example is the measurement of upper and lower aquifer boundaries of hydrostratigraphic layers required for the simulation of groundwater models (Mohammed *et al.,* 2006 and Meju *et al.,* 2000).

Developing a groundwater model of an area requires adequate knowledge of the subsurface geology/geohydrology. The mapping of subsurface geology/geohydrology is necessary for the description of the lateral extent of the geological facies, the depth it occurs and the thickness thereof, the texture and age of the water bearing formations and the confining layers. These properties define the transition from one geologic unit to another and are not uniformly distributed over an area as stated by Boonstra and de Rider (1981). Point information for groundwater studies can be obtained from boreholes but in isolation are not adequate when a model is required for a large area according to Gunther and Muller (2012). Geophysical techniques such as the electrical resistivity method, the electromagnetic method, and the

seismic method have been useful in describing subsurface structures for input in groundwater models (Christen and Sikander, 2012).

A geological formation is classified as an aquifer if it contains sufficient water and permeable materials to yield a significant amount of water when drilled into or as a discharge to springs and other drainage boundaries (rivers and lakes) (Christen and Sikander, 2012). Consequently, the Maputaland Formations form the primary aquifers in the Coastal Plains of north-eastern, KwaZulu-Natal (Worthington, 1978). Thornhill and Vuuren (2009) described the Pliocene Formation as the major aquifers around Richards Bay and are confined by the less permeable late Pleistocene Formations. The application of the electrical resistivity method to describe the facies between these aquifers exploits the anomaly resulting from particle sizes and degree of saturation of the different geologic units in the area (Refsgaard *et al.,* 2010).

In this study the electrical resistivity method was chosen for the characterization of the subsurface geology of the study because it has been successfully used by Worthington (1978; Mohammed *et al*., 2006 and Meju *et al*., 2000). The information from exploration boreholes drilled by DWS was used to calibrate the geophysical information. This study was aimed at conducting vertical electrical sounding that would be deep enough to detect the depth of the Cretaceous basement and also define the Miocene - Pleistocene and the Holocene units. Such a comprehensive survey of the entire study area would help to verify the spatial distribution of the geological facies (conceptual model) in the study area for input into a groundwater model.

A comprehensive geo-electrical investigation of the basement rocks to the upper Pleistocene/Holocene sediments around Richards Bay was presented by Worthington (1978) where the Schlumberger array was used to investigate resistivity anomalies due to contrast in geo-electric properties of the geologic units in the area. Worthington (1978) interpreted the Cenozoic sediments by dividing them into four Formations based on their geology and geo-electrical characteristics. The study described them as the Miocene Formations, the middle Pleistocene Formation, the upper Pleistocene Formation and the uppermost Pleistocene/Holocene Formations based on their different electrical conductivities.

These Formations correspond to the Formations proposed by Botha and Porat (2008) as the Uloa Formation (Miocene), Port Dunford Formation (middle Pleistocene), the Kosi Bay Formation (upper Pleistocene), and the Kwambonambi (uppermost Pleistocene) and Sibayi Formations (Holocene) respectively as shown in Figure 1. Worthington (1978) reported a high resistivity contrast at the interface between the Cretaceous sediments and the overlying

Miocene sediments which can be used to define the base of the Miocene sediments (Uloa and Umkwelane Formations). This resistivity anomaly distinguishes the Cretaceous sediments from the freshwater bearing Miocene/Pleistocene sediments.

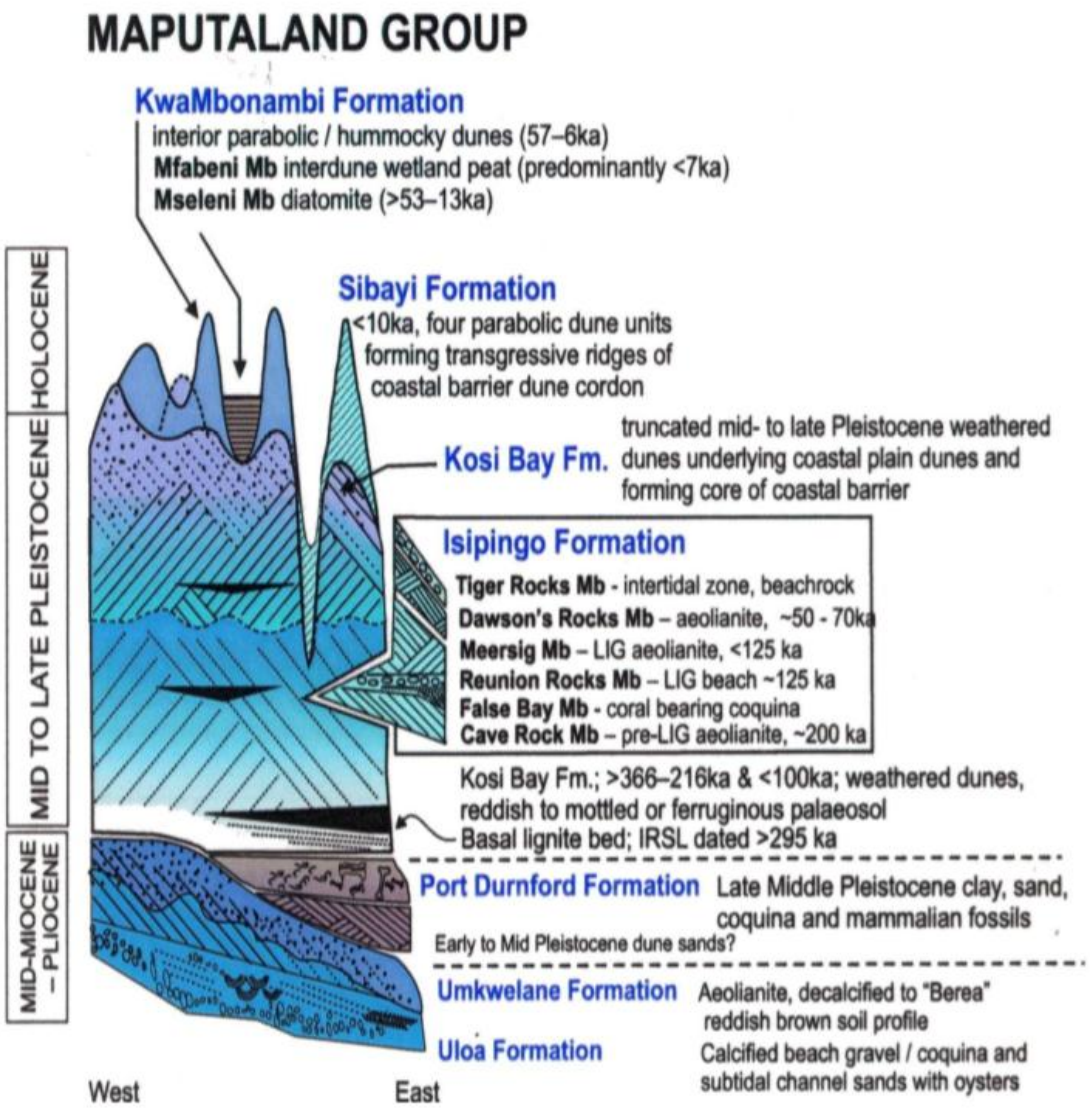

Figure 1: Generalized lithostratigraphic profile of the Maputaland after Botha and Porat (2008)

The geo-electric characteristics and the thickness of the Miocene sediments were not extensive enough to distinguish the facies between the overlying calcarenites of the Pliocene period from the underlying coquina and conglomerates of the Miocene period. A resistivity range of 24 to 175Ωm was reported for sediment of the Miocene to middle Pleistocene formations. Results

from pumping tests and borehole logs together with vertical electrical sounding results showed that the Miocene formations form the high yielding aquifer within the area (Worthington, 1978).

Worthington (1978) also reported a moderately resistive upper layer of the middle Pleistocene formation. A thin conductive layer separates the mid Pleistocene and the upper Pleistocene formations. The uppermost Pleistocene and Holocene formations are highly resistive to electric current, which can be attributed to grain size and saturation. The geo-electrical nature of these formations enables their easy identification or delineation by vertical electrical sounding. Vertical electrical sounding was integrated with borehole logs and micro paleontological data by Worthington (1978) to create a cross section which was described as the "post Palaeocene geology" of Maputaland. It was concluded that the major aquifers within the area are the Miocene sediments. However, there was no distinction between the Miocene and the upper Pliocene (Uloa and Umkwelane) Formations.

1.2 Study Area

1.2.1 Introduction

The Sodwana area falls within the Maputaland Coastal Plain which stretches through the north–eastern KwaZulu-Natal province of South Africa. The Plain is quite broad in southern Mozambique extending up to 80km in width and narrows down to about 3km wide at Mtunzini at its southern extremity (Porat and Botha, 2008). The Maputaland Coastal Plain is bounded in the east by the Indian Ocean (Figure 2) and in the west by the Lebombo Mountains (Grundling *et al*., 2013; Botha and Porat, 2007 and Watkeys *et al*., 1993).

The evolution of the Maputaland Coastal Plain dates back to the break-up of Gondwanaland during the Mesozoic era (Hobday, 1979 and Watkeys, *et al*., 1993). The second phase of the Gondwana break-up was marked by a succession of volcanic extrusion which forms the basement of the Maputaland Coastal Plain (Miller, 1998 and Hobday, 1979). The volcanic succession that extruded during the Jurassic period is overlain by Cretaceous, Tertiary and Quaternary sediments. The late Tertiary and Quaternary sediments of the Maputaland Coastal Plain are described as the Maputaland Formation (Botha, 1997).

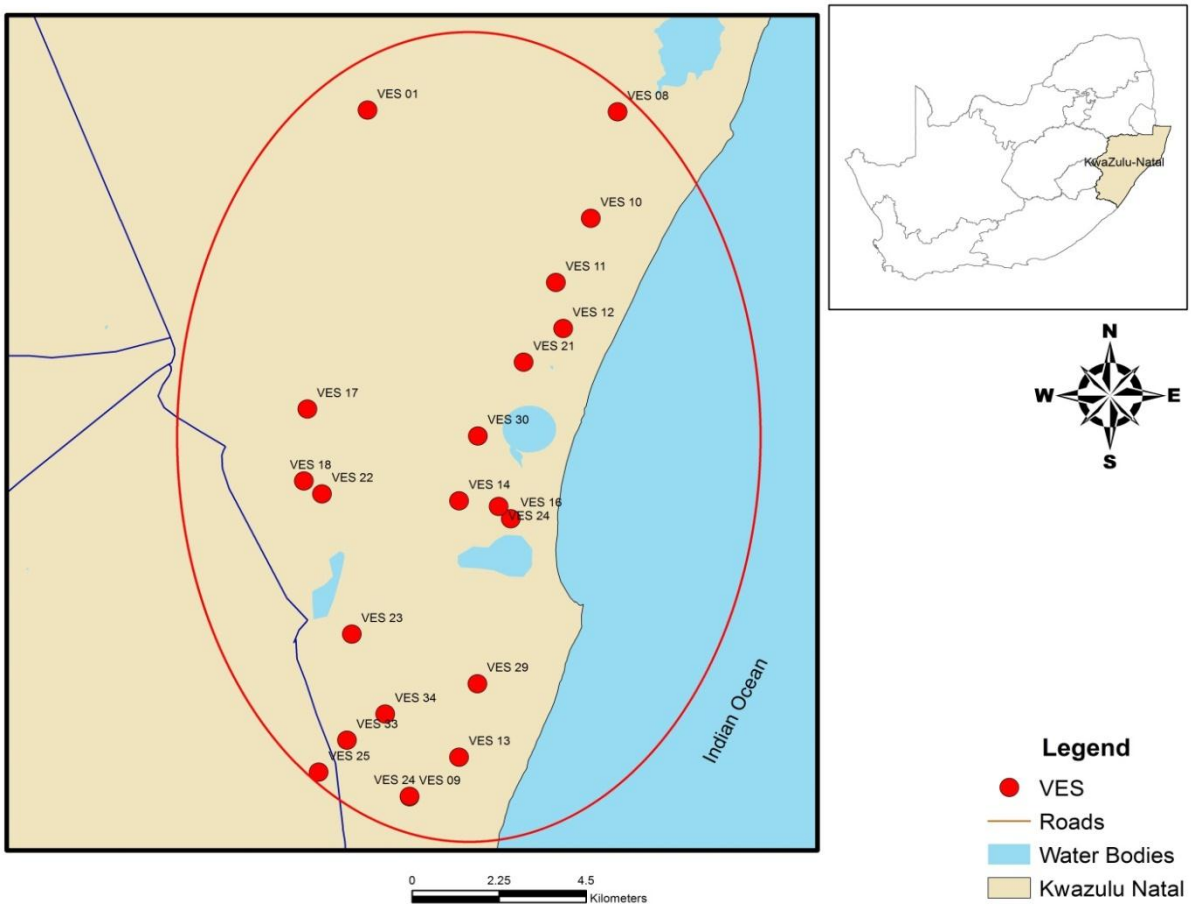

Figure 2: Study area (VES represents the vertical electrical sounding points)

The Maputaland Formation was deposited during periods of marine transgression and regression due to sea level changes. Sea level changes during the Cenozoic Era due to glaciation and de-glaciation and tectonic events resulted in marine transgression and regression periods (Hobday, 1979; Wright *et al*., 1993; Maud, 1980; Botha, 1997 and Miller, 1998). Transgression and regression periods resulted in the erosion and deposition of sediments followed by reworking and another phase of erosion and deposition by alternating events of transgression and regression (Cooper *et al*., 2013).

The resultant effect of periodic deposition and erosion is a group of sediments with complex geological properties. The complex nature of the Maputaland sediments coupled with few outcrops has limited research on the evolution and delineation of the lithostratigraphy of the Maputaland sediments (Wright *et al*., 2000). However, many authors such as Hobday (1979); Maud (1980) and Watkeys *et al*. (1993) have tried to describe the history and sequence of

deposition of the Maputaland sediments. The officially recognized stratigraphy of the Maputaland Formation was first presented by Botha (1997). The stratigraphy of the Maputaland Formation (Refer Figure 1) presented by Botha and Porat (2008) also suggested a sediment sequence with characteristic features of sea-level fluctuations.

1.2.2 Geological Formations

1.2.2.1 The Late Cretaceous Sediments

The Zululand Formation (Table 1) which is composed of sediments deposited during the late Cretaceous, lie unconformably on the volcanic basement rocks that dip eastward at 3-5^{o} according to Dingle *et al*. (1983). The late Cretaceous sediments are made up of the Makathini Formation, Mzinene Formation and the St. Lucia Formation. The Makathini Formation forms the base of the Zululand which directly overlies the Bumbeni complex and consists of non-marine coarse fluviatile sandstone and conglomerates which grade upward into fossiliferous shallow marine clays (Botha, 1997; Watkeys *et al*., 1993). It was deposited between 120 MA to 114 MA approximately.

Overlying the Makathini Formation is the Mzinene Formation, believed to be deposited between 114 MA to 91 MA. The Mzinene Formation consists of fossiliferous shallow marine silts and sand (Botha, 1997). The St. Lucia Formation (Figure 3) was deposited during the late Cretaceous epoch and lies unconformably on the Mzinene Formation. The St. Lucia Formation covers almost the entire Maputaland Coastal Plain but outcrops in few places such as around False Bay in Lake St. Lucia (Watkeys *et al*., 1993). The base of the St. Lucia Formation is predominantly composed of conglomerate which is overlain by cross-bedded silts and fine sand. The top is characterized by upward fining glauconitic silts and fine sand, clay lenses and hard concretions. It is also heavily fossiliferous (Dingle *et al*., 1983; Watkeys *et al*., 1993 and Miller, 1998).

1.2.2.2 The Maputaland Formation

The Maputaland Formation comprises sediments deposited during the Cenozoic era which overlie the Zululand Group in most parts of northern KwaZulu-Natal (Refer to Table 1). The cross-section of the Maputaland Formation proposed by Botha and Porat (2008) is presented in

Figure 1. The primary aquifers that occur in the Sodwana area and the entire coastal area are formed by the sediments of this group. The Uloa Formation and Umkwelane Formation (Figure 4) constitute the Tertiary sediments. Quaternary sediments consist of the Port Dunford, Kosi Bay and Kwambonambi Formations of the Pleistocene epoch, and the Sibayi Formation of the Holocene epoch.

Table 1: Geological succession of the Maputaland Coastal Plain

Era	Sub-Era	Period	Epoch	Group	Formation	Lithology
Cenozoic	Quaternary	Pleistocene	Holocene	Maputaland	Sibayi	High coastal dunes. Calcareous sand
			Pleistocene		Kwambonambi	Inland stabilized dune and redistributed sand. Diatomite
					Kosi Bay	Red sandy soil, cross-bedded sand, local calcarenites and lensoid carbonaceous sand
					Port Dunford	Beach rock, coral bearing coquina, lignite, fossiliferous mud rock and calcarenites
	Tertiary	Pliocene	Early To Late		Umkwelane	Red sandy soil, Aeolian cross-bedded calcarenites
					Uloa	Coquina and conglomerate
		Paleocene	Early			Fossiliferous shallow marine silts and hard concretional horizon
Mesozoic	Cretaceous		Late	Zululand	St. Lucia	Fossiliferous shallow marine silts and hard concretional horizon
			Early		Mzinene	Fossiliferous shallow marine silts and sand
					Makathini	Fossiliferous shallow marine clays and fluviatile sandstone
					Bumbeni Complex	Pyroclastic, Rhyolites and Trachyte
					Mpilo and Movene	Basalts
					Msudunze	Conglomerates
	Jurassic			Lebombo	Jozini	Rhyolites

Figure 3: St Lucia Formation (south of Mtubatuba)

1.2.2.3 Tertiary Sediments

The Tertiary sediments are comprised of the Uloa and Umkwelane Formations. These form a thin veneer of sediment that lie unconformably on the St. Lucia Formation in most parts of northern KwaZulu-Natal (Miller, 1998). These sediments were believed to have been deposited in the late Miocene to early Pliocene period. The Paleocene period of lower Tertiary sub-era was characterized by fossiliferous shallow marine silts, thin clay lenses and hard concretions. This layer was believed to have been eroded when the sea levels dropped 100m below their present level and does not exist in northern KwaZulu-Natal. Consequently, the Uloa and Umkwelane of the Miocene to Pliocene period lie unconformably on the Cretaceous sediments (Watkeys *et al*., 1993 and Miller, 1998).

Figure 4: Umkwelane Formation (Umkwelane Hill, Mtubatuba)

Glaciation during the last glacial maximum induced regression and a sea level drop to more than 100m below its present level (Watkeys *et al*., 1993). Pre-deposited Uloa and Umkwelane Formations were eroded during this regression period and consequently, these Formations occur as discontinuous strata in the Maputaland Coastal Plain (Watkeys *et al*., 1993). The Uloa and Umkwelane Formations were considered a single unit (McCarthy, 1988) but became separated and treated as individual units recently (Miller, 1998; Botha, 1997). The Uloa Formation consists of Miocene basal conglomerate (Botha and Porat, 2007) and an upper unit that is composed of coquina and tidal sands (Miller, 1998; Dingle *et al*., 1983). Outcrops of this Formation have been identified around Lake St. Lucia. The Umkwelane Formation (Figure 2 and Table 1) overlies the Uloa Formation and consists of calcified dune sands considered to be Pliocene in age (Porat and Botha, 2008).

1.2.2.4 The Quaternary Sediments

The Port Dunford Formation believed to have been deposited during the Pleistocene period forms the base of the Quaternary sediments in the Maputaland flats. It lies unconformably on the Tertiary sediments of the Uloa and Umkwelane Formations. Botha and Porat, (2007) stated that the Port Dunford Formation was deposited during the middle to late Pleistocene period and consists of coastal lake organic rich mud. Cooper *et al*. (2013); Maud and Orr (1975) described the Port Dunford formation as having a lithology that predominantly consists of mudstone, lignite, sand and corals. Maud and Orr (1975) reported a thin organic rich layer that separates a lower unit that consists predominantly of clay and an upper layer that is composed of fine to coarse sand. Worthington (1978) reported a thickness of about 20m – 40m and a maximum elevation of 40m above mean sea level for the Port Dunford Formation around the Richards Bay area.

The late Pleistocene Kosi Bay Formation overlies the Port Dunford formation. The regressive period was superimposed on sea-level fluctuations during the last interglacial maximum. This period of punctuated regression led to sub aerial weathering of the mid Pleistocene sediments. This process generated the Berea Red Sand of the Kosi Bay Formation (Wrigh*t et al*., 2000). The Kosi Bay Formation consists of an illuviated bottom soil that is rich in clay and an eluviated upper red soil that is overlain by younger dunes and diatomaceous reworked sand (Taylor *et al*., 2005). Wright *et al*. (2000) are of the opinion that the limited and poor description of the stratigraphy of the Maputaland Coastal Plain could be attributed to sediments reworked by periodic marine transgression and regression, non-uniformity in fossil distribution and the presence of only limited outcrop within the area. The Kosi Bay Formation is overlain by the younger dune cordon which constitutes the Kwambonambi Formation.

The Kwambonambi Formation consists of inland dunes, reworked sands and diatomite deposits. These dunes consist of aeolian sands and were formed by sand migration during the last glacial period according to Botha and Porat (1997). The architecture of the dunes' crest indicated filling of eroded surfaces of older dunes by mobilized sands. These dunes are aligned in a north – south direction and can be seen around Lake Sibaya as clusters of sub-rounded dunes with irregular surfaces. The periodic mobilization of sand across the dunes stopped some 7ka due to rising regional groundwater levels and consequently, vegetation preserved the dunes from further erosion (Botha and Porat, 2007). The Kwambonambi Formation is overlain by the high rising coastal dune cordons of the Holocene period.

The latest aeolian activity during the Holocene period generated the parabolic coastal dune barrier system which rises up to 120 – 170m in height and has been described as the Sibayi Formation (Botha and Porat, 2006). These dunes were formed when unconsolidated shelf sediments were eroded, transported and deposited during the last glacial maximum (Watkeys *et al*., 1993). The dunes contain some heavy minerals and are heavily vegetated (Watkeys *et al*., 1993) and also consist of marine washover and lagoonal deposit at the base (Miller, 1998).

1.2.3 Hydrology

Surface drainage is limited in Maputaland Coastal Plains due to high porosity and permeability of the top soil. The exposures of the water table in dune depressions forming drainage boundaries result in a system of streams within the Coastal plains (Kelbe and Germishuyse, 2001). There are such streams in the Sodwana area (study area) which start as springs and are augmented by groundwater seepage as they flow for a few kilometres before it emptying into Lakes Shazibe Mgobolezeni.

Seasonal ponding of water in inter dune depressions also occurs as a result of seepage along the contact between clay layers and the overlying high porosity top soil (Maud and Orr, 1975). There is also the occurrence of a number of lakes around the Maputaland Coastal Plain. Some of the more recognised lakes include Lake St. Lucia, Lake Sibayi and the Kosi Lake system. Lake Mgobolezeni and Lake Shazibe occur within the Mgobolezeni Catchment which is the study area for this research.

The Inland dunes prominent around Lake Sibayi together with reduced runoff, protects the lake from high sedimentation (Miller, 1998; Botha and Porat, 2007). Lake Sibayi is a freshwater lake and has direct interaction with groundwater. Groundwater recharges Lake Sibayi around the western area of the Catchment while the Lake recharges groundwater in the eastern area of the Catchment (Weitz and Demile, 2014). Lake Mgobolezeni and Lake Shazibe are freshwater lakes which are isolated from the ocean. They are continuously recharged by groundwater seepage (Porter and Clerk, 2012).

1.2.4 Geohydrology

Understanding the hydrology and geohydrology of the Maputaland Coastal Plain was prompted by the industrialization of some parts of the area such as Richards Bay (Rawlins, 1991). Adequate water supply was needed for sustaining the proposed industries in the Richards Bay area. This need induced the early studies of the surface water and groundwater conditions and, management thereof around Richards Bay. Industrialization and agricultural activities such as commercial forestry and sugarcane plantation are some of the major factors that prompted research on groundwater conditions in some parts of the Maputaland Coastal Plain. The Sodwana area experienced neither industrialization nor large scale agricultural activities (other than forestry). Therefore limited groundwater studies have been conducted around the Sodwana area (Jeffares and Green, 2012).

The geohydrology of the Maputaland Coastal area is controlled by the primary aquifer's hydraulic conductivity. Grain size, shape and sorting determine the transmissivity of the major aquifers that occur in the study area (Kelbe, 2014). The shallow aquifer in the area is formed by the Kwambonambi Formation. The groundwater potentials of the shallow aquifer are controlled by the lithology of the shallow aquifer itself, the lithology of the underlying Kosi Bay Formation and seasonal changes (wet and dry seasons) according to Maud (1998). The high clay content of the Kosi Bay Formation reduces percolation of groundwater from the shallow aquifer into the Uloa Formation creating a leaky aquifer. This interruption breaks the link between the shallow aquifer and the underlying formations. The shallow aquifer can be described as a "perched aquifer" under these conditions.

The deeper aquifer is composed of the Uloa/Umkwelane Formations. The Uloa/Umkwelane Formations are decalcified arenaceous deposits where hydraulic properties are controlled by the lithology of the sediments (Maud, 1998). They are considered to be semi confined by the overlying silty/clay units. Figure 5 shows the estimated transmissivity of the aquifers that occur in the study area. It was reported by Jeffares and Green (2012) that the transmissivity of the deeper aquifer varied from 110 – 587m^2/day while its hydraulic conductivity varied from 9 – 35m/day.

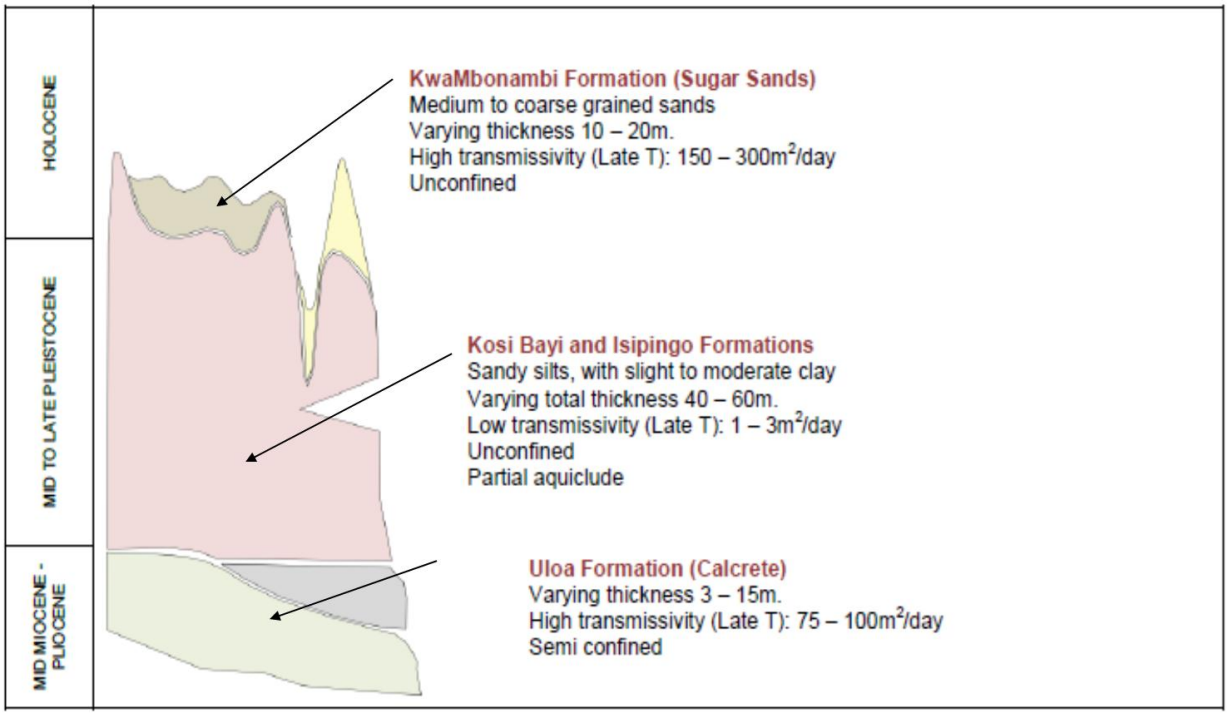

Figure 5: Hydrostratigraphy of Sodwana area (Schapers, 2011)

1.3 Problem Statement

Limited studies using geophysics for describing the subsurface structure have been conducted in the study area. Existing studies were mostly conducted using information gathered from exploration boreholes. The amount of information obtainable from such boreholes is limited to the locality of the drilled borehole. Such information cannot be expected to accurately interpolate the subsurface geology between boreholes. There is therefore a need to better understand the subsurface geology of the study area to accurately predict the geology and geohydrology of the area. This study was designed to use the electrical resistivity geophysical method in mapping the subsurface geology of the study area and the results would be calibrated using borehole drilling logs. This will enable the description of boundaries and aquifer geometry for input into a groundwater model for the study area.

1.4 Aim of the study

The aim of the study is to use of the electrical resistivity (geophysical) method to delineate the water bearing formations in the Lake Mgobolezeni Catchments, Sodwana and map their facies.

1.5 Objectives of the study

1. Conduct a literature survey to review the geophysical techniques and their applicability for mapping the facies of sedimentary deposits in low lying coastal plains. Define the spatial distribution of the geological units in the study area.
2. Interpretation, compilation and presentation of results.
3. Define the vertical and horizontal aquifer boundaries for input into a groundwater model.

1.6 Structure of thesis

Chapter 1 is an introduction to the study. It is made up of specific problems that this study was designed to solve.

Chapter 2 is composed of the literature review. All relevant literature surveyed for this study is presented.

Chapter 3 describes the methods that were used for this study. All the procedures used for data collection and analyses are described.

Chapter 4 consists of the interpretation of data and presentation of results. All data collected from the field and results obtained from the interpretation thereof, are presented.

Chapter 5 is composed of the discussion of results. The results from interpretation of vertical electrical sounding are described and correlated to the geology of the study area.

Chapter 6 consists of the conclusion deduced from the discussion of results.

CHAPTER TWO

2 LITERATURE REVIEW

2.1 Introduction

The literature survey focused on past studies conducted in the Sodwana area related to the geology, hydrology and the electrical resistivity method for groundwater exploration. Similar studies in some other parts of the Maputaland Coastal Plain were also reviewed. There was also a general survey of literature on the use of electrical resistivity method for aquifer characterization on unconsolidated sediments such as the Cenozoic sediments of the Sodwana area.

2.2 Hydrostratigraphic Units

Maxey (1964) defined hydrostratigraphic units as geological units for which hydraulic properties can be verified and which have reasonable lateral extent and also possess a lithological and structural framework for a particular hydrogeological system. Accordingly, groundwater units should be defined based on recharge, storage, discharge and, lithological properties. Seaber (1988) defined hydrostratigraphic unit based on hydraulic parameters such as porosity and transmissivity. He was of the opinion that hydrostratigraphic units could occur beyond a single lithological unit. While Maxey (1964) stated that identification of hydrostratigraphic units should be a function of groundwater flow and Seaber (1988) was of the view that hydrostratigraphic units should encompass any number of geological settings.

In sedimentary rocks or unconsolidated sediments such as the Maputaland Coastal Plains, hydrostratigraphic units must be a unit that can be mapped, and can be described based on lithological characteristics, stratigraphic association and contained fossils. These three factors formed the bases for the determination of the hydrostratigraphy of the Richards Bay area using the electrical resistivity geophysical method by Worthington (1978). The delineation of lithostratigraphic units is fundamental to defining the hydrostratigraphy of any geologic framework. The lithostratigraphic nomenclature adopted for the Maputaland Coastal Plains was proposed by Botha (1997). However, many authors such as Watkeys *et al*. (1993), Botha

(1997), Miller (1998), and Botha and Porat (2007) have conducted research aimed at defining the lithostratigraphy of the area.

Miller (1998) conducted a study on Lake Sibayi which is situated within the Maputaland Coastal Plain. One of the aims of the study was to determine the stratigraphy below the lake. Cored sediments from below the lake were analysed by Radioacarbon dating and fossil description and the stratigraphic units obtained were similar to those proposed by Botha (1997) and presented in Figure 1.

Botha and Porat (2007) studied the stratigraphy of the dunes along the coastal areas of the Maputaland Coastal Plain. Outcrops were studied and soil samples were collected and analysed to differentiate dune system and aeolian sand bodies. Botha and Porat (2007) determined soil development indices by soil profile description and sampling. Infrared stimulated luminescence dating was also employed to analyse soil evolution from the time of deposition. They concluded that the Quaternary sand dunes of the Maputaland Coastal Plain showed a pedogenic trend which is relative to the lithostratigraphy of the area from the oldest to the youngest formations.

The lithostratigraphy of the Tertiary and Quaternary sediments of the Maputaland Coastal Plain have been described with reference to chronology, clay content, colour and structure of the sediments (Botha, 1997 and Watkeys *et al*., 1993). These factors also play an important role in defining the hydrostratigraphy of unconsolidated sediments. Borehole logs obtained from groundwater monitoring boreholes in the Sodwana area showed a lithostratigraphic sequence based on field observation and description of samples (Jeffares and Green, 2012). Physical properties such as structure and colour of sediments were employed to describe the lithological units of the area. Pumping tests were conducted to determine the hydraulic parameters of various units within the boreholes. Water quality tests were also performed on water samples from the boreholes. Jeffares and Green's (2012) borehole logs showed the lithological units in conjunction with test pumping results which formed the basis from which to delineate aquifers within the Sodwana area.

Clay and silt content, and trend of texture (upward or downward coarsening) are some of the lithological factors that determine the water bearing capacity of the stratigraphic units of the Tertiary and Quaternary sediments of the study area according to Worthington (1978) and Jeffares and Green (2012). A schematic diagram showing the stratigraphy, lithology and hydrostratigraphy of the Cenozoic sediments of the study area is presented in Figure 5 (Refer to

Chapter 1). Table 2 is based on the study conducted by Botha (1997); Worthington (1978), Schapers (2011), and Jeffares and Green (2012) among others.

Table 2: Hydrostratigraphic units of the Sodwana area

Stratigraphy	Lithology	Hydrostratigraphy
Sibayi Formation	Calcareous sand and Lagoonal sand	Dry Sand
Kwambonambi Formation	Medium to Coarse grained sand	Unconfined Aquifer
Kosi Bay Formation	Sandy silt and Clay	Aquitard
Uloa/Umkwelane Formations	Calcrete and Conglomerate	Semi Confined Aquifer

Table 2 and Figure 5 show the uppermost Sibayi Formation that is composed of lagoonal sand. There is high infiltration into the Kwambonambi Formation as it is composed of coarse to medium grained sand. The Kwambonambi Formation forms the shallow unconfined aquifer that occurs in the Maputaland Coastal Plain. The Kosi Bay Formation is composed of sandy silt with clay. It has low transmissivity (Schapers, 2011, and Jeffares and Green, 2012) and can be described as an aquitard. The Uloa and Umkwelane Formations are composed of coquina and conglomerates. These units form the semi-confined deep aquifer that occurs in the Maputaland Coastal Plains.

2.3 Groundwater Exploration Using the Electrical Resistivity Method

The Electrical Resistivity (ER) geophysical method is an exploration technique that uses an externally controlled source to investigate naturally occurring electrical properties of rocks and sediments. Electrical resistivity has been a useful tool in solving many hydrogeological problems (Huntley, 1985; Aizebeokhai *et al.,* 2010; Boostra and de Ridder, 1981). The application of the electrical resistivity method for addressing hydrogeological problems is common among hydrogeologists due to its cost effectiveness and area of coverage compared with other

geophysical methods and down-hole measurement of geohydrological parameters (Huntley, 1985).

The use of the electrical resistivity method for geophysical prospecting started as early as 1906 in Sweden when potential electrodes were progressively moved while current electrodes were kept fixed for qualitative investigation. Loke (2000) stated that the electrical resistivity method developed in 1920 by the Schlumberger brothers was of a quantitative approach. They investigated the resistivity variation with depth by keeping the mid-point of the electrode configuration fixed while progressively increasing the electrodes' separation.

The electrical resistivity method is based on the phenomenon that the amount of current that passes through a rock or sediments is determined by the resistivity or conductivity of that geologic medium (Dobrin and Savit, 1988). Current can be conducted through a rock by electrochemical activity, electronic conduction or dielectric conduction. Reynolds (2000) explained that electrical conduction in most rocks is by electrochemical activity whereby pore fluids act as electrolytes and current is transmitted by the slow movement of ions within the pore fluid. The mineral grains of the rocks can only play an important role in current conduction when the grains are good electronic conductors according to Reynolds (2000).

The presence of water is a major factor that influences the flow of current in the shallow subsurface. The extent of water saturation and connectivity of pore spaces determine the conductivity (or resistivity) of the shallow subsurface (Dobrin and Savit, 1988). Resistivity increases when water saturation and connectivity of pore spaces are high. Resistivity reduces (high conductivity) when water saturation is low and the soil has a low pore space connectivity (Dobrin and Savit 1988). Jorgensen (1988) stated that the flow of current can also be controlled by the concentration of dissolved solutes and temperature in water.

Electrical resistivity decreases as concentration of dissolved solutes in water decreases, while conductivity increases with increasing concentration of dissolved solutes in water (Jorgensen, 1988 and Sabet, 1975). The electrical resistivity method can therefore be used for groundwater exploration to determine porosity and permeability; and to map contaminants and dissolved salts. It can also be useful in solving environmental and engineering problems (Abdul-Aziz, 2014 and Reynolds, 2000).

2.4 Relationship between ER and Aquifer Properties

The flow of current through the subsurface is a function of pore space connectivity as well as fluid characteristics. Many researchers have shown that a strong relationship exists between electrical resistivity and aquifer parameters such as porosity, hydraulic conductivity and transmissivity (Heigold *et al*., 1979; Huntley, 1985; Niwas and de Lima, 2003; Khali and Santos, 2009; Batayneh, 2009; Niwas and Celik, 2012). Most of the relationships between aquifer resistivity and aquifer parameters have been established by empirical and semi empirical methods and few by field observation. These relationships are mostly limited to the areas of study.

Khalil and Santos (2009) observed relationships between resistivity and hydraulic conductivity which were dependent on the degree of saturation. Their approach was based on a combined interpretation of hydrogeological and geophysical data. Three different situations exist between aquifer resistivity and hydraulic conductivity according to Khalil and Santos (2009). These situations are functions of porosity and saturation. They showed that when an aquifer is fully saturated and porosity equals saturation, there is an inverse power relation between aquifer resistivity and hydraulic conductivity.

Batayneh (2009) estimated the hydraulic conductivity and transmissivity of Central Jordan using the Vertical Electrical Sounding (VES) technique combined with pumping test results from boreholes in the study area. His approach was based on the assumption that groundwater flow is parallel to the stratigraphic layering and to longitudinal electric conductance. Batayneh (2009) computed the traverse resistance of the units in the study area using layer parameters (resistivity and thickness) obtained from vertical electrical sounding. A modification factor for water resistivity was also computed from water samples collected from sites in the study area. The traverse resistance and modification factor were multiplied to form a modified traverse resistance which was plotted against observed transmissivity to obtain a linear relationship between modified traverse resistance and transmissivity.

Niwas and de Lima (2003) stated that the relationship between aquifer hydraulic conductivity and electrical resistivity can be inverse or linear depending on the nature of the aquifer substratum. This condition exists when the aquifer dimension is big enough to correspond with the depth of VES investigation. They stated that for a highly resistive substratum, the current and hydraulic flows are dominantly longitudinal over a unit. Aquifer resistivity and hydraulic conductivity show an inverse relationship for this condition. However, when the aquifer

substratum is very conductive, the hydraulic flow is longitudinal but current flow is traversed and the relationship between aquifer resistivity and hydraulic conductivity is a direct relationship. Based on these conditions Niwas and Lima (2003) derived equations with which the transmissivity and hydraulic conductivity of an aquifer can be computed using electrical parameters obtained from the surface vertical electrical sounding geophysical method.

Kelly and Frohlich (1985) also explained the influence of the aquifer substratum on the aquifer resistivity and hydraulic parameters. They reviewed previous work on the aquifer resistivity and hydraulic conductivity relationship and concluded that when an aquifer substratum is resistive, the dominant electrical effect is the traverse resistance. According to them, the traverse resistance has a direct relationship with transmissivity since it is a product of aquifer resistivity and thickness. The longitudinal conductance cannot be used to estimate transmissivity in this condition since it is the ratio of aquifer thickness and resistivity. Kelly and Frohlich (1985) also concluded from a study conducted on Rhode Island that longitudinal conductance in isolation cannot be used to determine the hydraulic conductivity of an aquifer unit.

The transmissivity of an aquifer is a parameter that is estimated from the product of the hydraulic conductivity and aquifer thickness. Grain size analyses and pumping tests are some of the primary ways to determine an aquifer's hydraulic conductivity. Arshad *et al.* (2013) and Heigold *et al.* (1979) showed that the electrical resistivity method can be used to compute hydraulic conductivity as accurately as pumping tests and grain size analysis. Their approach was to calculate hydraulic conductivity and transmissivity using data obtained from sieve analyses conducted on samples collected from a drilling log and, also from a pumping test conducted on the same borehole. They also estimated hydraulic conductivity and transmissivity using bulk resistivity which was obtained from the VES method and water resistivity measured on water samples.

It was concluded by Arshad *et al.* (2013) that the electrical resistivity method can be used to determine aquifer hydraulic conductivity and transmissivity accurately and more cost effectively than traditional methods of pumping tests and grain size analyses. Heigold *et al.* (1979) concluded that an inverse geometric relationship exists between aquifer resistivity and hydraulic conductivity.

The relationship established between aquifer resistivity and hydraulic parameters by Heigold, *et al*. (1979); Kelly and Frohlich (1985); Niwas and Lima, (2003); Khalil and Santos, (2009); Batayneh (2009) and Arshad *et al.* (2013) were all based on the assumption that water

conductivity has to be constant over an area of study. Under such homogeneous conditions the formation factor computed from bulk resistivity and water resistivity can be used to determine aquifer hydraulic parameters such as permeability and transmissivity. Huntley, (1985) warned that some other phenomenon such as the matrix conductivity should be considered while relating aquifer resistivity with hydraulic parameters.

Huntley, (1985) considered the individual effect of the true formation factor, the apparent formation factor and matrix resistivity on permeability. His approach using empirical methods defined how these factors are related with permeability and hydraulic conductivity. He concluded that the formation factor is not always constant even within the normal range of groundwater salinity and can also be affected by clay content. For this reason, Huntley, (1985) cautioned that any relationship between the ratio of bulk resistivity and water resistivity should be limited to the geologic area where it was developed and to water with constant dissolved solute. He also concluded that a relationship exists between matrix resistivity and permeability which does not depend on the extent of dissolved solute and does not vary significantly with the geologic environment.

Aquifer bulk resistivity and fluid resistivity are fundamental in defining groundwater flow according to Archie (1942). The use of these two parameters in groundwater studies is only reliable in clean sand (without clay) as shown by Worthington (1993). In a situation where an aquifer contains little clay, surface conduction plays an important role in defining the formation factor of such an aquifer. In estimating the porosity and hydraulic conductivity of the aquifer, the apparent formation factor which is due to surface conductivity of clay particles is considered (Worthington, 1993). For a clay free aquifer, the intrinsic formation factor can be used for aquifer characterization. Soupios *et al.* (2007) however used bulk resistivity and pore fluid resistivity to determine the intrinsic formation factor. Aquifer porosity and hydraulic conductivity were consequently derived from the estimated intrinsic formation factor.

Worthington (1993) tried to modify Archie's Law by deriving an equation which combined the apparent formation factor and the intrinsic formation factor of an aquifer. He considered a situation whereby an aquifer may not be entirely clay free and therefore, derived his empirical equation which has the apparent formation factor and intrinsic formation factor as variables. This equation makes provision for any surface conduction which may be due to the presence of shale or clay.

Soupios *et al.* (2007) adopted the modified Archie's equation by Worthington (1993) to study aquifer parameters in Greece. Their approach was to conduct VES near existing boreholes and from the data develop a one dimensional resistivity model. The apparent formation factor was derived for each VES location using bulk resistivity and the water resistivity measured from the water sample of the corresponding borehole. The apparent formation factor was plotted against water resistivity and the intercept on the y-axis represented the inverse of intrinsic formation factor. They computed the porosity and hydraulic conductivity for the aquifer using the determined intrinsic formation factor. The computed porosity and hydraulic conductivity was then used to estimate the porosity and hydraulic conductivity for area without boreholes.

Soupios *et al.* (2007) concluded that the estimated or measured hydraulic conductivity had good correlation with the observed hydraulic conductivity. They also stated that electrical resistivity was used successfully to characterize the aquifer properties in the study area. It is cost effective and less time consuming than using pumping test and particle size distribution in estimating aquifer parameters as noted by Soupios *et al.* (2007).

Since electrical resistivity of water bearing formations (aquifer) vary with porosity, hydraulic conductivity and transmissivity, it can therefore be used to define the distribution of these parameters for any aquifer. Being able to estimate the distribution of porosity, hydraulic conductivity and transmissivity of the geologic units of an area would enable tracing the geometry of aquifer and confining layers in such area.

2.5 Aquifer Characterization Using VES

Abdul-Aziz (2014) integrated well log data with results from VES to define the aquifer distribution of the Nile Delta in Egypt. His approach was based on developing a model of the subsurface for a study area using resistivity logs and well logs. He conducted VES around the Nile Delta using the Schlumberger method. Resistivity logs were generated from the interpretation of the resistivity data obtained. Well logs were obtained from a well in close proximity to the sounding locations. These interpreted results (resistivity logs and well logs) were correlated with known stratigraphy of the Nile Delta. The aquifers and confining units were traced from the integrated resistivity and well log models.

Adagunodo (2013) studied the groundwater potentials of Oyo state in Nigeria using Schlumberger's method of VES. The study was aimed at using VES to define subsurface formations of the study area in terms of groundwater storage. They conducted VES using varying electrode spacing and were able to obtain knowledge of the boundaries of the various layers that compose the surface formations of the studied area. The results of their study showed areas with good groundwater potential and areas which did not have groundwater storage.

Ariyo and Adeyemi (2012) also used VES to characterize the hydrostratigraphy of Ishara in south-western Nigeria. Vertical Electrical Sounding by the Schlumberger method successfully separated the various layers of the sedimentary units and the fractured bed rocks. They concluded from their result that the potential aquifer in the area was within the shallow zone of the sedimentary units.

Khalil and Santos (2009) characterized the hydrostratigraphy of the Wadi El Natrun area in Egypt using the Schlumberger Method of VES. Their approach was based on the transformation of apparent resistivity data to true resistivity values for a non-homogeneous earth. They conducted VES to determine the depth of the various geologic units in the area. The depth of the units was combined with the volume of soundings to develop a 2 dimensional and 3 dimensional resistivity model of the area. The model defined the zones in the studied area that had abundant groundwater storage and also the zones which they considered as dry (contained no water).

2.6 Integration of VES into Geographical Information System (GIS)

The integration of the VES technique with a geospatial information system has enabled better understanding and interpretation of groundwater conditions. VES is capable of defining the depth and thickness of aquifer units and the incorporation of this data into groundwater models using GIS has improved groundwater studies over the years (Israil *et al.,* 2006). VES and GIS have successfully been used for groundwater studies (Israil *et al.,* 2006 and Nwachukwu *et al.,* 2013). Israil *et al.* (2006) integrated VES and GIS to interpret the groundwater potentials of an area in NW, India. A thematic map for the geomorphology and slope maps of the area in NW, India were initially constructed using data obtained from remote sensing and digitized with GIS. VES was also conducted in the area to define the resistivity, depth and thickness of the geologic

units. These results were integrated to define the groundwater potentials of the area (Israil *et al.*, 2006).

Besides VES, Nwachukwu *et al.* (2013) integrated down-hole logs and pumping test results into GIS to delineate the hydrogeological potential of the Imo River Basin in Nigeria. The approach was based on using data obtained from observation boreholes and from surface electrical resistivity methods to interpret groundwater distribution in the area. Aquifer resistivity and thickness were verified by VES. The mean value of the water table was estimated from down-hole log and pumping test results. GIS was finally used to produce thematic maps for the mean values of the water table, aquifer resistivity and thickness, as well as the groundwater distribution of the Imo River Basin in Nigeria.

2.7 Theory of Electrical Resistivity

The concept of electrical resistivity is based on Ohm's Law which relates the potential difference between the ends of a metallic conductor with the current applied through the conductor and the resistance of the metal to current flow. The potential difference between the ends of the metallic conductor (ΔV) is directly proportional to the applied current (I). According to Van Zijl (1985), the resistance to current flow equals the coefficient of proportionality in Ohm's Law as shown in equation (3.1).

$$\Delta V = IR \text{ (Ohm's Law)} \ldots\ldots\ldots \quad (3.1)$$

It is necessary to note that resistance R as contained in Ohm's Law does not consider the properties of the material medium through which current is flowing. Resistivity is more important and a basic property of the material medium through which current is flowing. When current (I) flows through a homogeneous material medium of length (L) and cross sectional area (a), potential difference (V) is set up across the ends of the medium as shown in Figure 6. Referring to Figure 6, the resistance R to current flow through the medium is proportional to the length of the medium and inversely proportional to the cross sectional area of it. Equation 3.2 indicates the relationship between the resistance, length and cross sectional area of any conductive material such as a length of wire (Reynolds, 2000) where the constant of proportionality is given by ρ.

$$R = \rho L / a \quad (\Omega) \ldots\ldots\ldots\ldots\ldots \quad (3.2)$$

$$\rho = R\,a\,/\,L \quad (\Omega.m) \ldots\ldots\ldots\ldots (3.3)$$

The coefficient of proportionality is given as resistivity ρ in (3.3). Resistivity is a function of the properties of the conductive material medium. The variables ρ L/a can be substituted for R in (3.1) to yield (3.4).

$$\Delta V = \rho\,(L/a)\,I \ldots\ldots\ldots\ldots\ldots\ldots (3.4)$$

$$\rho = \frac{\Delta V a}{IL}\ (\Omega.m) \ldots\ldots\ldots\ldots\ldots\ldots (3.5)$$

$$\frac{\Delta V}{I} = \rho\,\frac{L}{a} \ldots\ldots\ldots\ldots\ldots\ldots (3.6)$$

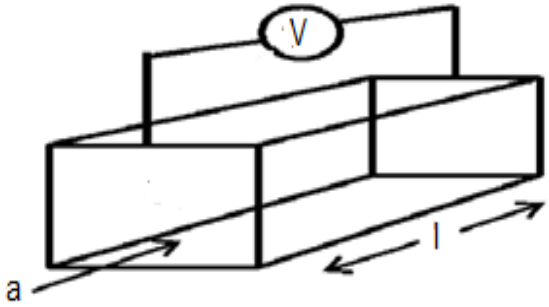

Figure 6: Concept of resistivity using a homogeneous material medium

The right-hand side of (3.6) is equal to current density **J** which can be defined as current intensity per unit area normal to the direction of flow of current. The electric field strength **E** can be defined also as the potential difference per unit length and is equal to the left-hand side of the equation. This implies that resistivity ρ can be defined in terms of current density and electric field strength by (3.7).

$$\mathbf{E} = \rho\,\mathbf{J} \ldots\ldots\ldots\ldots\ldots\ldots (3.7)$$

Therefore, $\rho = \mathbf{E}\,/\,\mathbf{J}\ (\Omega.m) \ldots\ldots\ldots\ldots\ldots$ (3.8)

2.8 Apparent Resistivity

Electrical resistivity is conducted in the field by passing a measurable amount of current into the ground through the current electrodes. As the current transits through the ground, the resulting potential difference is measured through the potential electrodes. Apparent resistivity ρ*a* is a measure of resistivity values by taking into account the electrodes' separations. Apparent resistivity depends on the depth of sounding and electrode separation. It is essential for the evaluation and interpretation of electrical resistivity data and can be regarded as true resistivity measured in a homogeneous earth. The concept of apparent resistivity can be illustrated using Figure 7. The current electrodes A and B are separated from each other as in Figure 7. The potential electrodes M and N are also separated from each other as illustrated in Figure 7.

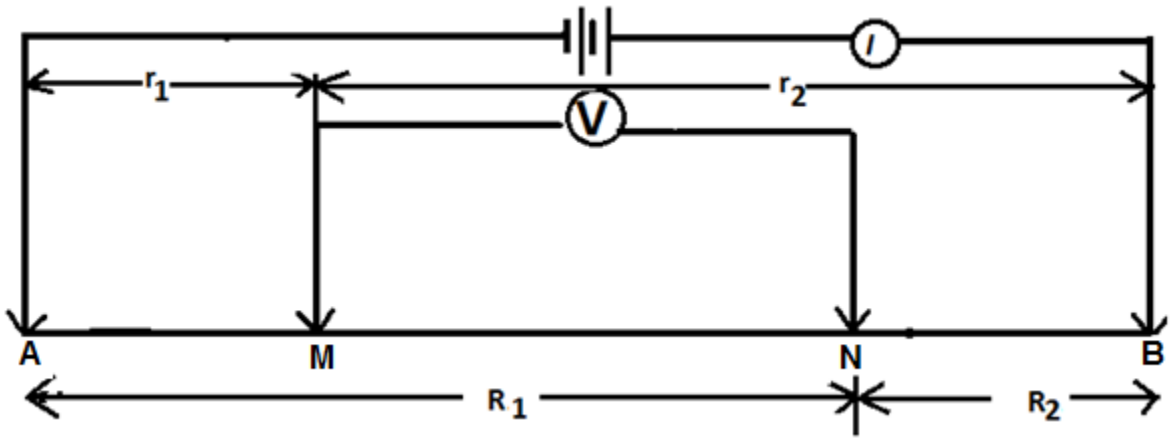

Figure 7: Measurement of apparent resistivity using four electrodes

When current I, is transmitted into the ground through A and B fixed on the ground surface in Figure 7, the resultant potential gradient is measured across the potential electrodes M and N. The potential difference at electrodes M and N are:

$$V_M = \frac{\rho I}{2\pi}\left(\frac{1}{r_1} - \frac{1}{r_2}\right) \quad \text{(3.9)}$$

$$V_N = \frac{\rho I}{2\pi}\left(\frac{1}{R_1} - \frac{1}{R_2}\right) \quad \text{(3.10)}$$

However, the potential difference across M and N can be measured by combining equations (3.9) and (3.10):

$$\delta V_{MN} = V_M - V_N = \frac{\rho I}{2\pi}\{[\frac{1}{r_1} - \frac{1}{r_2}] - [\frac{1}{R_1} - \frac{1}{R_2}]\} \ldots\ldots\ldots (3.11)$$

Solving for resistivity ρ in (3.11):

$$\rho_a = \frac{2\pi\delta V}{I}\{[\frac{1}{r_1} - \frac{1}{r_2}] - [\frac{1}{R_1} - \frac{1}{R_2}]\}^{-1} \ldots\ldots\ldots\ldots\ldots\ldots (3.12)$$

The expression ρ_a in equation (3.12) is the apparent resistivity which is computed for a non - homogeneous subsurface. Equation (3.13) is the geometric factor K measured in (m) and computed from electrode configuration. If R equals $\delta V/I$, therefore, KR equal apparent resistivity in equation (3.15).

$$K = 2\pi[\frac{1}{r_1} - \frac{1}{r_2} - \frac{1}{R_1} + \frac{1}{R_2}]^{-1} \ldots\ldots\ldots\ldots\ldots\ldots\ldots (3.13)$$

$$R = \frac{\delta V}{I} \ldots\ldots\ldots\ldots\ldots\ldots\ldots\ldots\ldots\ldots\ldots\ldots\ldots\ldots (3.14)$$

$$\rho_a = KR \ldots\ldots\ldots\ldots\ldots\ldots\ldots\ldots\ldots\ldots\ldots\ldots\ldots\ldots\ldots\ldots (3.15)$$

2.9 Electrode Configuration

The electrical resistivity method is conducted fundamentally by the use of four electrodes. The apparent resistivity measurement determined in the electrical resistivity survey is a function of the configuration of these four electrodes. A particular method for an electrical resistivity survey is achieved by keeping the separation of these electrodes constant or by varying their separations. The configuration or array of electrodes enables the computation of the geometric factor which is exclusive to that method. For the horizontal profiling technique, the electrodes' separations are kept constant and all the electrodes are moved by a constant distance for every measurement. This method is used to verify horizontal resistivity variation of ground subsurface. However, the method adopted for this study is the continuous electrode separation technique used for VES. Vertical Electrical Sounding for groundwater prospecting is commonly conducted using the Schlumberger method. The Schlumberger method is made up of two outer electrodes (current electrodes) A and B and, two inner electrodes (potential electrodes) M and N. To measure the resistivity of the different (non – homogeneous) earth layers at any point, the

electrodes are arranged as shown in Figure 8. A measurable amount of current is transmitted into the ground through A and B and the value of the current I is measured with an ammeter and recorded in (mA). The resultant potential gradient ΔV across M and N is determined by means of a voltmeter and recorded in (mV). Using the variables ΔV and I, and the geometric factor for the Schlumberger array, the apparent resistivity value for that depth can be calculated using equation (3.16).

$$\rho_a = \frac{\pi a^2}{b}\left[1 - \frac{b^2}{4a^2}\right] R \ldots\ldots\ldots\ldots\ldots \quad (3.16)$$

Where a and b in equation (3.16) equal potential and current electrodes' spacing respectively. In vertical electrical sounding, the potential electrodes are kept constant while the current electrodes are separated continuously until the measured current becomes too small and the potential electrodes have to be separated further apart. The depth of investigation increases as with current electrodes' spacing. The depth of investigation is equal to half the current electrodes' separation (AB/2). While conducting vertical electrical sounding, it is required that the potential electrodes' separation should always be less or equal to one fifth of current electrodes' separation (AB/2).

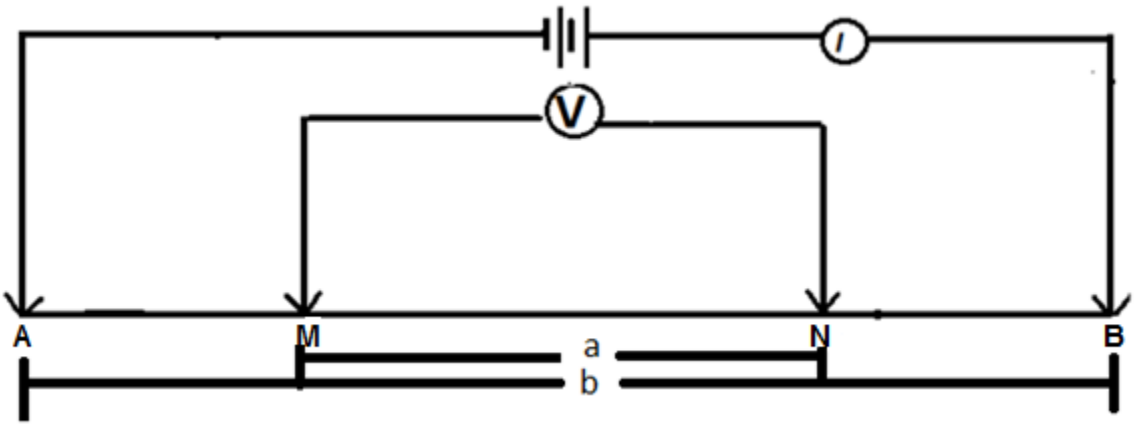

Figure 8: Electrode array for VES by Schlumberger Method

2.10 Dar Zarrouk Parameters

Thickness (h) and resistivity (ρ) are the two fundamental parameters of geoelectric sections that can be deduced from VES interpretation. These two parameters can be used to effectively describe geoelectric section generated from VES curves. The Dar Zarrouk parameters are relationships derived between h and ρ by Maillet (1947) and were called the traverse resistance (T_R) and longitudinal conductance (L_C). Traverse resistance and longitudinal conductance are important parameters in the electrical resistivity geophysical method and can be applied to define the aquifer hydraulic properties using VES.

The traverse resistance of a geoelectric unit is the product of the thickness h and the resistivity ρ of the unit. This can be written as:

$$T_R = h\rho \quad \text{(3.17)}$$

The longitudinal conductance of a geoelectric unit is the ratio of its thickness h to its resistivity ρ which can also be written as:

$$L_C = h/\rho \quad \text{(3.18)}$$

The flow of current through an aquifer is either perpendicular (traverse) or parallel (longitudinal) to the flow of groundwater. Since Dar Zarrouk parameters are bulk parameters deduced from the interpretation of VES curves, Zorhdy *et al*. (1974b) stated that the Dar Zarrouk parameters can be compared directly with hydraulic parameters. Niwas and Singhal (1981) showed that the current flow and hydraulic flow can be compared by relating Ohm's Law with Darcy's Law. They related the Dar Zarrouk parameters to transmissivity T and hydraulic conductivity K as follows:

$$T = Kh \quad \text{(3.19)}$$

$$T = K/\rho\, T_R \quad \text{(3.20)}$$

$$T = K\rho\, L_C \quad \text{(3.21)}$$

Where, T = transmissivity, K = hydraulic conductivity; h = aquifer thickness; ρ = resistivity derived from VES; T_R = traverse resistance derived from VES; and L_C = longitudinal conductance derived from VES.

Niwas and de Lima (2003) observed that electrical resistivity and transmissivity of a geoelectric unit can be influenced by clay content. The increasing amount of clay in such a unit increases

electrical conductivity and decreases hydraulic conductivity. Therefore, electrical resistivity and hydraulic conductivity varies directly with each other in a geoelectric unit that contains clay as shown in equation (3.22):

$$K = C_1\rho \ldots\ldots\ldots\ldots\ldots \quad (3.22)$$

$$K/\rho = C_R \ldots\ldots\ldots\ldots\ldots \quad (3.23)$$

In equation (3.23), C_R is a constant. Kelly (1977) reported an indirect inverse relationship between resistivity and hydraulic conductivity in a clay free geoelectric unit. This relationship can be described using equation (3.24):

$$K\rho = C_F \ldots\ldots\ldots\ldots\ldots \quad (3.24)$$

Where C_F in equation (3.24) is a constant and by substituting equations (3.23) and (3.24) in (3.20) and (3.21) respectively gives equations (3.25) and (3.26) as follows:

$$T = C_R T_R \ldots\ldots\ldots\ldots\ldots \quad (3.25)$$

$$T = C_F L_C \ldots\ldots\ldots\ldots\ldots \quad (3.26)$$

Equations (3.25) and (3.26) can be used to compute transmissivity values of the entire aquifer provided that pump test result exists for a few boreholes drilled in the area of study.

Niwas and Lima (2003) stated that in a clay rich geoelectric medium, K/ρ is expected to be constant. Equation (3.25) can be used to model transmissivity T. But in a clay free geoelectric medium, Kρ is expected to be constant. Therefore equation (3.26) should be used.

2.11 Resistivity of Geologic Materials

The flow of current through geologic materials occurs in a number of ways. One such way is the free movement of electrons in metals. This occurs mostly in ores and most metals (Reynolds, 2000 and Loke, 2004). Current flow through the subsurface most commonly occurs by electrolytic conduction. Electrolytic conduction occurs due to slow movement of ions in the mineralized pore fluids (Van Zijl, 1985).

Pore fluid of rocks and sediments contain some dissolved minerals or salts. When current is transmitted through such a geologic material, electrochemical action occurs which sets the

cations (+ charge) and anions (- charge) in an opposite direction. The movement of these ions conducts current through the rocks or sediments. Therefore, the conduction of current through a geologic material by electrolytic action is influenced by the dissolved solutes in the pore fluid, the amount of the pore fluid, and also by the nature of the host material (Van Zijl, 1985; Dobrin and Savit, 1988; Reynolds, 2000 and Loke, 2004).

In hard rocks, electrolytic conduction depends on the conductivity (inverse of resistivity) of water contained in the joints and fissures and, the amount of water that is contained in the joints and fissures. Reynolds (2000) also stated that the resistivity of hard rocks varies significantly with age. Older rocks are more resistive than younger ones. For example, volcanic rocks of the Precambrian age have higher resistivities than volcanic rocks of the Quaternary age. Different types of rocks exhibit different resistivity values (Figure 9).

Sedimentary rocks are more conductive than Igneous and metamorphic rocks due to a high fluid content and therefore have the lowest resistivity range. Igneous rocks have the highest resistivity values while metamorphic rocks exhibit an intermediate resistivity range (Reynolds, 2000).

The nature of geologic material as a factor that influences electrical conductivity (or resistivity) has to do with pore spaces and the proportion of the pore spaces filled with water (Van Zijl, 1985). The ratio of the pore spaces to the bulk volume of a rock or sedimentary unit defines the porosity of that unit. Therefore, porosity is a major factor that determines the electrical resistivity of rocks or sediments. In saturated sediments and rocks, the porosity, the electrical resistivity of the saturating fluid, the resistivity of the material medium and the interconnectedness of the pores determines the resistivity of the geologic unit (Huntley, 1985 and Arshad *et al,.* 2013). Archie's Law (equation 3.17) is a formula developed by empirical method which can be used to deduce the relationship between resistivity and porosity.

$$\rho_o = a\, \Phi^{-m}\, \rho_w \quad \text{..... (3.17)}$$

$$\rho_o / \rho_w = a\, \Phi^{-m} \quad \text{..... (3.18)}$$

Where

ρ_o = effective or bulk resistivity

ρ_w = resistivity of the pore water

ϕ = porosity

m = cementation constant given as 1.3 ≤ m ≤ 2.5 by Reynolds (2000)

a = constant given as 0.5 ≤ a ≤ 2.5 by Reynolds (2000)

The effective or bulk resistivity of the rock or sediment can be verified by conducting vertical electrical sounding while the resistivity of the pore fluid can be measured from samples taken from boreholes. Archie's Law assumes that the water bearing formation is clay free and also the saturating pore water resistivity is constant within any given geologic unit or basin. In this situation, the ratio ρ_o / ρ_w is described as the intrinsic formation factor F_1 (Worthington, 1993 and Soupios *et al*., 2007).

In a situation where an aquifer is composed of unconsolidated sediments and consists of clay, silt and gravel (such as Sodwana area), Soupios *et al*. (2007) explained that a modified form of Archie's Law should be used. To enable the application of a modified form of Archie's Law, the intrinsic formation factor F1 (for clean sand or crystalline rock) and the apparent formation factor Fa (for unconsolidated non-clean aquifer) were considered together. The ratio of the bulk aquifer resistivity to the resistivity of saturating water ρ_o / ρ_w becomes an apparent formation factor when the aquifer is unconsolidated and contains clay. Huntley (1985) and Worthington (1993) used equation (3.19) to compute the intrinsic formation factor and surface conductance P_m of the aquifer due to the presence of clay. When porosity (ϕ) is determined using equation (3.20), the bulk resistivity (ρ_o) can be determined using vertical electrical sounding while the saturating water resistivity can be determined from water samples taken from boreholes in the study location.

$$\frac{1}{Fa} = \frac{1}{F1} + \left(\frac{Pm}{F1}\right) \rho_w \ldots\ldots\ldots\ldots\ldots\ldots \quad (3.19)$$

When 1/Fa is plotted against ρ_w, the intercept of the straight line equals 1/F1 while the gradient equals Pm/F1. Since intrinsic formation factor F1 can be determined, Soupios *et al*. (2007) showed that porosity can also be determined using equation (3.20).

$$\phi = e^{\frac{1}{m}\ln(a)+\frac{1}{m}\ln\left(\frac{1}{F1}\right)} \ldots\ldots\ldots\ldots\ldots\ldots \quad (3.20)$$

Where a, in equation (3.20) equals 0.5 ≤ a ≤ 2.5 by Reynolds (2000)

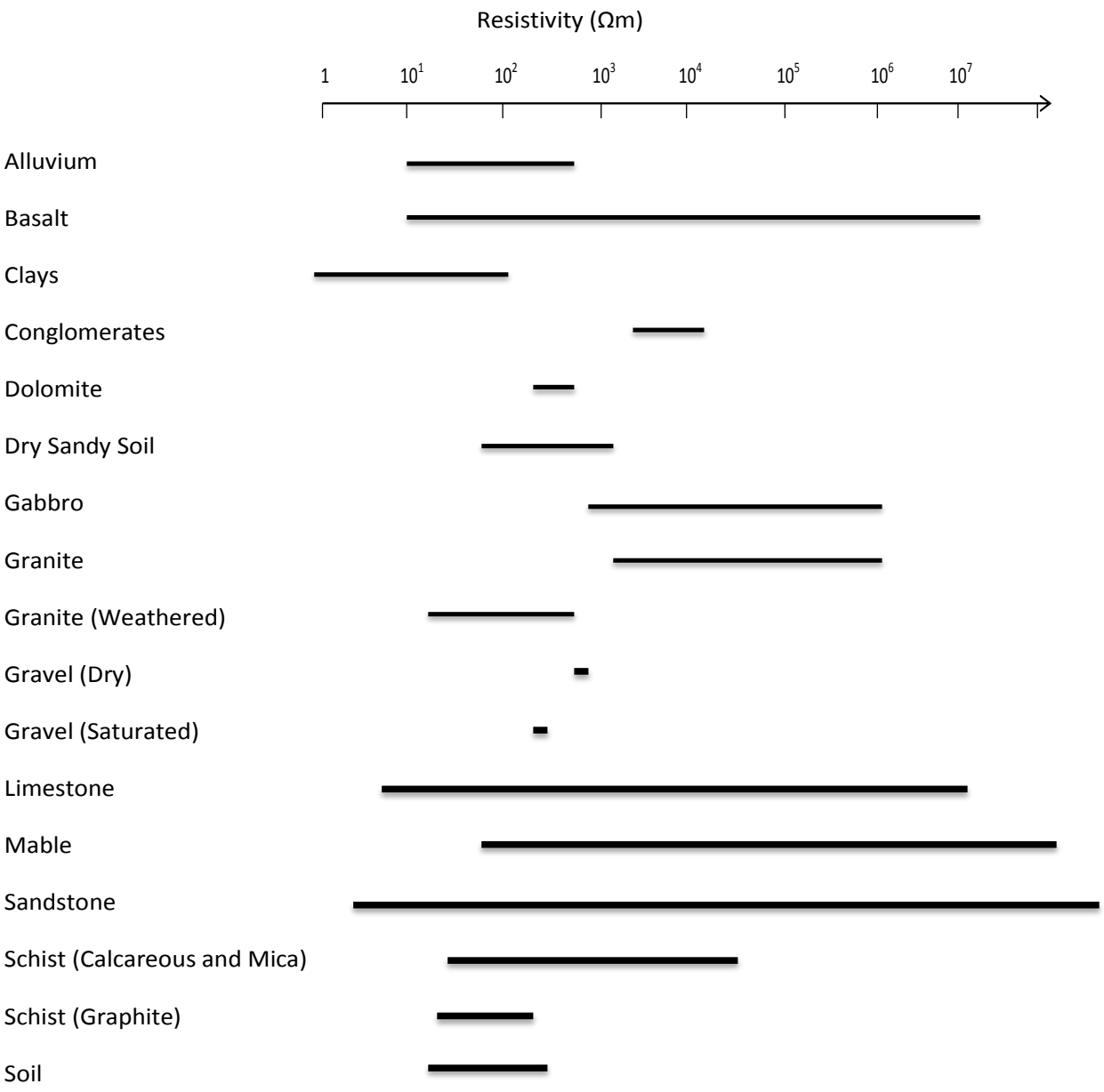

Figure 9: The resistivity of some geologic materials in ohmmeter *(Ωm);* thick line shows the resistivity range (Reynolds, 2000).

CHAPTER THREE

3 METHODOLOGY

3.1 Introduction

The study area was considered and the geophysical implementation plan was designed so that VES would be conducted at regular intervals in the study area in two roughly north - south transects running close to parallel to the coast line. Test locations were also aligned in a west - east direction. The Schlumberger electrodes' configuration and methodology was applied. The use of this method is applicable because of its sensitivity to variations in particle sizes (clay, silt, sand and gravel) and because of the successful use of the method in other areas (Worthington, 1978). The study area (Mgobolezeni Catchments) consists of sediments which are composed of clay, silt, sand and gravel (Jeffares and Green, 2012). The data collection for this study was designed to determine and verify the vertical variation of these characters (clay, silt, sand and gravel) in the north - south and east - west directions in the study area (Figure 10).

The monitoring boreholes (SOD 01, SOD 02, SOD 03, SOD 04, SOD 05, SOD 06, SOD 07 and SOD 08) form the basis of the two north - south transects, and were drilled along the eastern and western sides of Lake Mgobolezeni in the study area as presented in Figure 10. VES was conducted between the boreholes in a north – south direction along the western and eastern sides of Lake Mgobolezeni (Figure 10).

The field work was conducted in four phases as follows:-

a) The first phase was a reconnaissance visit to the study area in September, 2013. The purpose of this visit was to identify the monitoring boreholes in the study area and to trace transects and traverses for VES survey. Transects are lines running north – south with west - east controls along which the series of VES would be located. Traverses orientations for each vertical electrical sounding point were mostly in the north – south direction. The routes for movement within the study area were planned during this phase of the field work. b) The second phase commenced on the 7th of November and ended on the 6th of December 2013. VES were conducted along the western transect during this period.

c) The third phase was conducted between the 18th and 21st of March, 2014. VES were conducted along the eastern transect during this phase.

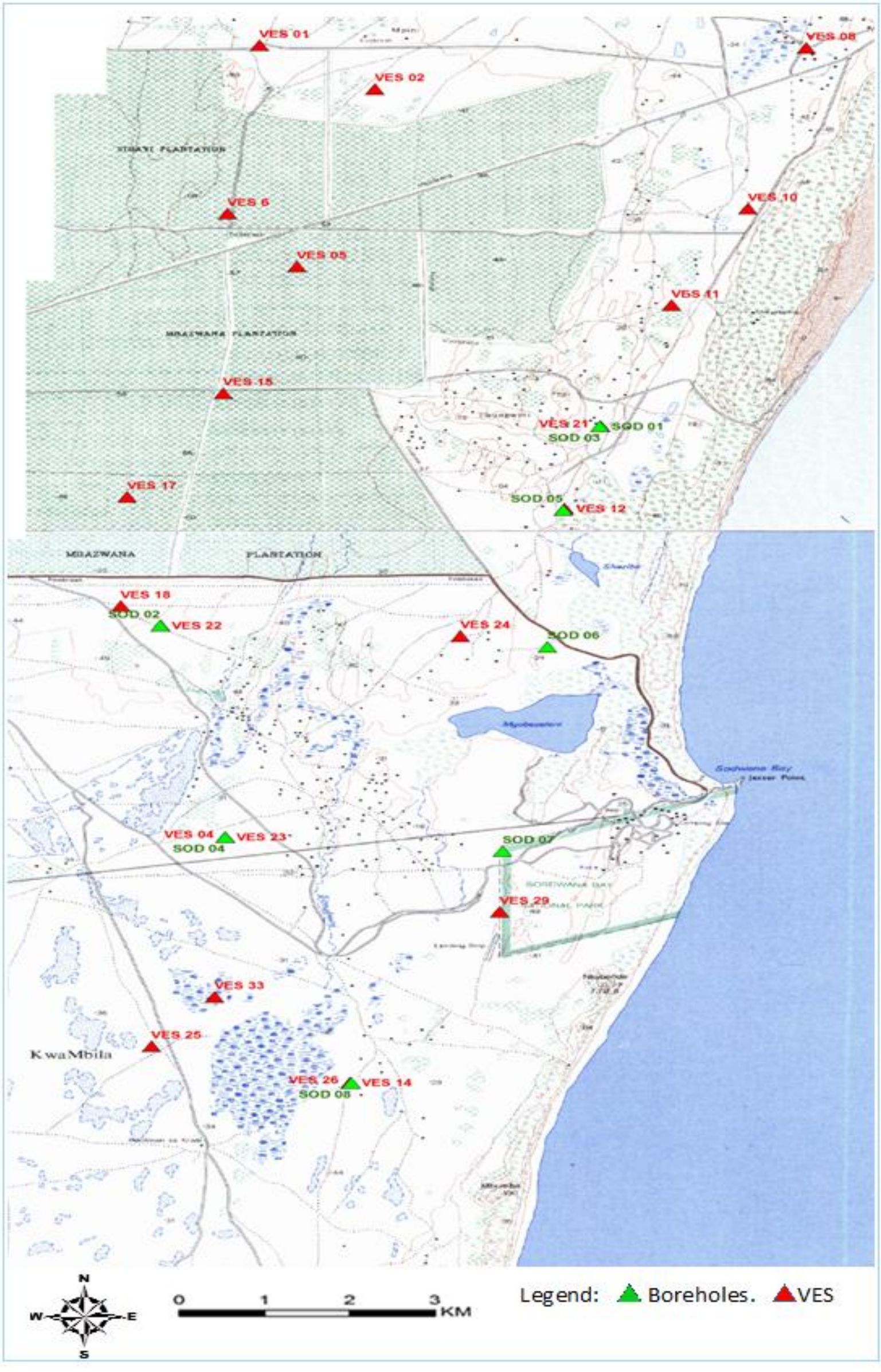

Figure 10: VES and borehole location

d) The fourth phase consisting mostly of infill test locations and was conducted from the 13th to 21st June, 2014.

3.2 Data Collection

3.2.1 Locating Vertical Electrical Sounding Points

Prior to the commencement of field work, the coordinates of the monitoring boreholes in the study area were sourced from Jeffares and Green (2012) and plotted on a map. VES was conducted in close proximity to the monitoring boreholes in order to calibrate results, and also in between them to increase the confidence in the lithology map.

Two roughly parallel lines or transects were generated. The first transect (AB) was called the eastern transect because it trends along a series of monitoring boreholes located in the eastern side of Lake Mgobolezeni. All boreholes and VES points located along this transect are denoted in this study as eastern boreholes and eastern VES points respectively. The second transect was called the western transect and this is because it runs through the series of monitoring boreholes located in the western side of Lake Mgobolezeni. All boreholes and VES points located along this transect are denoted in this study as western boreholes and western VES points respectively.

The distance between two adjacent boreholes along a particular transect was demarcated uniformly into 1km intervals with nodes. Starting from north to south, the first 1km node on the western transect (1W) was joined to the first 1km node on the eastern transect (1E) as illustrated in Figure 11. The second 1km node (2W) on the western transect was also joined to the second 1km node (2E) on the eastern transect. This procedure was repeated until all nodes on the western transect were joined to the corresponding node on the eastern transect (Refer to Figure 11).

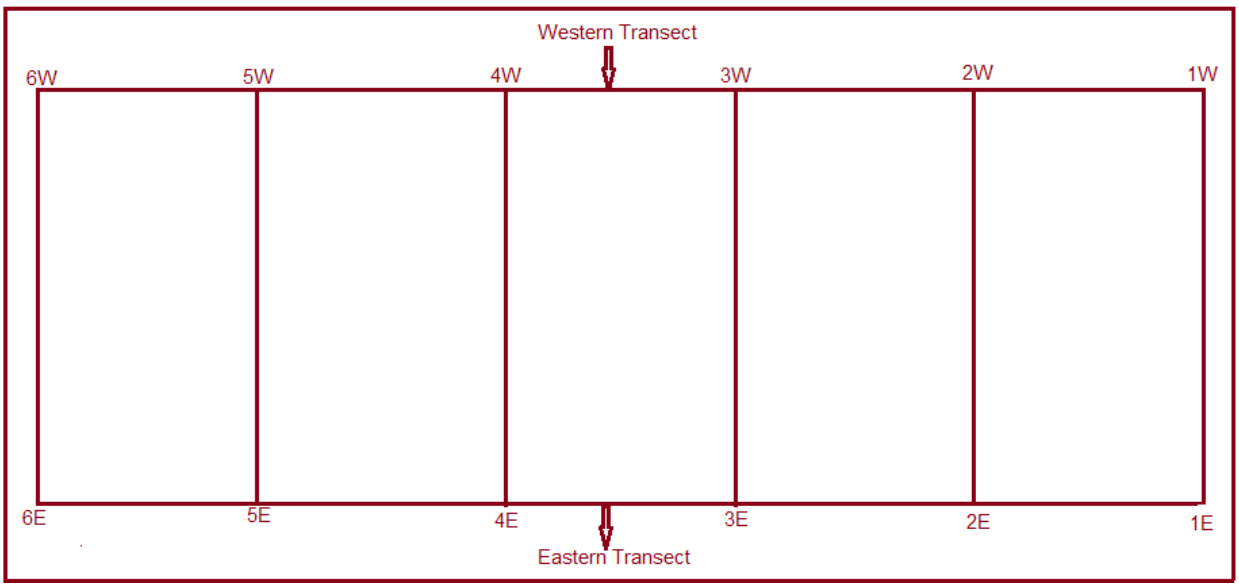

Figure 11: Demarcation of study area before the start of the field survey

The coordinates of nodes along each transect were determined from Google Earth and recorded in a field note book. The coordinates of each proposed VES point were numbered sequentially for each transect, starting from 01 to the final length of each transect. A suffix E or W was added to each number to denote eastern or western transect (Refer to Figure 11). These were the locations at which soundings were conducted to enable the survey of the entire study area.

3.2.2 Vertical Electrical Sounding

The Schlumberger method of VES was used for data collection in the field. A Geotron (G41) resistivity meter instrument was used for the survey. The instrument was made up of the resistivity meter, four stainless steel electrodes, four cable reels with wire and two (200m) tape measures. The field work commenced with conducting calibration soundings in close proximity to the DWA monitoring boreholes. A centre point was chosen approximately 10m away from each borehole and the coordinates of the point determined with a hand held GPS. All VES tests were aligned in a north – south direction to try to maintain consistency (based on the assumption that there is less horizontal variation in lithology parallel to the coast as opposed to perpendicular to the coast where it is likely that horizontal variation could be more noticeable). See Table 35 (Appendix 1) for the summary of VES test set.

3.3 Interpretation of Results

The apparent resistivity values for each location were plotted against AB/2 (half the current electrode separation) on a log – log graph. The MN overlap readings helped the removal of noise from the data. The smoothed values of apparent resistivity versus AB/2 were fed into IPI2Win (Lite) computer software for iteration. The software was used to generate an observed curve and a model curve. The inversion method was employed since the area of study is composed of non – homogeneous geologic materials.

The model curve was iterated to fit the observed curve until the minimum percentage error possible was obtained for each vertical electrical sounding location. When both curves fit with a minimum percentage error obtained, and then the observed geoelectric properties are considered to portray the geology beneath the ground surface for further interpretation.

The true resistivity value, the thickness, and depth of each layer that occurred in that location were determined and recorded in tables as presented in Chapter 5. The curves for each location and the corresponding geoelectric model for that location are also presented in Chapter 5. The depth and thickness of the layers that occur at each location in close proximity with DWS monitoring boreholes were compared with the borehole log for the corresponding borehole. Geoelectric models were developed for all locations in close proximity to monitoring boreholes and were used to interpret vertical electrical sounding data obtained at the nodes between the boreholes. The geoelectric model for all the locations, their coordinates and elevations (determined from Google Earth) were reviewed sequentially to show the spatial variation of the geoelectric layers in the study area.

The Dar Zarrouk parameters were combined with pumping test results from six boreholes in the study area to establish relationship between transmissivity and the Dar Zarrouk parameters. Transmissivity obtained from pumping tests for the five boreholes were plotted against traverse resistance for the deep aquifer. Relationships were established between transmissivity and traverse resistance using linear regression methods. These relationships were used to model transmissivity where there are no boreholes. The modelled transmissivity values were contoured over the surface of the deep aquifer in the study area.

CHAPTER FOUR

4 PRESENTATION OF RESULTS

4.1 Introduction

The interpretation of the VES data for this study was aided by the specialist knowledge of the geological succession of the study area from drilling of monitoring boreholes and the lithostratigraphic profile of the Maputaland Formation after Botha and Porat (2008). Additional information from Mark Schapers was taken into account. The information from the DWA borehole logs further enhanced the interpretation of the resistivity data. The instrument (Geotron – G41 – resistivity meter) used was designed to compute apparent resistivity values automatically from transmitted current, measured potential difference and electrode spacing. The values of the apparent resistivity, transmissivity current and potential difference displayed by the instrument were recorded in the data sheet (Refer to Appendix I) for further interpretation.

4.2 Presentation of Data

The VES locations in close proximity with the DWA (Refer to Figure 10) boreholes and the boreholes are as follows:-

a) VES 12 and borehole SOD 05
b) VES 21 and borehole SOD 01
c) VES 22 and borehole SOD 02
d) VES 23 and borehole SOD 04
e) VES 24 and borehole SOD 06
f) VES 25 and borehole SOD 03
g) VES 26 and borehole SOD 08
h) VES 29 and borehole SOD 07

4.2.1 VES Curves

The apparent resistivity values for the VES locations were plotted against AB/2 using IPI2Win computer software. The curves generated for each of the VES locations exhibited a continuously decreasing trend (Figure 12). The trend of the curves decreased progressively with increasing electrode spacing. This type of curve can be described as a QH-type curve and was experienced throughout the study area.

Figure 12 shows the VES curves and the corresponding geoelectric model generated for calibration VES surveys. The geoelectric models are made up of five columns which describe the properties of each geoelectric layer observed from the VES curves. The five columns making up the geoelectric model are described as follows:-

a) Column N shows the layers comprising up a curve

b) Column ρ provides the apparent resistivity for each layer

c) Column h represents the thickness of each layer

d) Column d shows the surface of the immediately underlying layer.

The resistivity curves and models for all the VES conducted for this study are presented in Appendix 11. The resistivity curves and models observed for the entire VES survey show a minimum of four geoelectric layers and a maximum of five geoelectric layers.

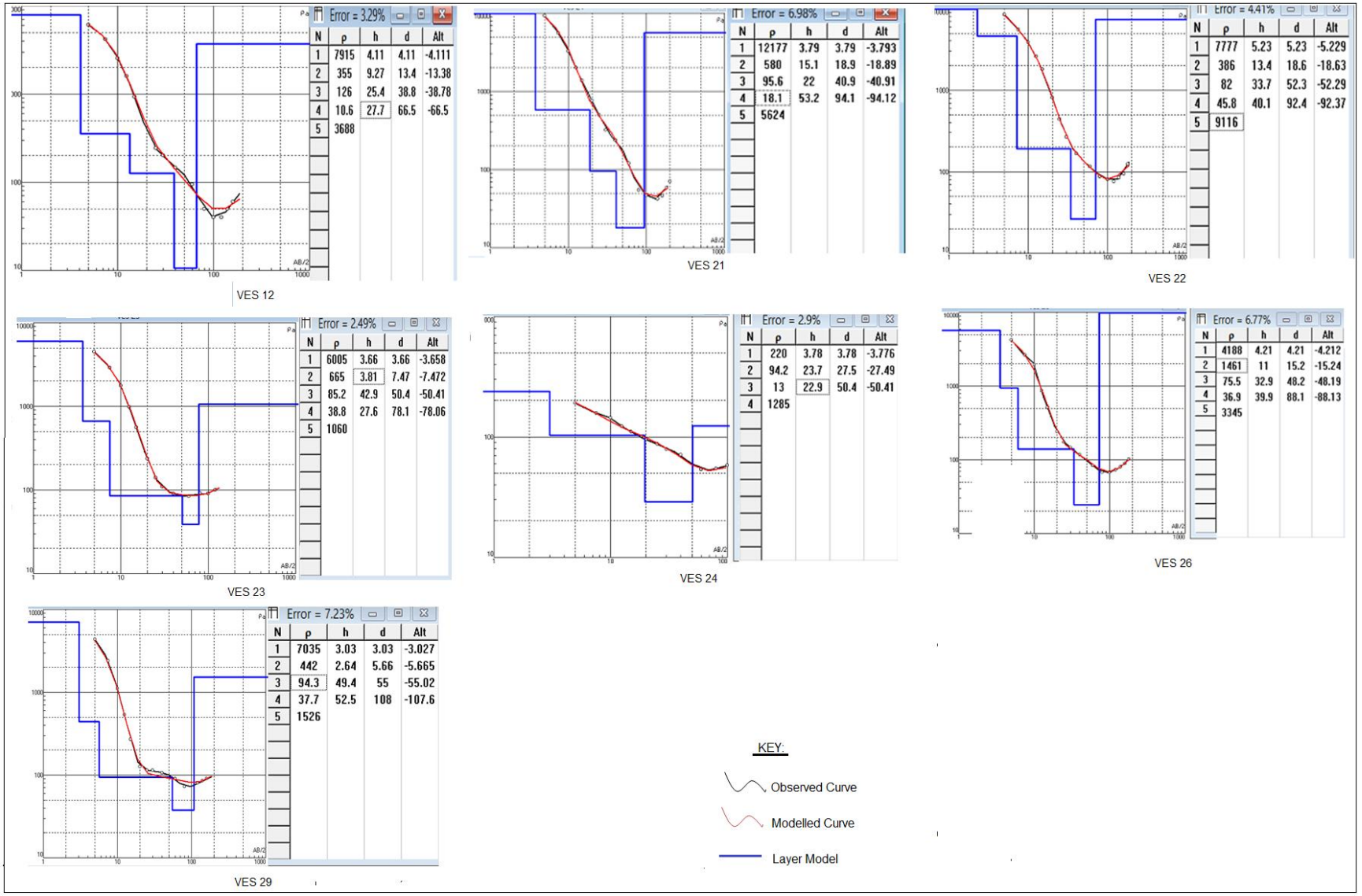

Figure 12: Resistivity curves for the seven calibration VES locations

4.2.2 Observed Geoelectric Properties

The interpretation of all the VES conducted (points in close proximity with monitoring boreholes and points in between the monitoring boreholes) are summarized in Table 3 and Table 4. Tables 3 and 4 present the geoelectric properties of each individual layer observed from the VES survey. Table 3 consists of the VES points along the western transect of the study area while Table 4 consists of VES points along the eastern transect (Refer to Figure 13 for western and eastern transect).

The highlighted columns in Tables 3 and 4 indicate the depth to the Cretaceous layer at each VES location. The thickness (H), apparent resistivity (ρ) and depth (D) of the individual layers observed for all the VES locations are also presented in Tables 3 and 4.

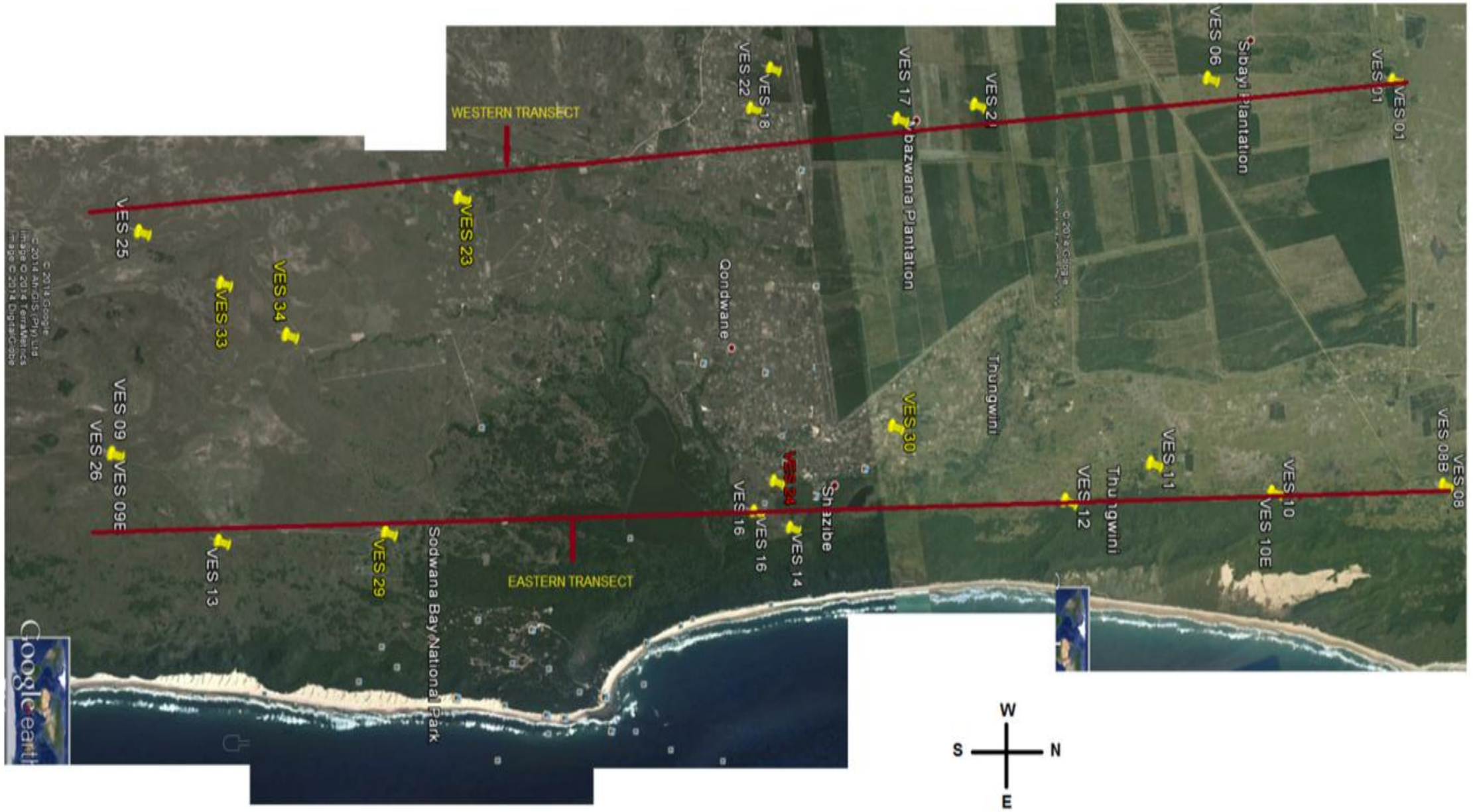

Figure 13: VES points along eastern and western transects

Table 3: Results for VES locations along the western transect

	LAYER 1			LAYER 2			LAYER 3			LAYER 4			LAYER 5		
ID	ρ(Ωm)	H(m)	D(m)	ρ(Ωm)	H(m)	D(m)	ρ(Ωm)	H(m)	D(m)	ρ(Ωm)	H(m)	D(m)	ρ(Ωm)	H(m)	D(m)
VES 01	6195	3	3	859	6	9	198	36	45	14	43	87	1442	∞	∞
VES 06	6098	3	3	971	6	9	194	36	45	14	42	87	1330	∞	∞
VES 17	2491	2	2	724	10	12	112	38	50	43	40	90	6688	∞	∞
VES 18	7441	2	2	3140	10	12	178	37	47	20	33	80	4139	∞	∞
VES 21	8141	4	4	518	15	19	97	19	39	21	59	98	6285	∞	∞
VES 23	6005	4	4	665	4	8	85	43	50	39	28	78	1060	∞	∞
VES 24	0	0	0	220	4	4	94	24	28	13	23	50	1285	∞	∞
VES 25	8213	3	3	189	31	33	72	19	52	28	34	86	1729	∞	∞
VES 33	6654	2	2	724	10	12	112	38	50	43	40	90	1592	∞	∞

The columns circled in red in Table 3 and Table 4 show the depth of the Cretaceous basement at VES locations. It can be observed from Table 3 that the VES locations along the western transect exhibited a 5-layer model except in VES 24 where the top soil was not present therefore reducing it to a 4 layer model. The high apparent resistivity values observed for the layer 1 (top soil) at other VES locations was not observed at VES 24. This is because the top layer was composed of peat at VES 24. Table 3 shows that the geoelectric layer 1 has thicknesses that ranged between 2 – 4m and also exhibited very high apparent resistivity values along the western transect. The thicknesses of geoelectric layer 2 varied from 4 – 15m with one exception. The thickness (31m) observed for layer 2 at VES 25 was considered out of range and attributed to possible instrument error. The geoelectric layer 3 has thicknesses that varied from 19 – 43m while the geoelectric layer 4 exhibited thicknesses that varied from 23 – 59m.

Table 4: Results for VES locations along the eastern transect

	LAYER 1			LAYER 2			LAYER 3			LAYER 4			LAYER 5		
ID	ρ(Ωm)	H(m)	D(m)	ρ(Ωm)	H(m)	D(m)	ρ(Ωm)	H(m)	D(m)	ρ(Ωm)	H(m)	D(m)	ρ(Ωm)	H(m)	D(m)
VES 08	3502	5	5	1238	4	9	159	34	43	48	25	68	1433	∞	∞
VES 9	3641	9	9	1214	4	13	147	29	42	20	18	60	3374	∞	∞
VES 10	3298	7	7	738	20	27	115	12	39	28	25	64	7225	∞	∞
VES 11	6403	5	5	850	11	16	133	36	52	25	56	108	3583	∞	∞
VES 12	7915	4	4	355	9	13	126	25	39	11	28	67	3688	∞	∞
VES 13	10155	2	2	1334	8	9	99	32	41	12	26	67	6216	∞	∞
VES 14	4687	3	3	852	3	5	82	23	29	21	29	58	10910	∞	∞
VES 22	7777	5	5	386	13	19	82	34	52	45	40	92	9116	∞	∞
VES 26	4188	4	4	1661	11	15	76	33	48	37	40	88	3345	∞	∞
VES 29	7035	3	3	442	3	6	94	49	55	38	53	108	1526	∞	∞
VES 30	15543	4	4	0	0	0	142	21	24	13	29	53	2397	∞	∞

Table 4 gives a summary of the interpretation of the VES locations along the eastern transect. A total of 11 VES points were conducted along the eastern transect. Five-layer resistivity models were observed at 10 locations while a four-layer model was observed at VES 30. Layer 2 was not observed at VES 30 possibly having been eroded completely at this location. Table 4 shows that thicknesses of geoelectric layer 1 varied from 2 – 9m along the eastern transect. It also exhibited very high apparent resistivity values. The thicknesses of geoelectric layer 2 varied from 3 – 20m. The thicknesses of geoelectric layer 3 varied from 11 – 49m while the thicknesses of the geoelectric layer varied from 18 – 53m.

4.2.3 Correlation of Borehole Logs with VES Logs

A resistivity log showing the thickness and depth of the geoelectric layers comprising a VES point was generated for each VES survey. The logs for the VES locations in close proximity of DWA monitoring boreholes were compared with the corresponding borehole logs in Figures 14 - 19. The legend shows the resistivity range at which each geoelectric layer was observed. The purpose for comparing the two logs is to enable correlation between the resistivity profile and the observed geology.

Zorhdy *et al*. (1974b) noted that water conductivity can cause a geoelectric boundary that is different from the geological boundary on one hand and lithologies of different ages. However, having the same resistivity can cause discordance between geoelectric boundaries and resistivity boundaries. The boundaries of interpreted geoelectric layers do not always coincide with the observed boundaries of geologic formations but did show some good correlation as can be observed from Figures 14 to Figure 19.

The correlation of borehole logs (geology) for borehole SOD 01 and the resistivity log for VES 21 are presented in Figure 14. It can be observed from the borehole log that actual changes in lithologies occurred at depths of 7m, 14m and 42m while changes in geoelectric properties were observed at 5m, 18m, 40m and 96m. The deep aquifer (Uloa/Umkwelane) was not drilled at this location as can be observed from the borehole logs. The VES log shows that the layer 4 is separated from the underlying unit at the 96m depth. This depth (96m) marks the interpreted boundary between the Cenozoic sediments (Refer to Table 1) and the Cretaceous unit. The geoelectric boundaries show good correlation with the lithologic boundaries.

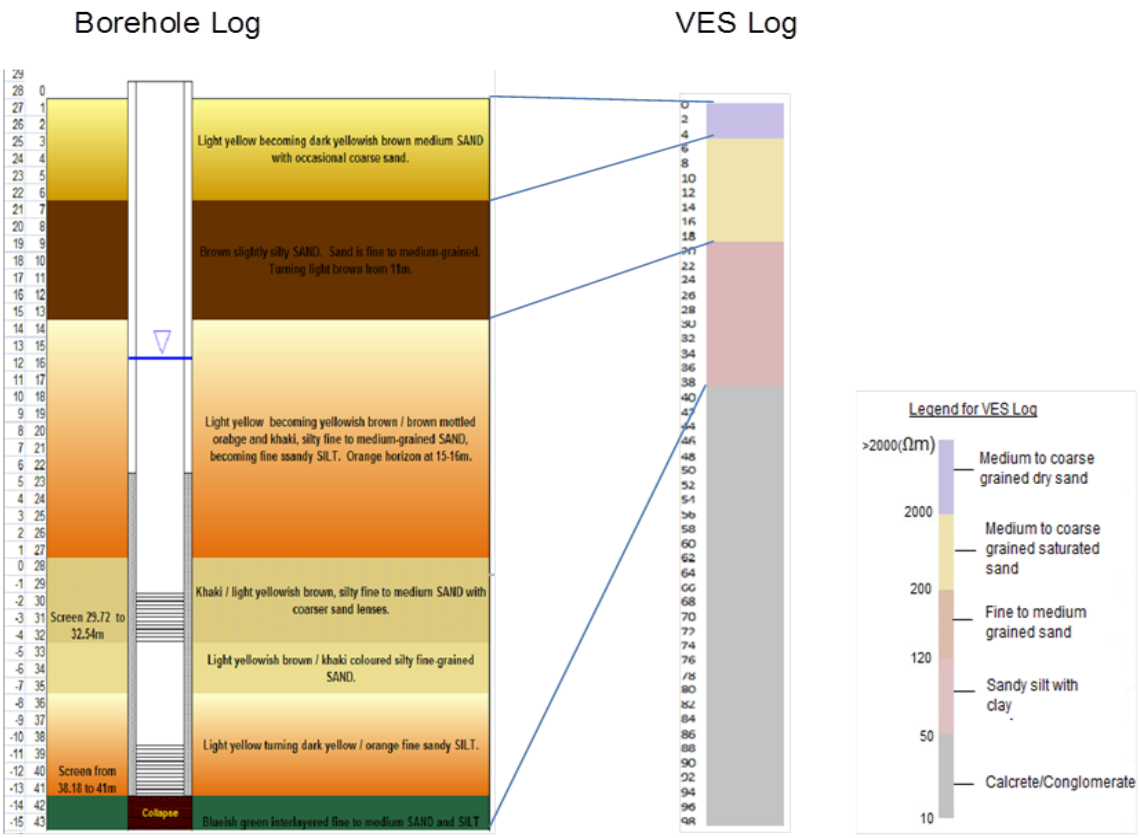

Figure 14: Correlation of borehole SOD 01geology with VES 21 survey. Note: The change in scale of the log depths.

VES 22 was conducted in close proximity with borehole SOD 02 and the two logs are presented in Figure 15. The borehole log shows lithological boundaries which do not coincide perfectly with the geoelectric boundaries. There are nine observed lithological changes in the borehole log. These nine lithological units can be grouped into four geologic sections with three geologic boundaries at 12m, 34m and 52m. The resistivity log shows four geoelectric layers with boundaries at 5m, 19m, 52m and 92m. The boundary between the third and fourth layer is the same (52m) for both the geologic and geoelectric sections. There is a good correlation between the two logs at 52m depth.

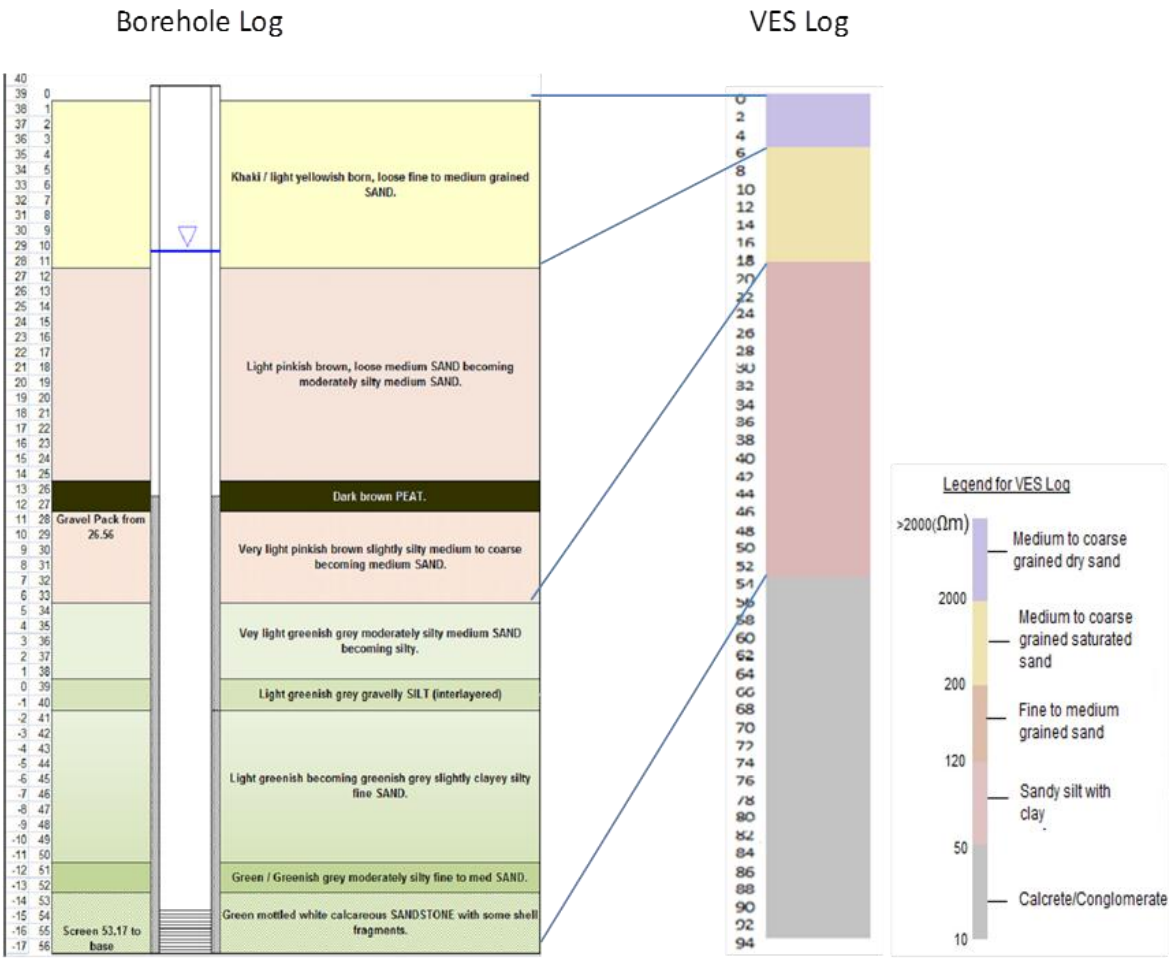

Figure 15: Correlation borehole SOD 02 geology with VES 22 survey. Note: The change in scale of the log depths.

The logs for borehole SOD 04 and resistivity log for VES 23 which are presented in Figure 16 correlate well. Three geological sections can be observed from the borehole logs (SOD 04). The geologic sections are based on lithological (not colour) variation. The geologic boundaries occur at depths of 22m and 49m. On the resistivity log, four geoelectric sections were observed at VES 23 which was conducted in close proximity with SOD 04. The geoelectric boundaries were observed at 5m, 8m, 53m and 80m.

In Figure 16, the borehole logs for SOD 04 and VES 23 are presented together. The boundary between the fourth and fifth sections on the borehole log was observed at 49m. On the resistivity log, the boundary between the third and the fourth layers was observed at 53m. The fourth and the fifth sections on the borehole log show good correlation with the third and fourth layers on the resistivity log as can be observed in Figure 16. The layer 4 in the resistivity log coincides with calcrete section (deep aquifer) in the borehole log.

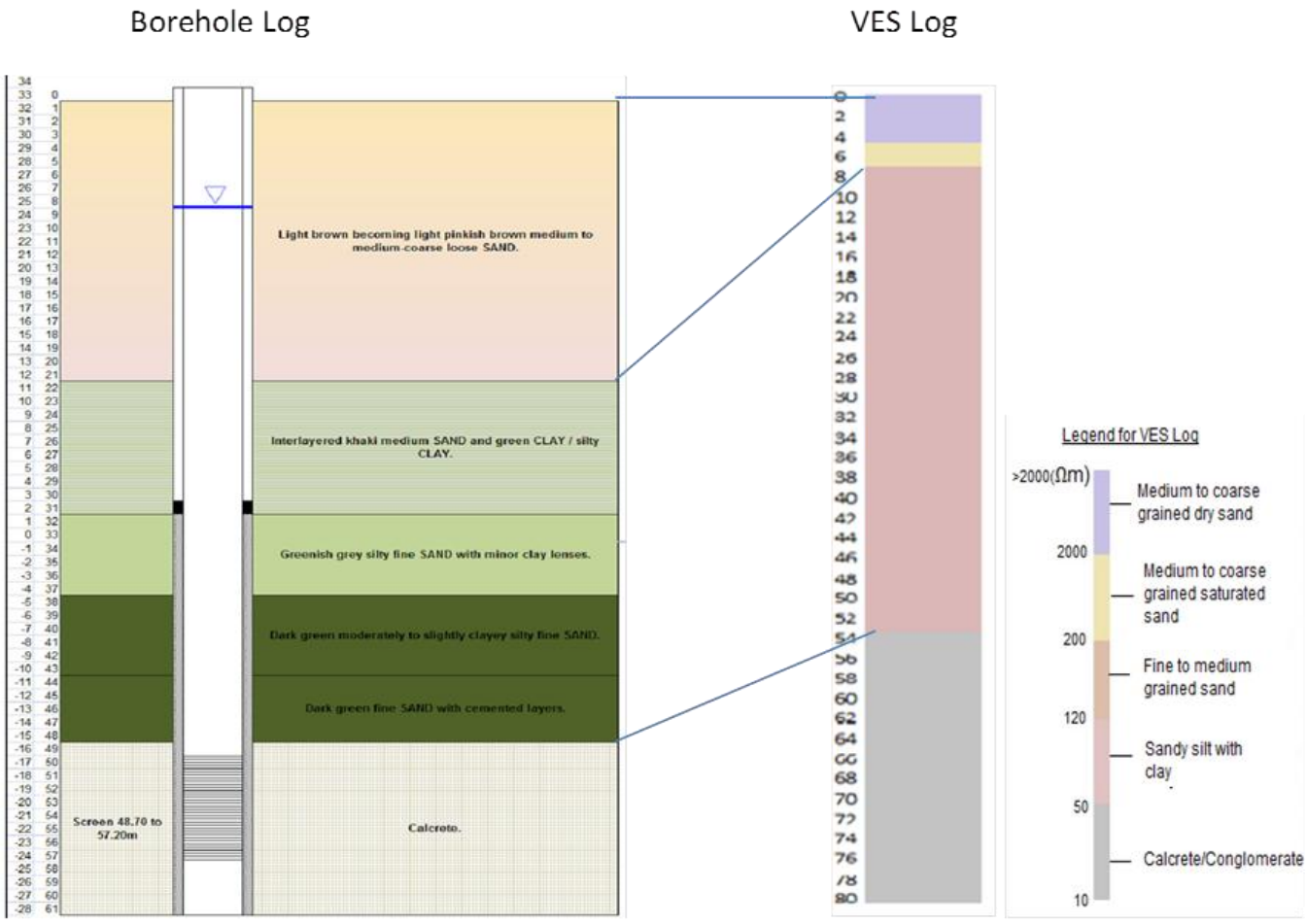

Figure 16: Correlation borehole SOD 04 geology with VES 23 survey. Note: The change in scale of the log depths.

VES 24 was conducted in close proximity with borehole SOD 06. The correlation of the resistivity log with borehole log is presented in Figure 17. The borehole log showed that the Cretaceous basement was intersected at 46m depth while the resistivity log observed it at 50m depth. The borehole log also showed that a calcrete layer which directly overlies the Cretaceous basement was encountered at 36m depth. The resistivity log observed layer 4 (which correlates with the calcrete in borehole log) at 30m depth. There is a moderately good correlation between the borehole log and the resistivity log for this location.

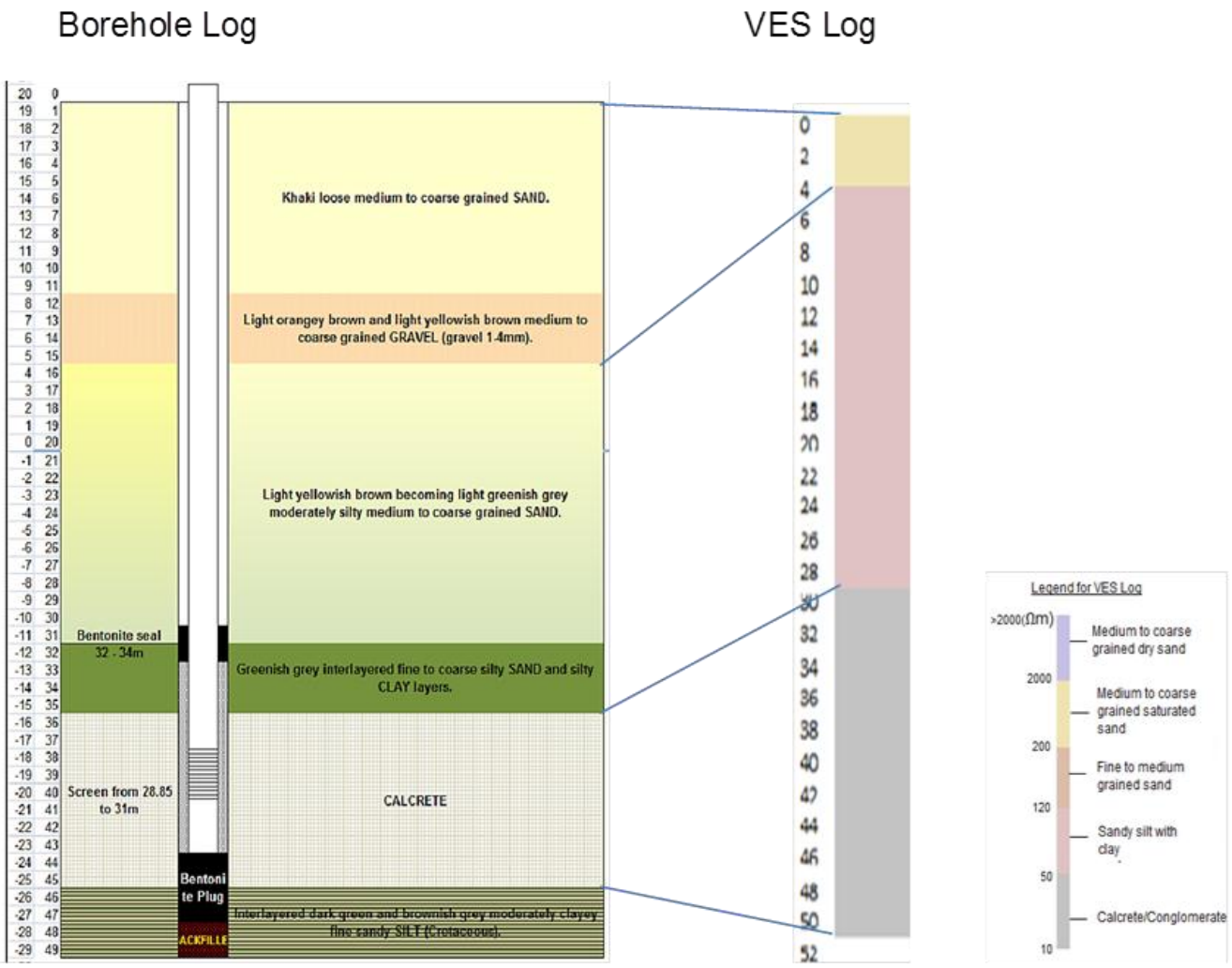

Figure 17: Correlation of borehole SOD 06 geology with VES 24 survey. Note: The change in scale of the log depths.

Figure 18 presents the correlation of the borehole log and VES logs for borehole SOD 03 and VES 25. Seven lithological changes can be observed on the borehole logs. These changes can be grouped into three geologic units. Fine to medium grained sand forms the top layer which is immediately underlain by a silty/clay section. The boundary between these two units was observed at 27m depth. Immediately underlying the silty/clay unit is the calcrete unit (deep aquifer). The boundary between the calcrete and the top two units was observed at 45m depth. The resistivity log for VES 25 showed three geoelectric layers. The top layer is separated from the immediately underlying layer at 31m depth. Layer 2 is separated from layer 3 at a depth of 54m. The top of the Cretaceous basement was observed at 86m depth. The 27m and 45m depths on the borehole log correlate with 31m and 54m depths on the resistivity log.

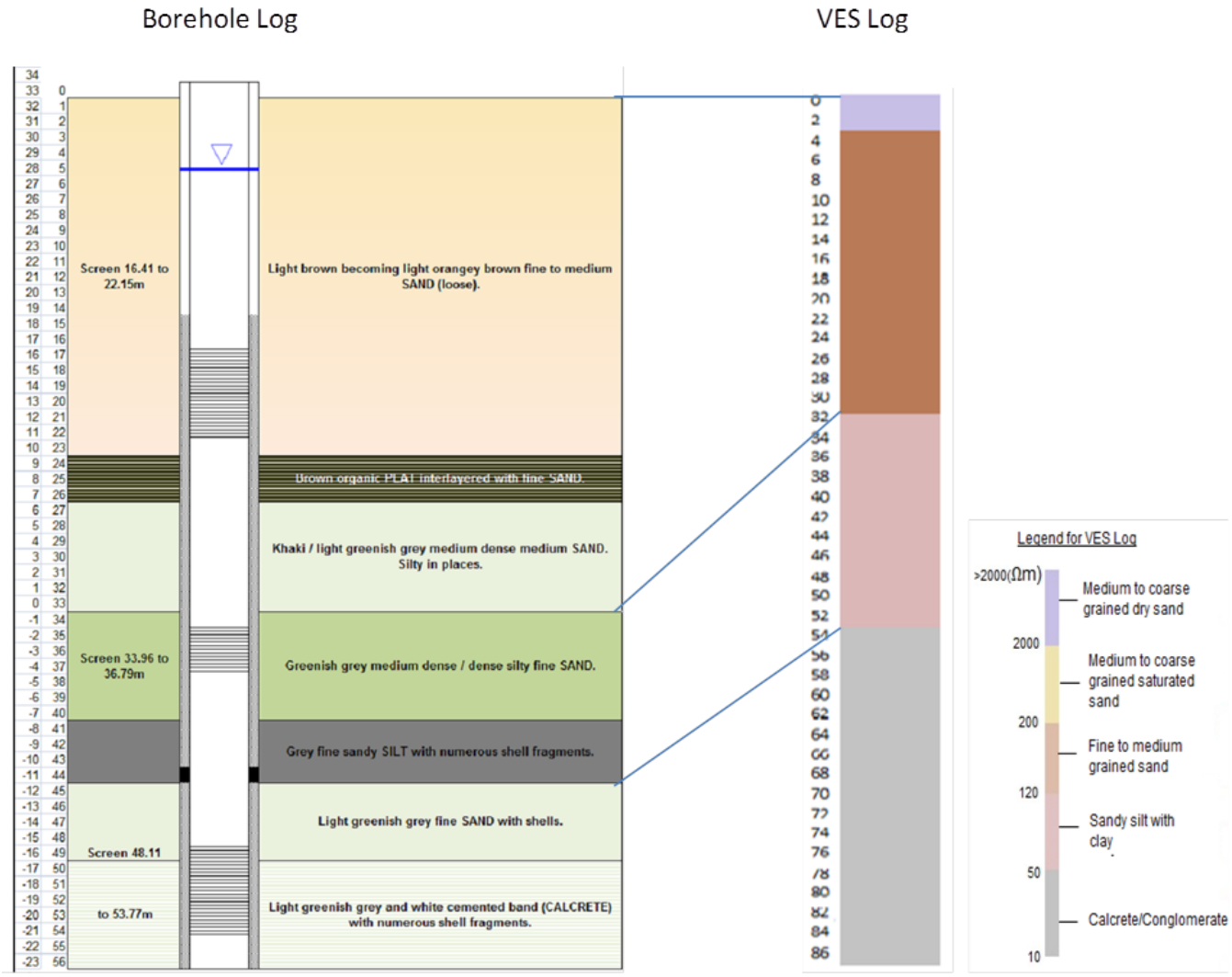

Figure 18: Correlation borehole SOD 03 geology and VES 25 survey. Note: The change in scale of the log depths.

In Figure 19, the lithological changes observed on the borehole log for SOD 08 can be grouped into two geologic units with a boundary at 13m depth. The resistivity log for VES 26 showed four geoelectric layers with boundaries at 5m, 15m, 48m and 88m (Figure 19). The 12m boundary on the borehole log coincides with the 15m boundary on the resistivity log.

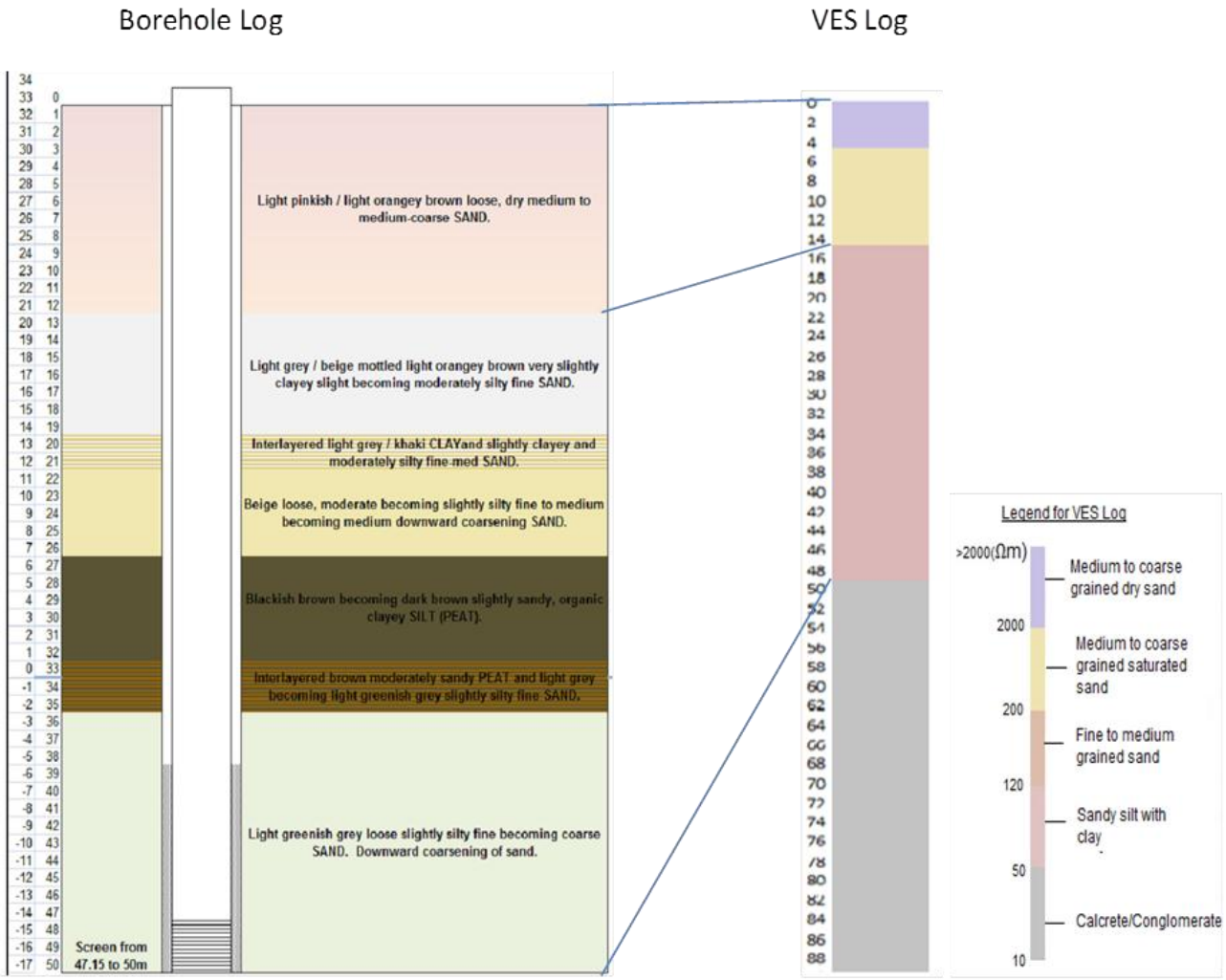

Figure 19: Correlation of borehole SOD 08 geology and VES 26 survey. Note: The change in scale of the log depths.

4.3 Interpretation of Results

4.3.1 Observed Geoelectric Layers

Correlating the resistivity logs with the borehole logs and with reference to Worthington (1978) and Reynolds (2000), apparent resistivity ranges were developed for the relevant formations making up the Cenozoic age sediments. Table 5 contains the apparent resistivity ranges, the corresponding lithology, the period of formation, and the hydrostratigraphy of the various formations detected by the VES. The resistivity ranges and lithological properties presented in Table 5 form the base model for interpretation of the VES data observed for this study.

Table 5: Apparent resistivity range for the Cenozoic sediments in study area

Resistivity (Ωm)	Lithology	Period	Formation	Hydrostratigraphy
>2000	Medium to coarse sand	Late Pleistocene	Kwambonambi	Dry sand
200 - 2000	Medium to coarse sand	Late Pleistocene	Kwambonambi	Shallow aquifer
120 - 200	Fine to medium sand	Pleistocene	Kosi Bay	Aquiclude
50 - 120	Silty sand with clay	Pleistocene	Kosi Bay	Aquiclude
10 - 50	Gravel/Conglomerate	Miocene - Pliocene	Uloa/Umkwelane	Semi confined aquifer

The lithologies are presented in column 2. The hydrostratigraphy describes the groundwater characteristics of each lithological unit.

The geoelectric, lithologic and hydrostratigraphic properties presented in Table 5 served as a model for the interpretation of VES result in the areas without boreholes. The geoelectric, lithologic and hydrostratigraphic properties of the geoelectric layers observed for the seven (7 No.) calibration VES surveys are presented in Tables 6 to 12. The tables for the other VES conducted where there are no boreholes are presented in Appendix 2. Each table defines the number of observed geoelectric layers for a particular VES location. The parameters shown in each table includes:-

a) Apparent resistivity values of each geoelectric layer
b) Thickness of each geoelectric layer
c) Depth of a layer

d) Lithology that is characteristic of each geoelectric unit
e) Period to which each geoelectric unit correlates within the Maputaland Formation
f) Formation that defines the geologic formation in the Maputaland Formation that corresponds to each geoelectric unit
g) Hydrostratigraphy that defines the aquifer classification of the geoelectric layers

Table 6: Summary of VES 12

Layer	Resistivity (Ωm)	Thickness (m)	Depth (m)	Lithology	Age	Formation	Hydrostratigraphy
1	7915	4	4	Medium to coarse grained sand	Pleistocene	Kwambonambi Formation	Dry sand
2	859	9	13	Medium to coarse grained sand	Pleistocene	Kwambonambi Formation	Unconfined aquifer
3	126	25	39	Fine to medium grained sand	Pleistocene	Kosi Bay Formation	Aquiclude
4	11	28	67	Calcrete/con-glomerate	Miocene to Pliocene	Uloa/Umkwelane Formations	Semi confined aquifer
5	3688	∞	∞	Siltstone	Cretaceous		Aquitard

Table 7: Summary of VES 21

Layer	Resistivity (Ωm)	Thickness (m)	Depth (m)	Lithology	Age	Formation	Hydrostratigraphy
1	8141	4	4	Medium to coarse grained sand	Pleistocene	Kwambonambi Formation	Dry sand
2	510	15	19	Medium to coarse grained sand	Pleistocene	Kwambonambi Formation	Unconfined aquifer
3	97	19	39	Sandy silt with clay	Pleistocene	Kosi Bay Formation	Aquiclude
4	21	59	97	Calcrete/con-glomerate	Miocene to Pliocene	Uloa/Umkwelane Formations	Semi confined aquifer
5	6285	∞	∞	Siltstone	Cretaceous		Aquitard

Table 8: Summary of VES 22

Layer	Resistivity (Ωm)	Thickness (m)	Depth (m)	Lithology	Age	Formation	Hydrostratigraphy
1	7777	5	5	Medium to coarse grained sand	Pleistocene	Kwambonambi Formation	Dry sand
2	386	13	19	Medium to coarse grained sand	Pleistocene	Kwambonambi Formation	Unconfined aquifer
3	82	34	52	Sandy silt with clay	Pleistocene	Kosi Bay Formation	Aquiclude
4	46	40	92	Calcrete/con-glomerate	Miocene to Pliocene	Uloa/Umkwelane Formations	Semi confined aquifer
5	9116	∞	∞	Siltstone	Cretaceous		Aquitard

Table 9: Summary of VES 23

Layer	Resistivity (Ωm)	Thickness (m)	Depth (m)	Lithology	Age	Formation	Hydrostratigraphy
1	6005	4	4	Medium to coarse grained sand	Pleistocene	Kwambonambi Formation	Dry sand
2	665	4	8	Medium to coarse grained sand	Pleistocene	Kwambonambi Formation	Unconfined aquifer
3	85	43	50	Sandy silt with clay	Pleistocene	Kosi Bay Formation	Aquiclude
4	39	28	78	Calcrete/con-glomerate	Miocene to Pliocene	Uloa/Umkwelane Formations	Semi confined aquifer
5	1060	∞	∞	siltstone	Cretaceous		Aquitard

Table 10: Summary of VES 24

Layer	Resistivity (Ωm)	Thickness (m)	Depth (m)	Lithology	Age	Formation	Hydrostratigraphy
1	220	4	4	Medium to coarse grained sand	Pleistocene	Kwambonambi Formation	Unconfined aquifer
2	94	24	28	Sandy silt with clay	Pleistocene	Kosi Bay Formation	Aquiclude
3	13	23	50	Calcrete/con-glomerate	Miocene to Pliocene	Uloa/Umkwelane Formations	Semi confined aquifer
4	1285	∞	∞	Siltstone	Cretaceous		Aquitard

Table 11: Summary of VES 26

Layer	Resistivity (Ωm)	Thickness (m)	Depth (m)	Lithology	Age	Formation	Hydrostratigraphy
1	4188	4	4	Medium to coarse grained sand	Pleistocene	Kwambonambi Formation	Dry sand
2	1461	11	15	Medium to coarse grained sand	Pleistocene	Kwambonambi Formation	Unconfined aquifer
3	76	33	48	Sandy silt with clay	Pleistocene	Kosi Bay Formation	Aquiclude
4	37	40	88	Calcrete/con-glomerate	Miocene to Pliocene	Uloa/Umkwelane Formations	Semi confined aquifer
5	3345	∞	∞	Siltstone	Cretaceous		Aquitard

Table 12: Summary of VES 29

Layer	Resistivity (Ωm)	Thickness (m)	Depth (m)	Lithology	Age	Formation	Hydrostratigraphy
1	7035	3	3	Medium to coarse grained sand	Pleistocene	Kwambonambi Formation	Dry sand
2	442	3	6	Medium to coarse grained sand	Pleistocene	Kwambonambi Formation	Unconfined aquifer
3	94	49	55	Sandy silt with clay	Pleistocene	Kosi Bay Formation	Aquiclude
4	38	53	108	Calcrete/con-glomerate	Miocene to Pliocene	Uloa/Umkwelane Formations	Semi confined aquifer
5	1526	∞	∞	Siltstone	Cretaceous		Aquitard

4.3.2 Western Transect

The western transect corresponds to a roughly north to south trending transect running through the DWA monitoring boreholes on the western side of Lake Mgobolezeni. VES logs at the borehole positions on this transect, as well as the 1km nodes in between these monitoring boreholes, were plotted and presented in Figure 20. Refer to Figure 13 for the locations of each VES point along the western transect. This was for the purpose of comparing the variations of the geology along the western transect. The VES logs presented in Figure 20 were interpolated to generate a cross section showing the extent of the geoelectric layers along the western transect (Refer to Figure 21).

It can be visualized in Figure 21 that layer 1 (top soil) and layer 2 have higher relative elevation to average mean sea level in the north than in the south. This is because the inland dunes are more prominent in the northern part of the study area than in the southern part. The layers 3 and 4 also have higher relative elevation to average mean sea level in the north than in the south. This suggested that there was more potential for erosion during transgressive conditions in the south after the deposition of layer 4 and also after the deposition of layer 3. The inferred

water table in layer 2 (shallow aquifer) indicates the possible trend of a water table along the western transect.

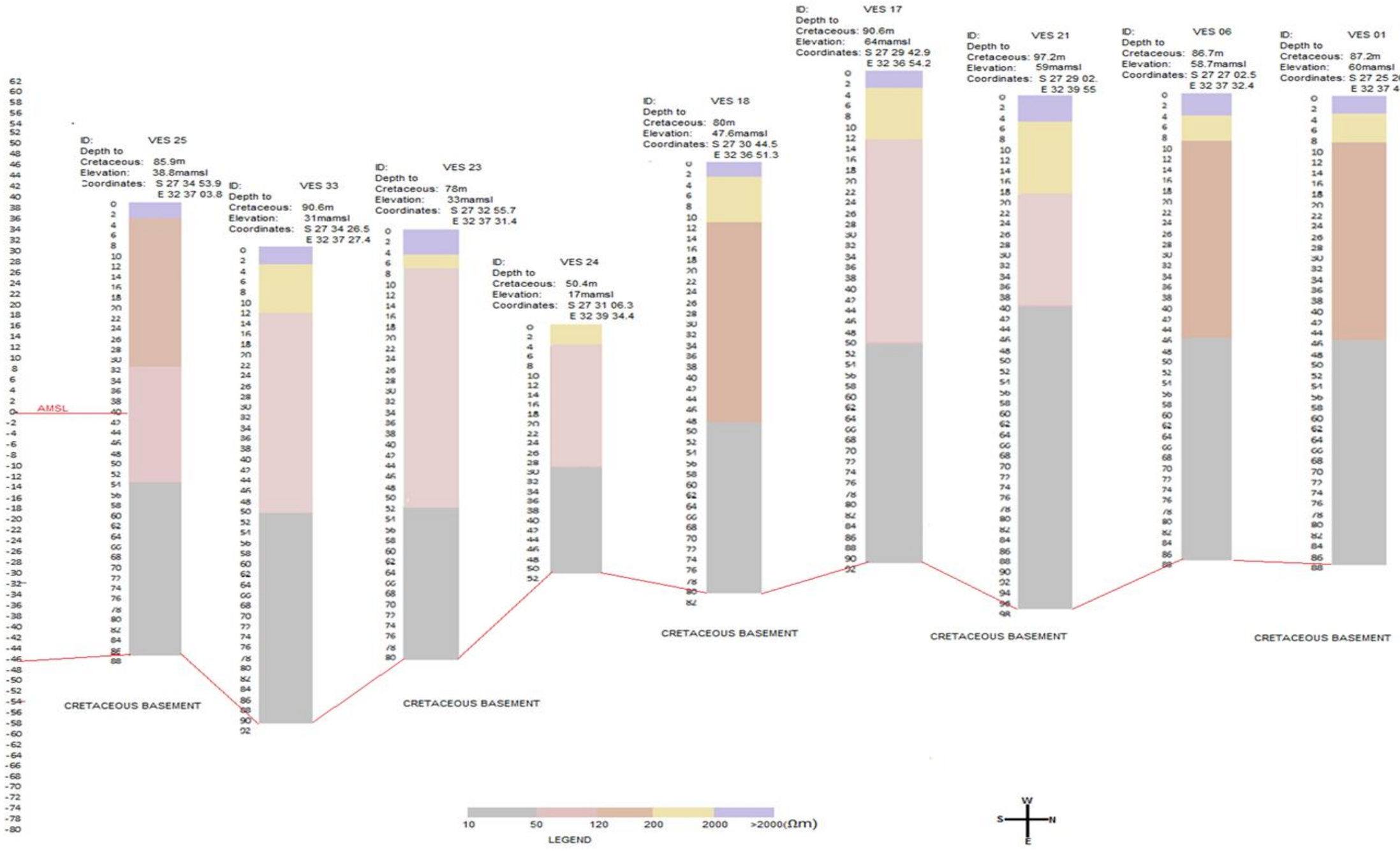

Figure 20: Resistivity logs along western transect

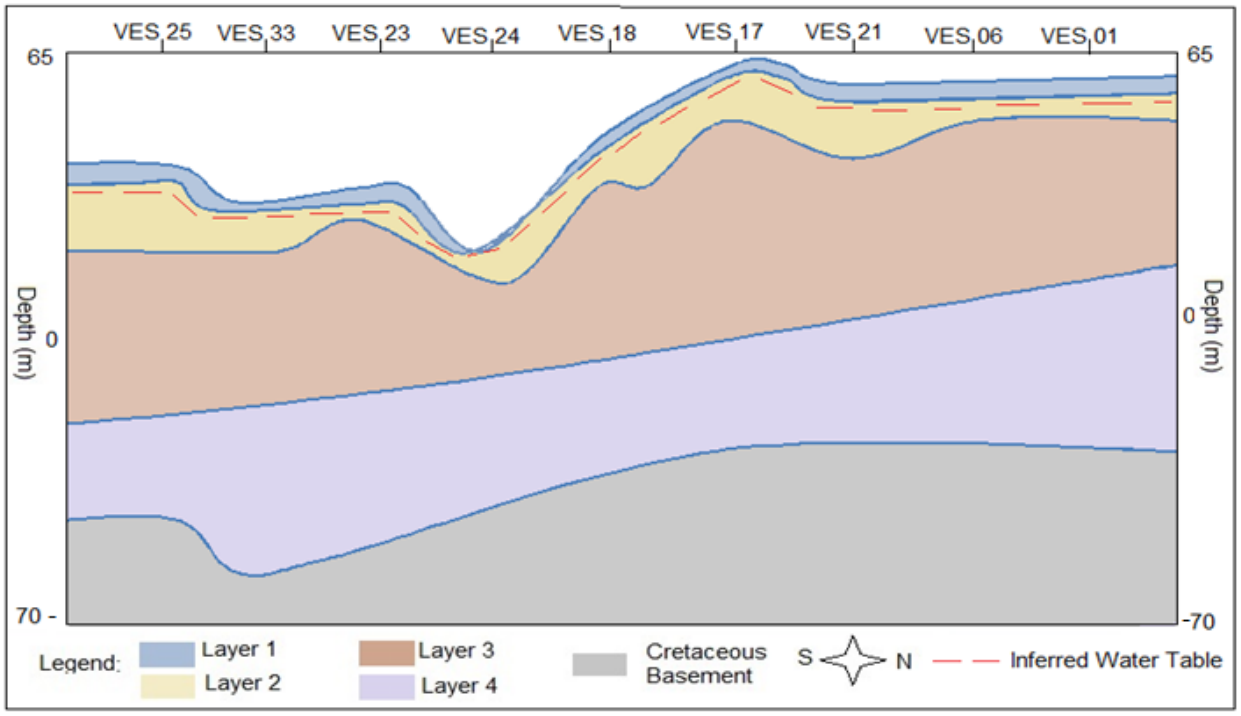

Figure 21: Cross section of the western transect

4.3.3 Eastern Transect

The eastern transect similarly corresponds to a roughly north - south trending transect trending through the DWA monitoring boreholes on the eastern side of Lake Mgobolezeni. The VES logs (showing geoelectric layers) and coordinates of each VES point were plotted together and presented in Figure 22. Refer also to Figure 13 for VES points along the eastern transect. The VES logs along the eastern transect were interpolated to develop a cross section for the geoelectric layers in the eastern transect (Refer to Figure 23). This was for the purpose of comparing the variation of the geology along the eastern transect.

The relative elevations of the geoelectric layers to average mean sea level do not vary much from north to south along the eastern transect. This is because the topography along the eastern transect does not vary much except at VES 12 which was conducted in an inter-dune depression. The inferred water table indicates the trend of water table in the shallow aquifer along the eastern transect (Refer to Figure 23).

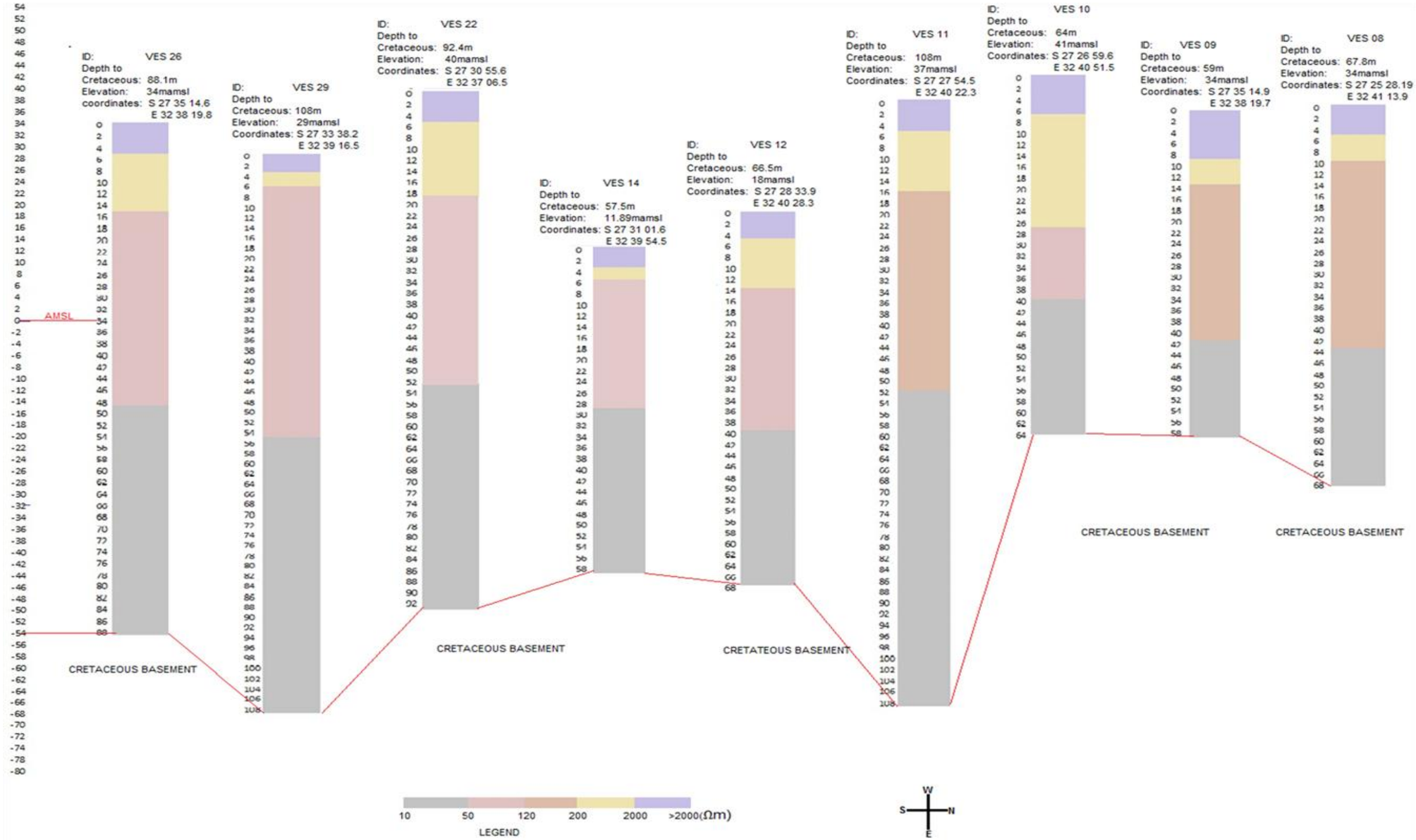

Figure 22: Resistivity logs along eastern transect

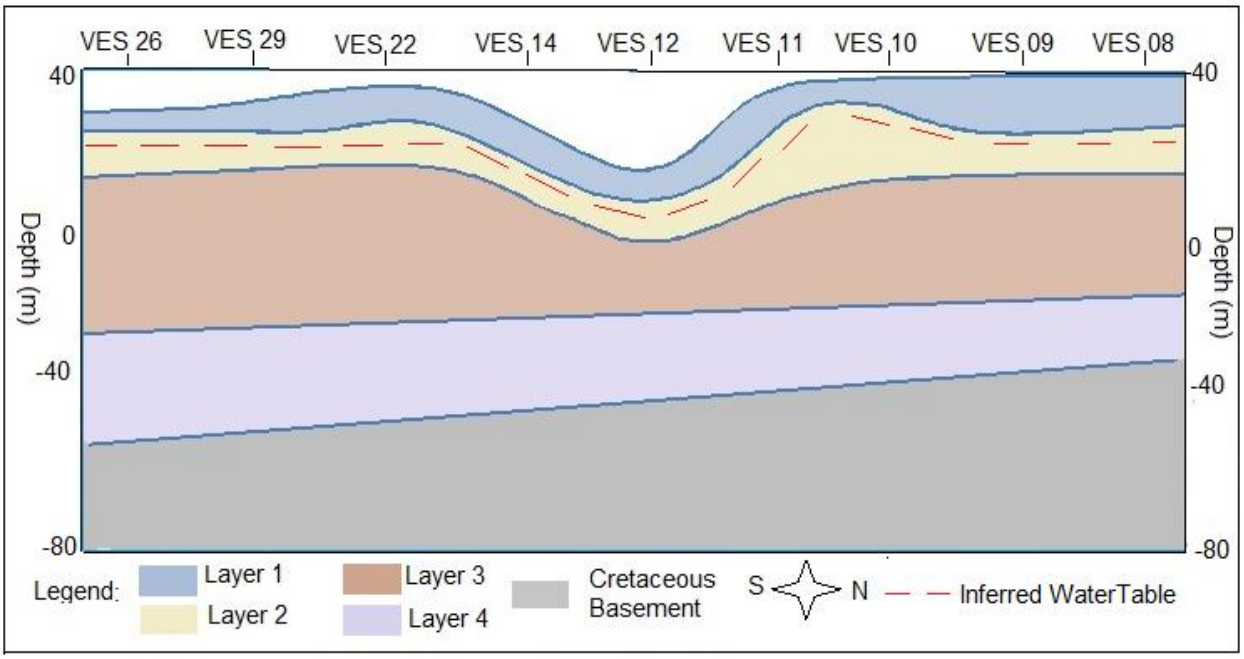

Figure 23: Cross section of the eastern transect

4.3.4 Topography of the Observed Geoelectric Layers

The geoelectric models presented in Tables 6 to 12 showed that layer 1 corresponds to the windblown dry fine to medium cover sand; layer 2 corresponds to the saturated medium sand hosting the shallow aquifer (Kwambonambi Formation); layer 3 corresponds to the moderately silty to silty-fine sand with clay lenses with low transmissivity of the Kosi Bay Formation; and layer 4 corresponds to the medium to coarse sand overlying calcrete of high transmissivity of the Uloa/Umkwelane Formations.

This conceptual model can be used to delineate a contoured map of the interfaces between layers. Figure 24 shows the contoured surfaces of the layers lettered A – D representing the base of layers 1 to 4, derived from the VES points. The contour values at any point indicate the depth from surface at such point relative to average mean sea level. The top layer is not included because it is relatively thin throughout the surveyed area. The bottom of a layer corresponds to the surface of the immediately underlying layer.

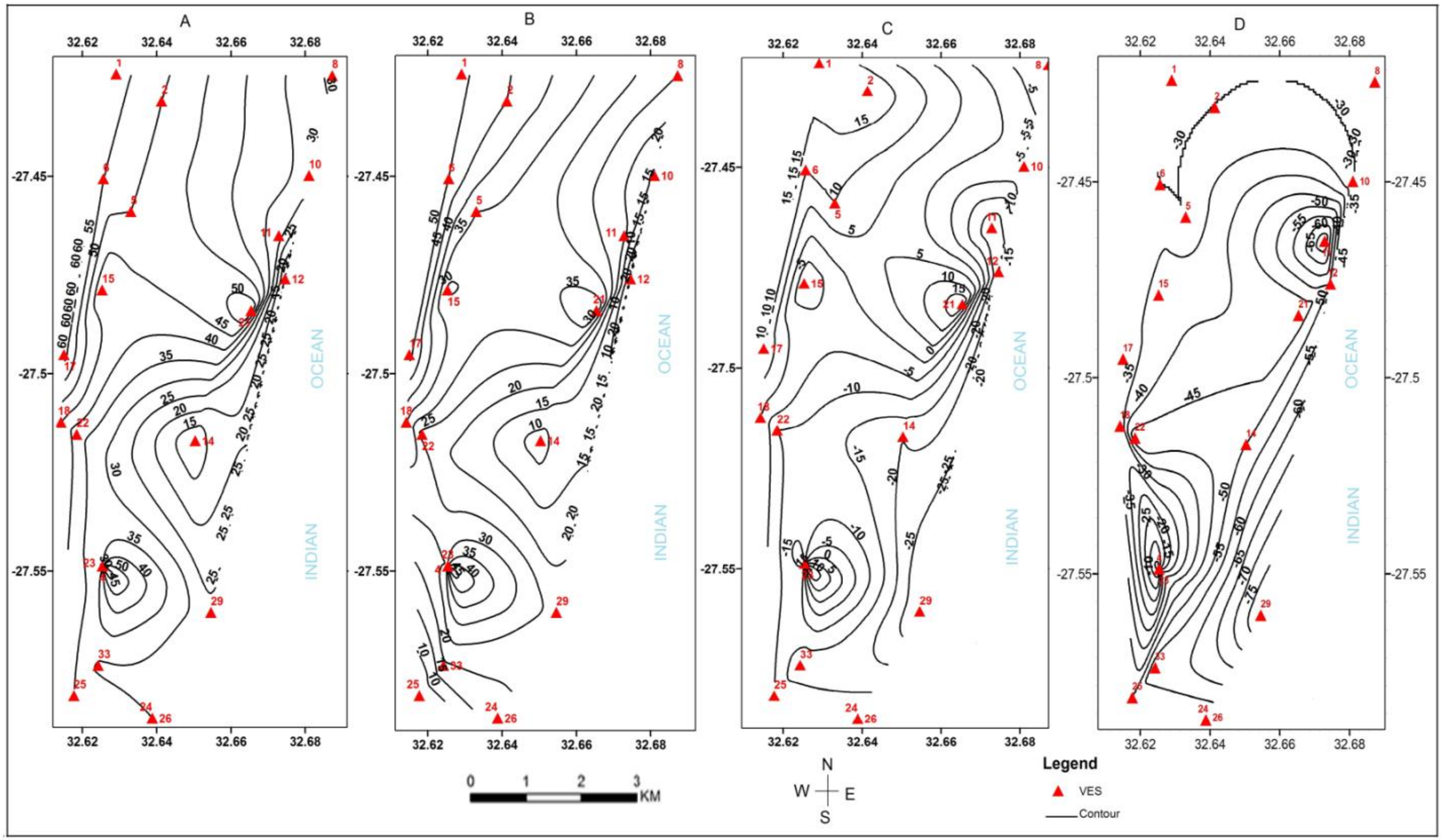

Figure 24: Contoured geoelectric facies and VES points (A = Layer 2; B = Layer 3; C = Layer 4 and D = Cretaceous Basement

It can be observed from Figure 24 that the geoelectric layers are deeper in the eastern transect than in the western transect of the study area, which corresponds well with the inferred geological formations of the Maputaland Coastal Plain dipping eastwards or towards the ocean (Watkeys *et al*., 1993). It can be inferred from Figure 24 that:-

- The top of geoelectric layer 2 has average surface elevations of 60m above mean sea level (amsl) in the western side and 20m (amsl) in the eastern side.
- The top of layer 3 has average surface elevations of 50m (amsl) in the western side and 15m (amsl) in the eastern side.
- The top of layer 4 has average surface elevations of 15m (amsl) in the western side and 20m below average mean sea level (bmsl).
- The top of the Cretaceous layer has average surface elevations of 35m (bmsl) in the western side and 60m (bmsl) in the eastern side.

4.4 Deeper Aquifer

The transmissivity values observed from pumping tests conducted on the deeper aquifer (Uloa/Umkwelane Formations) using Cooper Jacob's method were obtained from DWA (2012). The pump tests were conducted on 6 of the 7 monitoring boreholes that were used for VES calibration. Traverse resistance (product of layer thickness and layer resistivity) of layer 4 was computed for the 6 VES points close to the 6 calibration boreholes. A linear regression was evident between the transmissivity of the deeper aquifer for the 6 boreholes and the traverse resistance of the 6 VES points. A negative but strong correlation (R^2 = 0.99) was observed between transmissivity and traverse resistance (Figure 25). The linear relationship developed for transmissivity and traverse resistance was integrated into equation (3.25) to compute transmissivity in areas without borehole coverage.

The hydraulic conductivity of the deeper aquifer was also investigated as a ratio between the modelled transmissivity and aquifer thickness obtained from the VES survey.

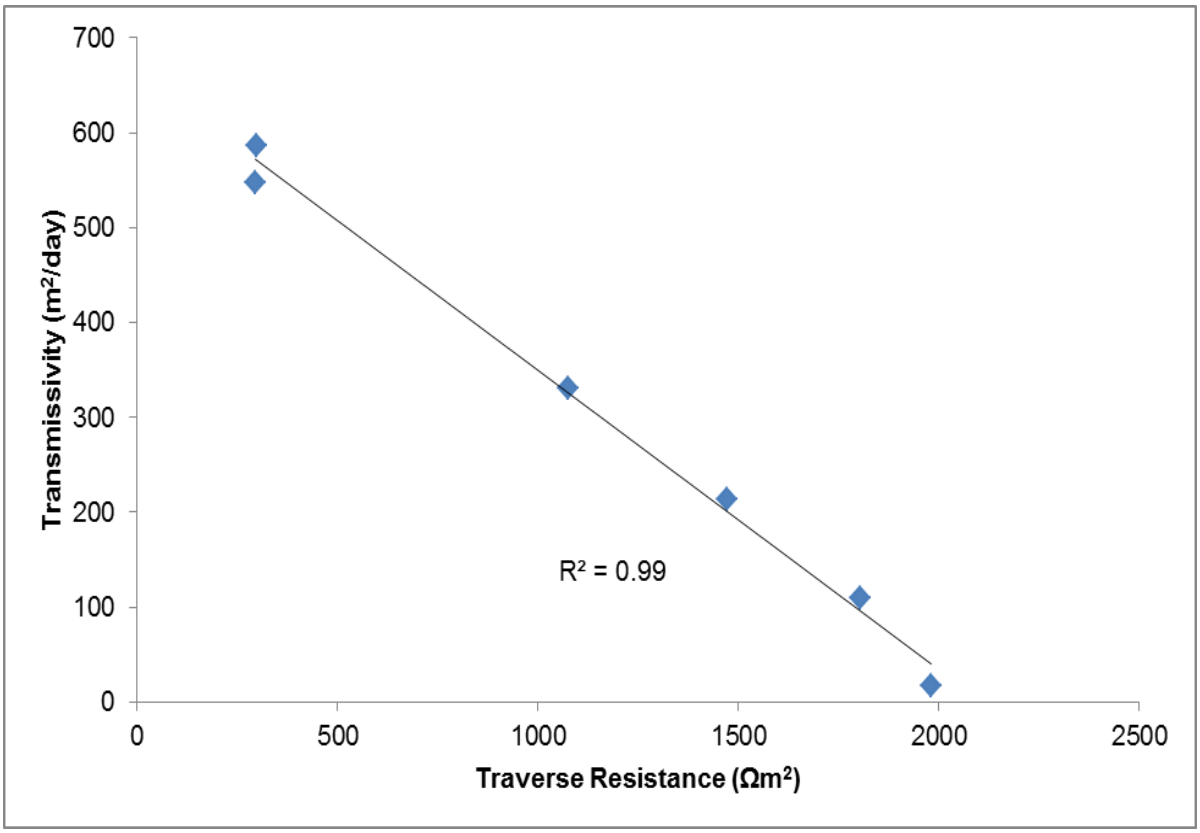

Figure 25: Transmissivity and traverse resistance at five locations

The measured transmissivity obtained from pumping tests and modelled transmissivity computed using VES data are presented in Table 13. The modelled transmissivity was calculated using the relationship established between the observed transmissivity and traverse resistance. There is correspondence between the measured transmissivity and the modelled transmissivity. There is also a close relation between the hydraulic conductivity measured from pumping tests and hydraulic conductivity computed from VES data using equation (3.19). The measured transmissivity observed from pumping tests was compared with the calculated transmissivity obtained using VES data. The linear regression between the measured transmissivity and the modelled or computed transmissivity exhibited a very good correlation of $R^2 = 0.99$ (Figure 26).

Table 13: Modelled transmissivity and hydraulic conductivity

Location	Resistivity (Ωm)	Thickness (m)	Traverse Resistance (Ωm²)	Measured Transmissivity (m²/day)	Modelled Transmissivity (m²/day)	Measured Hydraulic Conductivity (m/day)	Modelled hydraulic conductivity (m/day)
1	14	43	588	-	479	-	11
6	14	42	577	-	482	-	12
8	48	25	1203	-	285	-	12
9	20	18	352	-	553	-	32
10	28	25	719	-	438	-	17
11	25	56	1414	-	219	-	4
12	11	28	294	547	571	35	21
13	12	24	289	-	573	-	24
14	21	29	607	-	473	-	16
17	43	40	1741	-	116	-	3
18	20	33	662	-	456	-	14
21	21	59	1233	-	276	-	5
22	45	40	1805	110	96	16	2
23	39	28	1074	331	326	28	12
24	13	23	298	587	570	24	25
25	28	34	933	-	370	-	11
26	37	40	1472	213	200	9	5
29	38	53	1979	17	41	-	1
30	13	28	302	-	569	-	21
33	43	40	1741	-	116	-	3

Table 13 shows the following parameters:-

a) Location represents each VES point.
b) The resistivity column represents the measured apparent resistivity values of layer 4 (deeper aquifer) at each location.
c) The thickness shows the measured geoelectric thickness of layer 4 at each VES location.
d) The traverse resistance in (Ωm^2) indiates the product of apparent resistivity and thickness of layer 4 at each VES location
e) Measured transmissivity is the transmissivity obtained from pumping tests for the six boreholes in close proximity to the corresponding VES locations.

f) The modelled transmissivity refers to the transmissivity computed using the modelled transmissivity and traverse resistance.

g) Measured hydraulic conductivity is the hydraulic conductivity obtained from pumping tests for the six boreholes.

h) The modelled hydraulic conductivity was computed from modelled transmissivity and thickness obtained from VES.

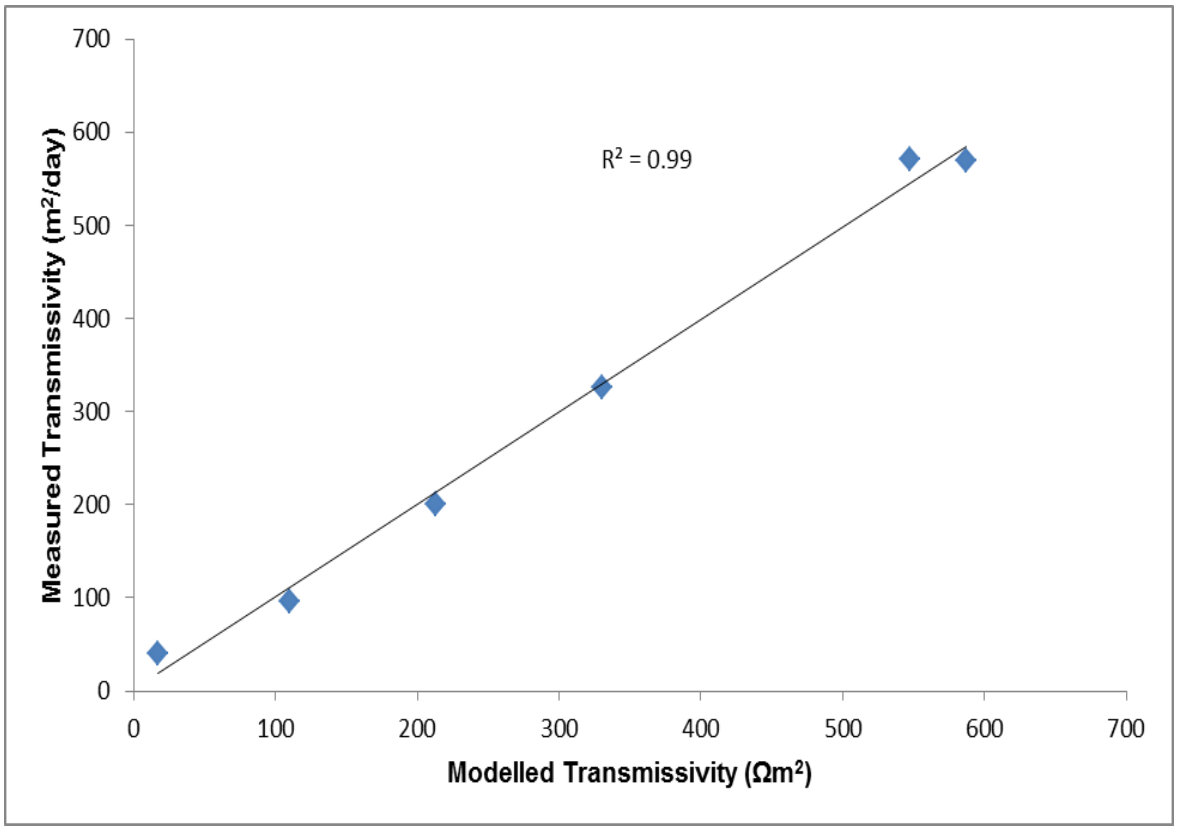

Figure 26: Observed transmissivity compared with computed transmissivity for six locations.

CHAPTER FIVE

5 DISCUSSION

5.1 Introduction

The results presented in Chapter 4 were obtained from VES conducted at 20 locations in the study area. The correlation of interpreted geoelectric layers derived from VES results together with borehole logs, combined with the literature, was used to assign resistivity ranges to the various lithological units in the study area. The DWS monitoring boreholes' logs were used in developing the conceptual model for interpretation of the VES data.

The interpretation of VES data was made by inputting the field observations into the IPI2Win software package. The inversion method (conversion of geoelectric plots into distinct geoelectric layers) was performed to generate geoelectric models for each VES location. The measured or observed curve for each VES point was adjusted (iterated) to fit the modelled curve (Refer to Figure 12). When a best fit curve was obtained, geoelectric properties (apparent resistivity, thickness and depth) were derived for each layer.

The inversion and iteration processes were initially performed for VES locations in close proximity to the DWS monitoring boreholes in the study area (Figures 14 to Figure 19) to calibrate the results in accordance with observed lithological changes. The resistivity ranges that were established for geoelectric layers and lithological properties from boreholes' logs were integrated to develop an improved model for interpretation and extrapolation of lithological layers for VES data in areas without boreholes.

5.2 Discussion of the Results

VES results can provide information on the nature and depth of subsurface lithological units. This may not always be accurate due to lateral heterogeneous variation and difficulty in defining the vertical geoelectric properties of two adjacent layers according to the literature discussed previously (Chapter 2) two major factors potentially influence the electrical resistivity of the geological units of the study area, that being the clay and silt content, and degree of saturation of the units.

The VES results showed apparent resistivity values decreasing continuously once saturated, from the top layer to the bottom layer as current transited through the Cenozoic Formations. This was followed by a rise in apparent resistivity values as current penetrated the Cretaceous layer. The results showed a 5 layer VES curve which can be described as follows:-

a) Apparent resistivity of layer 1 is greater than the apparent resistivity of layer 2

b) Apparent resistivity of layer 2 is greater than the apparent resistivity of layer 3

c) Apparent resistivity of layer 3 is greater than the apparent resistivity of layer 4

d) Apparent resistivity of layer 4 is lower than the apparent resistivity of layer 5

$\rho1 > \rho2 > \rho3 > \rho4 << \rho5$ (where $\rho1$ = apparent resistivity of top layer, $\rho2$ = apparent resistivity of layer 2, $\rho3$ = apparent resistivity of layer 3, apparent resistivity of layer 4, $\rho5$ = apparent resistivity of layer 5 which is the Cretaceous unit).

The borehole logs (Jeffares and Green, 2012) showed that three hydrostratigraphic sections exist in the study area. The hydrostratigraphic sections were correlated with the 5 layers observed from VES results (Refer to Tables 6 to 12). The correlation of the hydrostratigraphic units and geoelectric layers are as follows:

a) Geoelectric layers 1 and 2 correlate stratigraphically with the high transmissivity Kwambonambi Formation (Shallow aquifer)

b) Geoelectric layer 3 correlates stratigraphically with the low transmissivity Kosi Bay Formation

c) Geoelectric layer 4 which correlates stratigraphically with the higher transmissivity Uloa/Umkwelane Formations (Deeper aquifer).

5.2.1 Geoelectric Layer 1

The apparent resistivity values measured for layer 1 (top layer) at all VES locations are much higher than the apparent resistivity values measured for the underlying layers. As discussed by Niwas and Celik (2012) the electrical resistivity of ground layers decreases as the amount of water saturating the ground layers increases. This condition is only possible if the electrical resistivity of the ground layer is higher in a dry state than when saturated or filled with water. Therefore, the very high apparent resistivity values (>2000Ωm) recorded for layer 1 can be best explained as a combination of dryness and grain size.

The resistivity values observed for layer 1 were in accordance with the resistivity values reported for dry sand in Worthington (1978); Van Zijl (1985) and Reynolds (2000). High resistivity values observed for layer 1 can be attributed to coarseness of the sand grains because the surface conductance of sediments decreases as the grain sizes increase. Electrical resistivity increases as surface conductance decreases and it results in high apparent resistivity values that can be observed for sediments. Therefore medium to coarse nature of the cover sand (also reported in Jeffares and Green, 2012) was considered a contributing factor that caused poor electric conductivity and therefore resulted in high apparent resistivity values for layer 1.

The drilling results and VES results showed that the top layer is thin throughout the surveyed area with an average thickness of approximately 4m. It was considered to be part of the Late Pleistocene Kwambonambi Formation. The apparent resistivity values of the layer 1 are higher in the northern part of the study area compared with the southern part (Figure 27) suggesting more potential infiltration of rain in the western part.

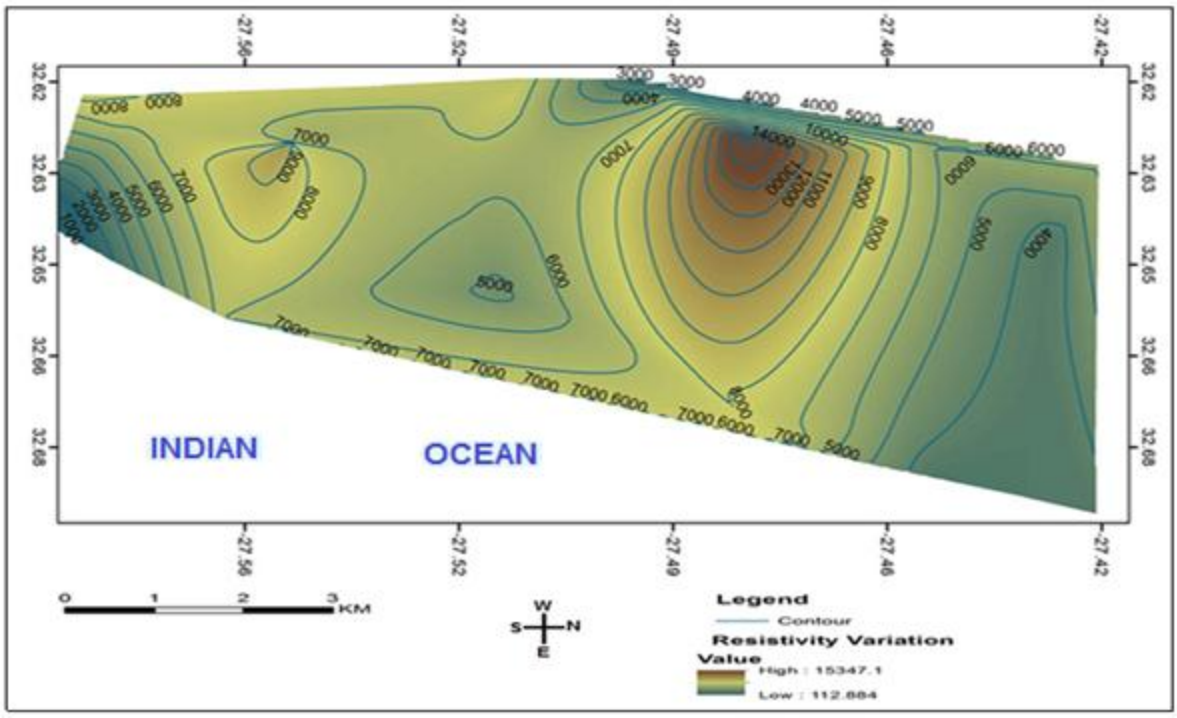

Figure 27: Average apparent resistivity variation over the layer 1

5.2.2 Geoelectric Layer 2

Layer 2 immediately underlies layer 1 and exhibited a wide apparent resistivity range of 200 - 2000Ωm (Figure 28). The apparent resistivity values observed for layer 2 at all the VES locations were much lower than the values observed for layer 1 for each respective VES. It was observed from borehole logs that layer 1 and layer 2 possess the same lithological properties of medium to coarse grained sand. Background resistivity (the resistivity of unsaturated sand) was deemed the major contributing factor for differentiating layer 2 from layer 1.

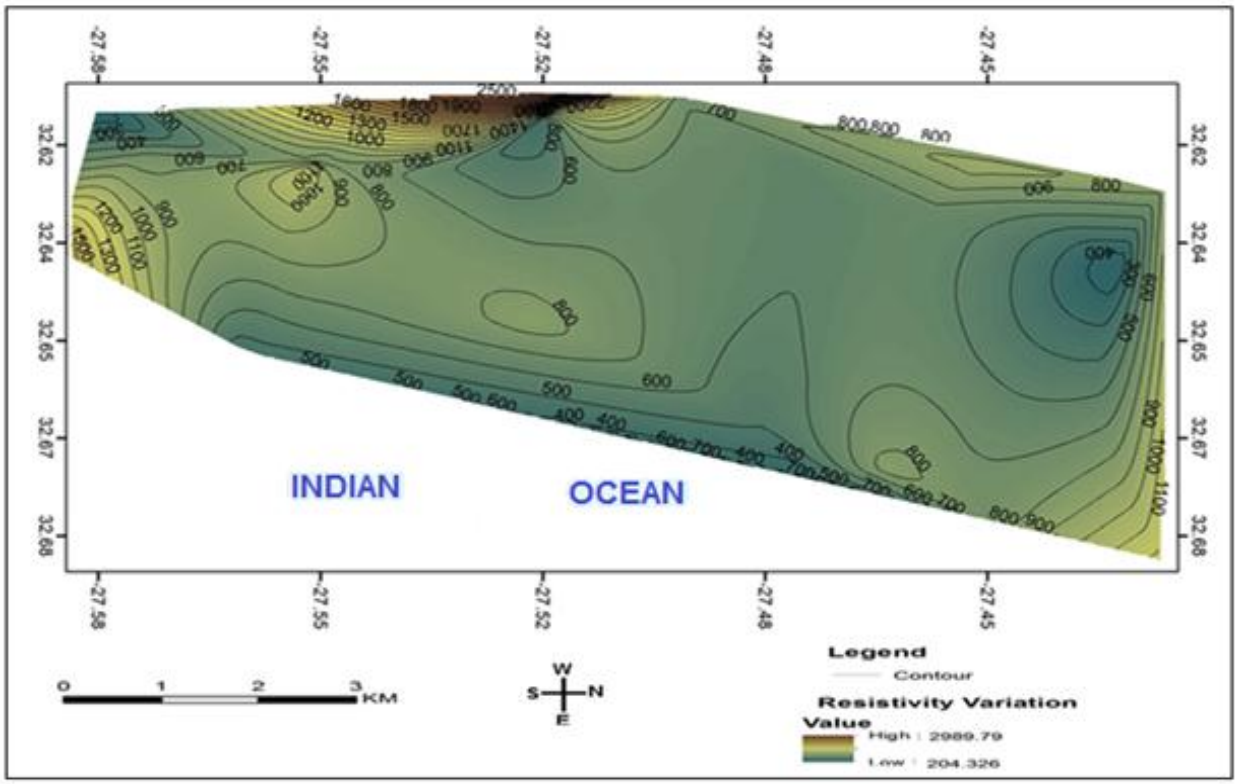

Figure 28: Average apparent Resistivity Variation over layer 2

DWA (2012) indicated that the shallow aquifer exhibited high productivity at boreholes SOD 02, SOD 03, and SOD 04. The VES 22, 25 and 23 which were conducted in close proximity of SOD 02, 03 and 04 respectively indicated that layer 2 (which correlates with the shallow aquifer) exhibited apparent resistivity values of 386Ωm for VES 22, 189Ωm for VES 25 and 665Ωm for VES 23. These apparent resistivity values were in accordance with the values reported for porous and permeable sand filled with water (Van Zijl, 1985 and Reynolds, 2000). The depth of layer 2, derived from VES results, ranged from 6m – 27m while the depth of the corresponding shallow aquifer in Jeffares and Green (2012) ranged from 5m – 24m. An average thickness of 7.9m (6.9m standard deviation) was observed for layer 2 from all the VES results.

With reference to Worthington, (1978); Van Zijl, (1985); Reynolds, (2000); Niwas and Celik, (2012) and correlation of VES results with borehole logs, it was observed that apparent resistivity values of an aquifer can be greater than 500Ωm where the saturation of the aquifer is low. The apparent resistivity values of the same aquifer can be lower than 500Ωm when water content of the aquifer is high. The high apparent resistivity values observed for layer 2 at some

VES locations in the study area suggests low groundwater availability. Apparent resistivity values are low around the centre of the study area suggesting higher groundwater availability around this region (Refer to Figure 28).

According to Kelbe (2014), there is continuous groundwater movement or interaction between the shallow aquifer (Kwambonambi Formation) and the immediately underlying low transmissive Kosi Bay Formation. The presence of groundwater in the shallow aquifer is significantly influenced by the lithology of the Kosi Bay Formation. Groundwater moves much slower in the Kosi Bay Formation creating a partially confining layer over the underlying units. The groundwater saturating the shallow aquifer slowly infiltrates into the Kosi Bay Formation and ultimately into the Umkwelane and Uloa Formation below. The infiltration of groundwater into and through the Kosi Bay Formation is slowed where silt and clay are more apparent. Therefore groundwater cannot drain rapidly from the shallow aquifer into the Uloa Formation creating a difference in the peizometric head.

5.2.3 Geoelectric Layer 3

Layer 3 was sub-divided into two units based on the variation of apparent resistivity values primarily attributed to grain size variations. The first unit showed apparent resistivity values of 120 to 200Ωm. This was considered to be composed of medium to fine sand and silt. It forms part of the low transmissivity Pleistocene Kosi Bay Formation. The second unit in this layer showed resistivity values of 50 to 120Ωm, and is composed of silty sand with clay. The finer particles of this unit caused higher conductivity than the overlying unit. It also forms part of the low transmissivity Pleistocene Kosi Bay Formations. The low apparent resistivity values observed for layer 3 resulted from medium to fine sand, silt and clay which are more conductive than the coarse to medium sand making up the overlying layers 1 and 2.

The amount of clay and silt present influenced the hydraulic and geoelectric properties of layer 3. Borehole lithological logs and pumping test results (Jeffares and Green, 2012) showed that increasing clay and silt content reduced the transmissivity of the Kosi Bay Formation such that it forms a confining or semi-confining layer between the shallow (Kwambonambi Formation) and the deep aquifer (Uloa/Umkwelane Formations). The thickness of layer 3 varies in the surveyed area as summarized in Table 3 and Table 4 while Figure 29 shows variation of its apparent

resistivity. It has an average thickness of 32m (7.5m standard deviation) in the western side and 30m (8.5m standard deviation) in the eastern side.

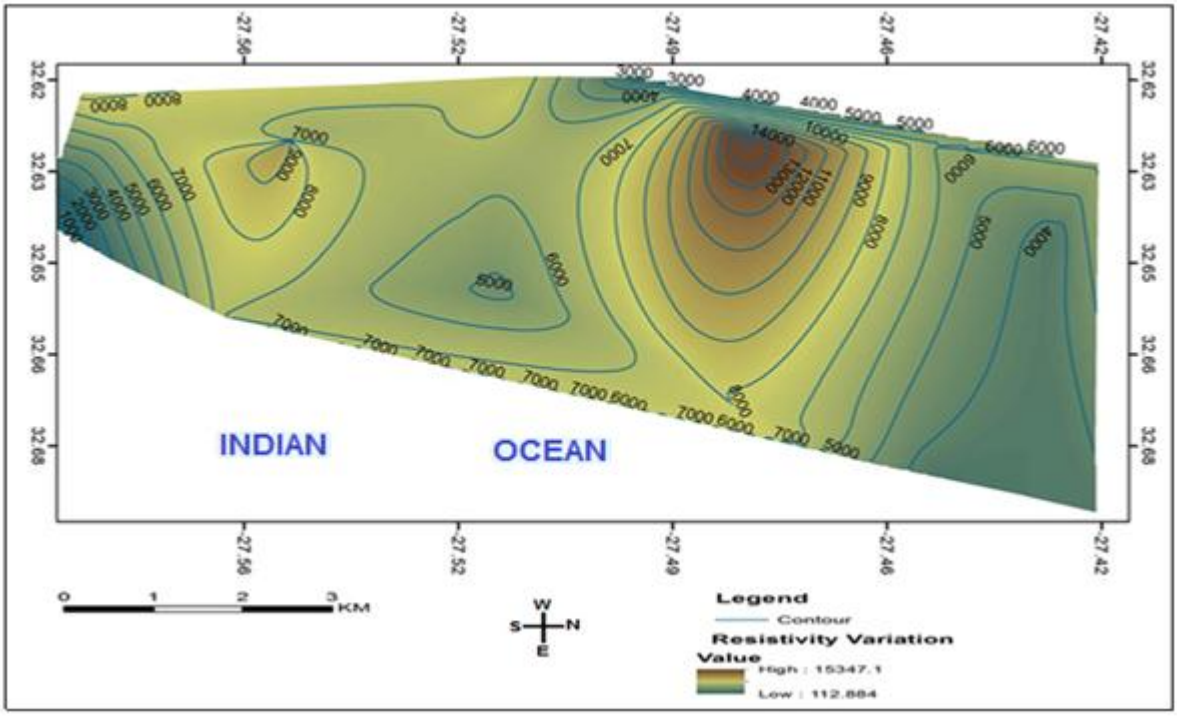

Figure 29: Average apparent resistivity variation over layer 3

5.2.4 Geoelectric Layer 4

The apparent resistivity values observed for layer 4 ranged between 10 and 50Ωm (Figure 30). The VES results showed that layer 4 occurs throughout the study area. The correlation of VES logs with borehole logs indicated that layer 4 corresponds to the deeper aquifers of the Uloa and Umkwelane Formations. The Uloa/Umkwelane Formations are decalcified arenaceous deposits with hydraulic properties that are controlled by the lithology of the sediments. Electrical properties of these essentially clay-free sediments are controlled by the fluid saturating the pores (Refer to literature review in Chapter 2). Therefore, the apparent resistivity values observed for layer 4 were considered related more to water than grain size.

The Uloa and Umkwelane Formations have good groundwater potentials (high porosity and permeability). The depths of the Uloa and Umkwelane formations as indicated in the borehole logs were compared with the depths of layer 4 obtained from the VES results. The depth of

layer 4 in both boreholes and VES logs conducted in close proximity to the boreholes are summarized in Table 14.

Table 14: The comparison of the VES & BH logs for the upper surface of Layer 4

Locations		Depth (m)		Elevation (m)	
VES	BH	VES	BH	VES	BH
12	SOD 05	39	36	-19	-8
22	SOD 02	52	52	-12	-13
23	SOD 04	51	48	-17	-15
24	SOD 06	28	35	-10	-15
26	SOD 08	48	50	-14	-18
29	SOD 07	55	43	-26	-12

The depth to the top of layer 4 observed from VES results is the depth to the top of the deep aquifer (Uloa/Umkwelane Formations) inferred from the borehole logs. The negative sign indicates that the top of the geoelectric layer 4 and the top of the deep aquifer are below mean sea level at these locations. The VES results showed that the top of layer 4 was below average mean sea level at some locations (Refer to Figure 21 and Figure 23). Layer 4 has an average thickness of 35m (12m standard deviation) for the entire VES survey.

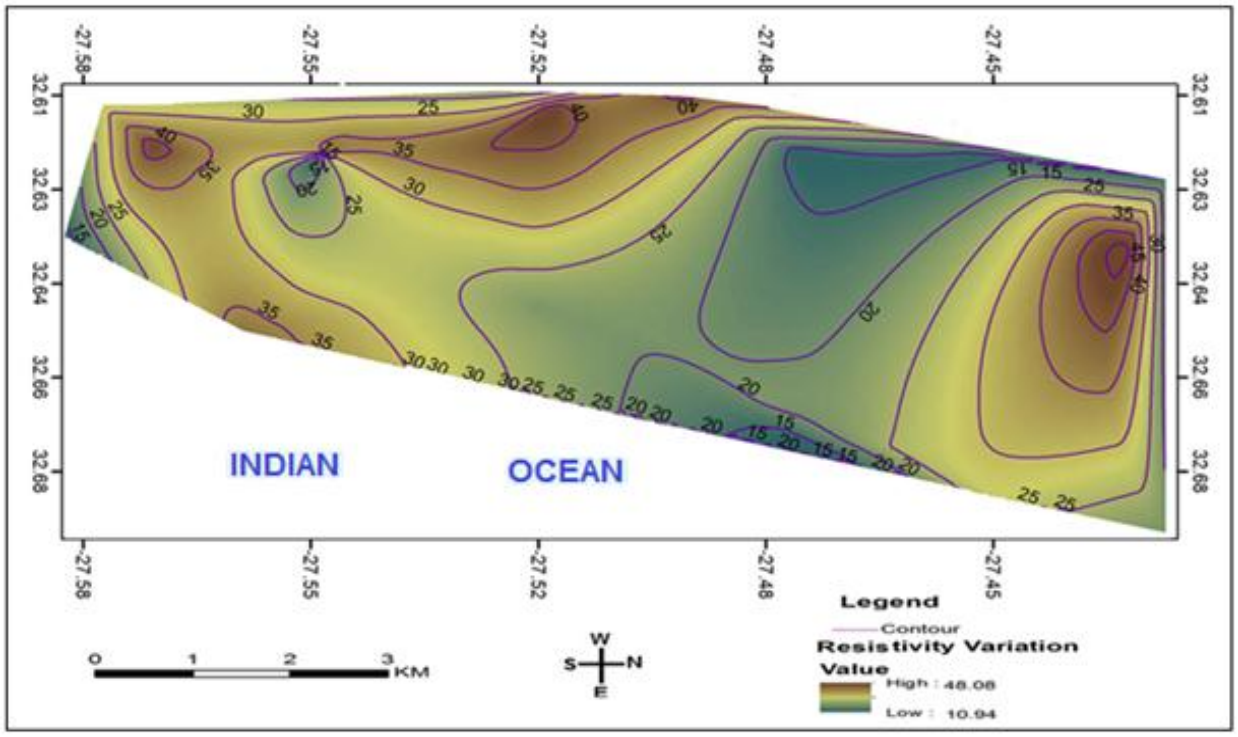

Figure 30: Average apparent Resistivity Variation over layer 4

5.2.5 Transmissivity of Layer 4 (Deep aquifer)

The geoelectric parameters of thickness and resistivity were used to calculate the traverse resistance of layer 4 at all VES locations. The traverse resistance varied from 294 – 1979 Ωm^2 (Table 13). The measured transmissivity obtained from borehole information was observed from pumping tests conducted on the six boreholes using the Cooper-Jacob method by Jeffares and Green (2012). It was stated in Jeffares and Green (2012) that the pumping tests were conducted very soon after the drilling process. It was therefore possible that the drilling fluid affected the results of the pumping tests but it was stated that the results were reliable representations of the aquifer properties.

The measured transmissivities varied from 110.1 – 587m^2/day with an average transmissivity of 365.60m^2/day. The modelled (calculated using equation 3.25) transmissivity varied from 40.78 – 572.76m^2/day with an average transmissivity of 307.50m^2/day (Table 13). The modelled transmissivity was compared with calculated transmissivity using the linear regression method. A very good statistical correlation coefficient of R^2 = 0.99 was observed between the measured

transmissivity and the modelled transmissivity (Refer to Figure 26). The contoured transmissivity variation in the study area and the model of the calculated transmissivity are shown in Figure 31.

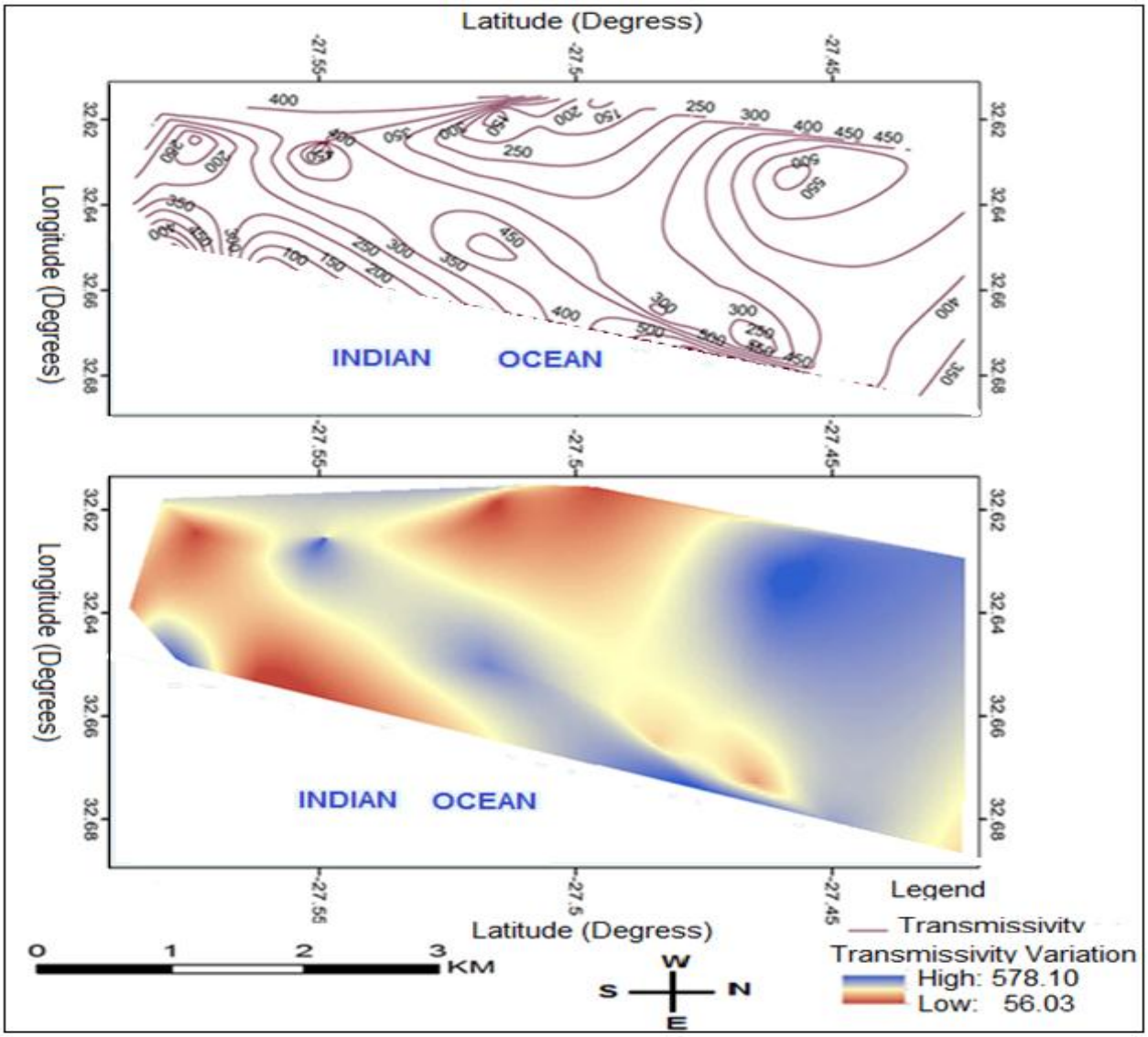

Figure 31: Transmissivity distribution of the deep aquifer

It can be seen from Figure 31 that the transmissivity of layer 4 (deep aquifer) is higher in the north than in the south, and appears to form linear zones of heightened potential.

The modelled transmissivity and the thicknesses of layer 4 at VES locations were used to estimate the hydraulic conductivity of the deep aquifer where no control boreholes exist. The measured hydraulic conductivity varied from 9 – 35m/day with an average hydraulic conductivity of 22m/day. The modelled or calculated hydraulic conductivity varied from 1 – 30m/day with an average hydraulic conductivity of 13m/day.

5.2.6 Western Transect

Figure 21 shows the depth of each geoelectric unit at the VES locations on the western transect and the inferred water table in the shallow aquifer. It can be seen from Figure 21 that geoelectric layer 1 and layer 2 correspond to the cover sand and the Kwambonambi Formation respectively. Each has higher relative vertical elevations to average mean sea level in the north than in the south. This is because the inland dunes are more prominent in the northern part of the study area than in the southern part.

The inferred thickness and depth of the deep aquifer or layer 4 (which corresponds to the Uloa/Umkwelane Formations) also varies from north to south. It has an approximate depth of 6m (amsl) in the northern part and 12m (bmsl) in the southern part. The Formations might have been eroded much more in the southern part of the study area than in the northern part. The average depth of the deeper aquifer along the western transect is about 2m below mean sea level.

At VES 33 located at the southern end of the western transect, the top of the Cretaceous unit was inferred at -50m (bmsl). The surface of the Cretaceous unit at the northern end of the western transect is about -28m (bmsl). The depth remained relatively constant (with minor variation), except towards the southernmost end, where the depth increased to -48m (bmsl) at VES 23 and 25 suggesting more potential erosion before the formation of the Cenozoic sediments (Refer to Figure 32).

Similarly, the Kosi Bay Formation is also shallower at the northern end and deeper in the southern end. Conversely the Kwambonambi Formation is thicker in the northern end than in the southern end, which suggests greater aquifer thickness and more available water in the northern reaches than in the southern reaches of the study area. VES 24 was conducted on a peat land and therefore, the cover sand was not detected. The presence of peat and also the thinness of layer 2 at VES 24 is shown in Figure 20. The presence of peat results in reduced

infiltration while the thinness suggests less available water at VES 24. Jeffares and Green (2012) indicated that the shallow aquifer at borehole number SOD 06 (in close proximity with VES 24) exhibited very low groundwater potential. The presence of peat and the thickness thereof can influence and affect the availability of groundwater in layer 2.

5.2.7 Eastern Transect

The eastern transect trends roughly north to south running through the DWA monitoring boreholes on the eastern side of Lake Mgobolezeni. The cover sand is relatively thicker along the eastern transect (Refer to Figure 23) than that of the western transect. Layer 2 (deep aquifer) is thicker at VES 10, 11 and 22 suggesting more available water at these areas. VES results showed that apparent resistivity values observed for the Kosi Bay Formations were higher in the southern reaches than those in the northern reaches of the study area. This suggests that silt and clay content appears to increase from north to south of the study area.

The thickness and depth of the deeper aquifer (Uloa/Umkwelane Formations) did not vary as much along the eastern transect as in the western transect, except at VES 11. It has an average elevation of -12m (bmsl) along the eastern transect. The deep aquifer is relatively deeper along the eastern transect (average elevation of 12mbmsl) than along the western transect (average elevation of 2mbmsl).

The depth to Cretaceous unit showed more variation along the eastern transect than the western transect. The upper surface occurs at an elevation -32m (bmsl) at VES 08 in the extreme north and at -71m (bmsl) at VES 11 in the south (Refer to Figure 23). It can be observed from Figure 32 that the Cretaceous unit is deeper along the eastern side than the western side of the study area. The -71m (bmsl) observed for the Cretaceous unit at VES 11 and 29 also suggests more potential erosion at these areas prior to the formation of Cenozoic sediments.

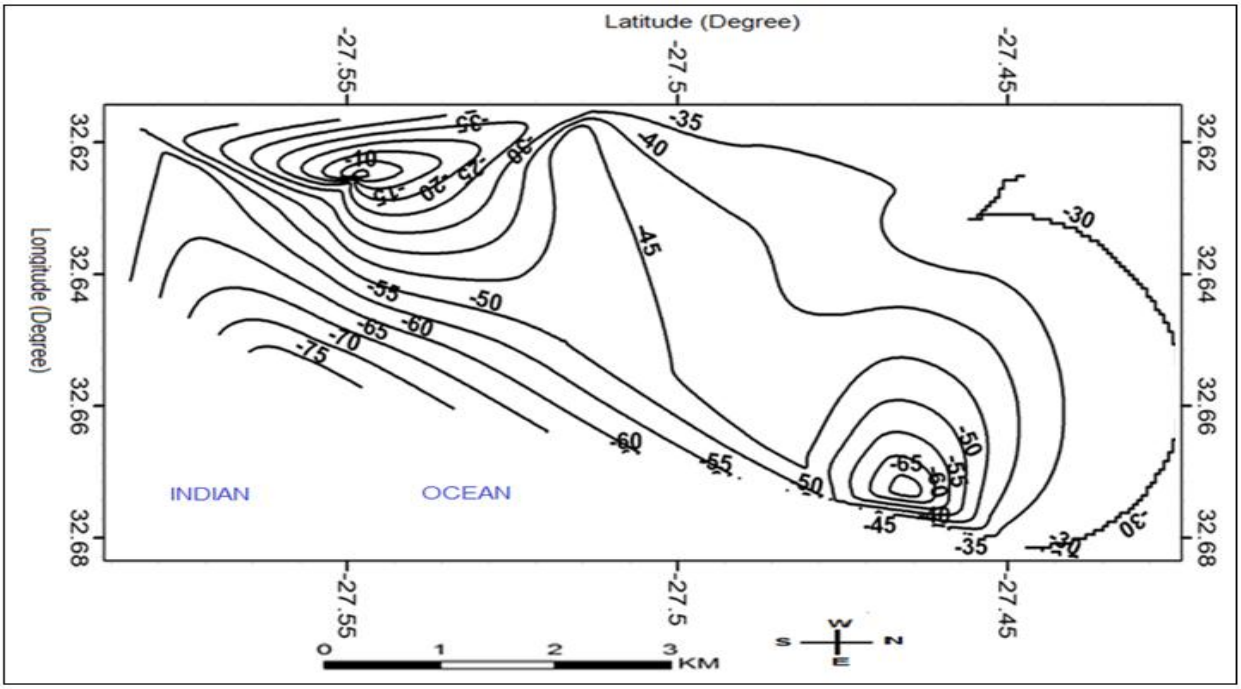

Figure 32: Surface of the Cretaceous Basement in the study area

CHAPTER SIX

6 CONCLUSIONS AND RECOMMENDATIONS

6.1 Conclusions

The applicability of VES in groundwater exploration is due to its cost effectiveness and clarity. The use of computer programmes also enhances the interpretation of VES data. The choice of the method for this study was based on its successful application for similar studies in other areas of the coastal plain.

The main aim of this study was to define the hydrostratigraphic units of the study area using the electrical resistivity method and to interpolate between boreholes with known geological logs. The response of the geologic units to current flow was used to define their hydrostratigraphy. This was possible because porosity and moisture content influence current flow through geologic materials, as well as the predominantly downward fining of sediments in the study area.

The correlation of the DWS monitoring borehole logs with VES logs enabled the delineation of the geoelectric units generated from the VES results. The information on the local geology of the study area was gathered from literature and local knowledge which also helped with the comparison of the geoelectric units with geology. The various apparent resistivity values' ranges obtained for the geoelectric units were in accordance with those assigned to similar geological units. The VES therefore successfully defined the geoelectric units in the study area.

The very high resistivity values observed for layer 1 (cover sands) were attributed to very low moisture (dry) conditions above the natural water table. The borehole logs confirmed a thin cover sand that was dry at all borehole locations. Layer 1 was considered to be the zone of aeration overlying the shallow aquifer in most parts of the study area.

Geological logs showed that the shallow aquifer (layer 2) varies in thickness throughout the study area. Lower resistivity values observed for layer 2 (shallow aquifer) in comparison to layer 1 were attributed to the presence of groundwater (saturated). The cover sand and the shallow aquifer are composed of similar lithology consisting of coarse to medium grained sand; both layers are considered part of the Kwambonambi Formation. The top of layer 2 therefore coincides with the water table. Since the thickness of an aquifer also determines its groundwater

potential, the parts of the study area where the thickness of the shallow aquifer is greater by deduction possess more available groundwater.

Layer 3 was considered to correspond with the low transmissivity Kosi Bay Formation which forms confining to semi confining units over the deeper aquifer. The decreasing resistivity values observed for layer 3 are attributed to increasing silt and clay content. The areas with lower resistivity values (50 to 120Ωm) were considered to contain more silt and clay. The deeper aquifer was considered to be more confined in those areas. The areas with higher resistivity values (120 to 200Ωm) were considered to contain lower amounts of silt and clay and the deeper aquifer was considered more semi confined in these areas. It forms a partial Aquiclude between the shallow aquifer and the deep aquifer. The apparent resistivity values recorded for layer 3 are higher around the area S 27.46° and S 27.49°. The deeper aquifer is therefore possibly semi-confined in this area.

The occurrence of the deeper aquifer in the study area was defined. The parts of the deeper aquifer considered to be confined (or semi-confined) by the overlying Kosi Bay Formation showed higher transmissivity values. The similarity between the thicknesses of the geoelectric layers (obtained from VES) and the thicknesses of the corresponding geologic units (obtained from drilling logs) indicated moderate to good accuracy of the method of this study. The good statistical correlation (R^2 = 0.9) between observed and modelled transmissivity also showed very good accuracy of the method.

The surface of the layer 5 (Cretaceous unit) was observed to be deeper to the eastthan in the west. This is in agreement with literature that the geologic units in the study area dip towards the east.

6.2 Recommendations

The interpretation of VES data was conservative to avoid over interpretation, as the geoelectric boundary does not always clearly coincide with geologic boundaries. Similarly the geoelectric units presented in this study may not coincide exactly with the geologic boundaries in the study area. Due to limited time and expenses not enough VES were conducted.

The results were interpolated to create a three dimensional surface of the various geoelectric layers obtained from this study. With the addition of more survey points the resolution can be improved.

Therefore it is recommended that:-

a) Additional VES be conducted around the study area to obtain a larger data set
b) Drilling some of the surveyed locations be conducted to verify results
c) The use of higher precision two dimensional instruments with multiple electrode arrays for improved accuracy, and a quicker field survey.

It can be concluded that the VES method used for this study successfully defined the geologic facies in the study area. Many previously published works on the VES method suggest a wide application of the method. The accuracy of the results of this study showed that the method can be applied successfully in unconsolidated sediments such as the Maputaland Formation. It is more cost effective than some other geophysical methods such as seismic and electromagnetic methods.

7 References

Abdul-Aziz, M.A., 2014. Hydrostratigraphic Characterization of Groundwater Systems in Khatatba area using Vertical Electric Sounding and Well log data, SW Nile Delta, Egypt. International Journal of Advancement in Earth and Environmental Sciences 2(1), Pages 39 – 50.

Adagunodo, T.A., Sunmonu, L.A., Ojoawo, A., Oladejo, P., and Olafisoye, R.E., 2013. The Hydro Geophysical Investigation of Oyo State Industrial Estate Ogbomosho, Southwestern Nigeria Using Vertical Electrical Soundings. Research Journal of Applied Sciences, Engineering and Technology 5(5), Pages 1816-1829.

Aizebeokhai, P.A., Olayinka, A.I., and Singh, V.S., 2010. Application of 2D and 3D Geoelectrical Resistivity Imaging for Engineering site Investigation in a Crystalline Basement Terrain, Southwestern Nigeria. Environmental Earth Science. DOI 10.1007/s12665-010-0464-z.

Archie, G.E., 1942. The Electrical Resistivity Log as an Aid in Determining some Reservoir Characteristics. Dallas meeting, 194. http://www.pe.tamu.edu/blasingame/data/z_zcourse_archive/P663_03C/P663_03C_TAB_Ref_FormEval/SPE_Trans_1942_Archie_Reservoir_Char_from_Resistivity_Logs.pdf. Accessed 12/7/2014.

Ariyo, S.O., and Adeyemi, G.O., 2012. Geoelectrical Characterization of Aquifers in the Basement Complex/sedimentary Transition Zone, Southwestern Nigeria. International Journal of Advanced Scientific Research and Technology 2(1), ISSN: 2249-9954.

Arshad, M., Shakoor, A., Ahmad, I., and Ahmad, M., 2013. Hydraulic Transmissivity Determination for the Groundwater Exploration using Vertical Electric Sounding Method in Comparison to the Traditional Methods. Parkistanian Journal of Agricultural Science. 50(3), Pages 487-492. http://www.pakjas.com.pk. Accessed 14/6/2014.

Batayneh, T.A., 2009. A Hydrogeophysical Model of the Relationship between Geoelectric and Hydraulic Parameters, Central Jordan. Journal of Water Resource and Protection, 1, Pages 400-407. http://www.scirp.org/journal/jwarp. Accessed 05/02/2014.

Boonstra, J., and de Ridder N.A., 1981. Numerical Modeling of Groundwater Basins. International Institute for Lands Reclamation and Improvement (ILRI), P. O. Box 45, 6700 AA Wagenningen, The Netherlands

Botha, G.A., and Porat, N., 2007. Soil Chronosequence Development in the Dunes on the Southeast African Coastal Plain, Maputaland, South Africa. Quaternary International 162 – 163, pages 111 – 132.

Botha, G.A., 1997. Maputaland: Focus on the Quaternary Evolution of the Southeast African Coastal Plain. Field Guide and Abstracts. INQUA commission of Quaternary Shorelines, Africa Sub-commission, 104

Bredehoeft, J., 2005. The Conceptualization Model Problem – Surprise. Hydrology Journal 13, pages 37 – 46.

Christen E. W., and Sikandar. P., 2012. Geoelectrical Sounding for the Estimation of Hydraulic Conductivity of Alluvial Aquifers. Water Resource Management 26, pages 1201 – 1215.

Cooper, J.A.G., Green, A.N., and Smith, A.M., 2013. Vertical Stacking of Multiple Highstand Shoreline Deposits from the Cretaceous to the Present: Facies Development and Preservation. Journal of Coastal Research, Special Issue No. 65.

Dingle, R.V., Siesser, W.G., and Newton, A.R., 1983. Mesozoic and Tertiary Geology of Southern Africa. Balkema, Rotterdam.

Dobrin, B.M., and Savit, H.C., 1988. Introduction to Geophysical Prospecting, Fourth Edition. McGraw – Hill Book Company, New York.

Grundlin, T.A., van den Berg, C.E., and Price, S.J., 2013. Assessing the Distribution of Wetlands over Wet and Dry periods and Land-use change on the Maputaland Coastal Plain, North-eastern Kwazulu-Natal, South Africa. Journal of Geomatics 2(2).

Gunther, T., and Muller-petke, M., 2012. Hydraulic Properties at the North Sea Island of Borkum Derived from Joint Inversion of Magnetic Resonance and Electrical Resistivity Soundings. Hydrology and Earth Systems Sciences 16, 3279 – 3291.

Heigold, P.C., Gilkerson, R.H., Cartwright, K., and Reed, C.P., 1979. Aquifer Transmissivity from Surficial Electrical Methods. Groundwater 17(4).

Herckenrath, D., 2012. Informing Groundwater Models with Near Surface Geophysics Data. Ph.D. Thesis Submitted to Department of Environmental Engineering, Technical University of Denmark, page 17.

Hobday, D.K., 1979. Geological Evolution and Geomorphology of the Zululand Coastal plain in Lake Sibaya (B.R. Allanson, ed.) Monographiae Bibliogicae 36, pages 1 – 19.

Huntley, D., 1985. Relationship between Permeability and Electrical Resistivity of Granular Aquifers. Groundwater 24(4).

Israil, M., Al-hadithi, M., Singhal, D.C., 2006. Application of a Resistivity Survey and Geographical Information System (GIS) Analysis for Hydrogeological Zoning of a Piedmont Area, Himalayan Foothill Region, India. Hydrogeology Journal 14, pages 753–759.

Jeffares and Green, 2012. uMkhanyakude District Municipality Groundwater Monitoring Network. Implementation Report. Jeffares and Green (Pty) Ltd. Project Number 2911.

Jorgensen, G.D., 1988. Using Geophysical Logs to Estimate Porosity, Water Resistivity and Intrinsic Permeability. United States Geological Survey Water-Supply Paper 2321.

Kelbe, B., and Germishuyse, T., 2001. Geohydrological Studies of the Primary Coastal Aquifer in Zululand, Richards Bay Region, Water Resource Commission, Report No: 720/1/01.

Kelbe, B.E., Taylor, R.H., and Bate, G.B., 2013. The linkage between hydrological and ecological drivers: Mgobezeleni Studies. Annual Report to WRC, Pretoria.

Kelbe, B., 2014. Progress Report. Department of Water Affairs and Forestry – University of Zululand Sodwana Conference.

Kelly, W., 1977. Geoelectric Sounding for Estimating Aquifer Hydraulic Conductivity, Ground Water, 15(6).

Kelly, E.W., and Frohlich, K.R., 1985. Relations between Aquifer Electrical and Hydraulic Properties. Groundwater 23(2).

Khalil, A.M., and Santos, M.A.F., 2009. Influence of Degree of Saturation in the Electric Resistivity–Hydraulic Conductivity Relationship. Survey Geophysics 30, pages 601–615.

Loke, M.H., 2000. Electrical Imaging Surveys for Environmental and Engineering Studies. A practical guide to 2-D and 3-D surveys http://www.cas.umt.edu/geosciences//faculty/sheriff/495 subsurface%20imaging%20in%20archaeology/Sources/Loke_elect_tutorial.pdf. Accessed 21/04/2014.

Loke, M. H., 2004. Tutorial: 2-D and 3-D Electrical Imaging Survey. http://www.cas.umt.edu/geosciences//faculty/sheriff/495 subsurface%20imaging%20in%20archaeology/Sources/Loke_elect_tutorial.pdf. Accessed 21/04/2014.

Maillet, R., 1947. The Fundamental Equations of Electrical Prospecting, Geophysics 12(4), Pages 529-556.

Maud, R.R., and Orr, W.N., 1975. Aspects of post-Karoo Geology in the Richards Bay area. Geological Society of South Africa 78, pages 101 – 109.

Maud, R.R., 1980. The Climate and Geology of Maputaland in studies on the Geology of Maputaland. Rhodes University and the Natal branch of the Wildlife Society of Southern Africa, pages 1 – 7.

Maud, R.R., 1998. A brief summary of the hydrogeology of the Maputaland Coastal Plain. Proceedings of the Maputaland Groundwater resource Conference, St Lucia, 17/03,1998.Chief Directorate Environmental Affairs, KZN Department of traditional and Environmental Affairs, Pages 7-11.

Maxey, G.B., 1964. Hydrostratigraphic Units. Journal of hydrology 2, pages 124 – 129.

McCarthy, M. J., 1988. Some Observations on the Occurrence of "Berea-type" red sand along the Natal coast. Ext. Abstract. 22nd Biennial Congress, Geological Society of South Africa. 403b - d

Meads, N. L., Bentley, R. L., and Mendoza, A. C., 2003. Application of Electrical Resistivity Imaging to the Development of a Geologic Model for Edmonton Landfill Site. Geotechnical Journal 40, pages 551 – 558.

Meju, M. A., Fenning, P. J., and Hawkins, T. R. W., 2000. Evaluation of Small-Loop Transient Electromagnetic Sounding to Locate the Sherwood Sandstone Aquifer and Confining Formations at Well Sites in the Vale of New York. Journal of Applied Geophysics 44, pages 217 – 236.

Miller, W.R., 1998. The Sedimentology of Lake Sibaya, northern Kwazulu-Natal. Report, Council for Geoscience, Private Bag 112, Pretoria, 0001 1998-0318.

Miller, W. R., 2001. The bathymetry, Sedimentology and Seismic Stratigraphy of Lake Sibaya, KwaZulu-Natal. Bulletin No. 131, Council for Geosciences, Pretoria.

Mohamed, A. K., Metwaly, M., Khalili, M., and Al Sayed, E., 2006. Evaluation of the Transient Electromagnetic Method as Applied to Wadi-Fill Deposits, South Sinai, Egypt. Egyptian Geological Society Journal 4(1), pages 189 – 198.

Niwas, S., and de Lima, L.A.O., 2003. Aquifer Parameter Estimation from Surface Resistivity Data. Groundwater 41(1), Pages 94 – 99.

Niwas, S., and Celik, M., 2012. Equation Estimation of Porosity and Hydraulic Conductivity of Ruhrtal Aquifer in Germany using Near Surface Geophysics. Journal of Applied Geophysics 84, Pages 77 – 85.

Niwas, S and Singhal, D.C., 1981. Estimation of Aquifer Transmissivity from Dar Zar Rouk Parameters in Porous Media. Journal of Hydrology 50, Pages 393- 399.

Nwachukwu, A.M., Aslan, A., and Nwachukwu, I.M., 2013. Application of Geographic Information System (GIS) in Sustainable Groundwater Development, Imo River Basin Nigeria. International Journal of Water Resources and Environmental Engineering 5(6), pages 310-320.

Porat, N., and Botha., 2008. The Luminescence Dating of Dune Development on the Maputaland Coastal Plain, Southeast Africa. Quaternary Science Reviews 27, pages 1024 – 1046.

Porter, N.S., and Clark, B.M., 2012. UMkhanyakude District Municipality Environmental Management Framework. Coastal Estuarine Discipline. Anchor Environmental, 8 Steenberg House, Silverwood close, Tokai 7945.

Rafsgaard, C. J., Hojberg, L. A. L., Moller, I., Hansen, M., and Sondergaard, V., 2010. Groundwater Modeling in Integrated Water Resources Management – Vision 2020. Groundwater journal 48 (45), pages 633 – 648.

Rawlins, B.K., 1991. Geohydrological Assessment of the Behaviour and response of the Zululand Coastal Plain to both Environmental influences and human activity. Submitted to the Faculty of Science and Agriculture in partial fulfilment of the requirements for the degree of Master of Science in the Department of Hydrology at the University of Zululand, South Africa.

Reynolds, J.M., 2000. An introduction to Applied and Environmental geophysics. John Willey and Sons, New York. Pages 417- 491.

Saad, R., Nawawi, N. N. M., and Mohamed, T. E., 2012. Groundwater Detection in Alluvium Using 2-D resistivity Tomography. Electronic Journal of Geotechnical Engineering 17, pages 369 – 377.

Seaber, P.R., 1988. Chapter 2: Hydrostratigraphic Units. The Geology of North America 0 – 2.

Sabet, A.M., 1975. Vertical Electrical Resistivity Soundings to locate Groundwater Resources: A Feasibility Study. A publication of Virginia Water Resources Research Center, Virginia Polytechnic Institute and State University, Blacksburg, Virginia 24061. Bulletin 75.

Schapers, M., 2011. Characterization of the Kwangwanase Airfield Aquifer. A Dissertation Submitted in Accordance with the Fulfilment of the Requirements for the Award of Master of Science Degree in the Faculty of Natural Sciences, Department of Groundwater Studies, University of Free State, Bloemfontein, South Africa.

Soupios, M.P., Kouli, M., Filippos, V., Antonis, V., and Stavroulakis, G., 2007. Estimation of Aquifer hydraulic parameters from Surficial Geophysical Methods: A Case Study of Keritis Basin in Chania (Crete – Greece). Journal of Hydrology 338, Pages 122 – 131.

Taylor, R., Kelbe, B., Haldorsen, S., Botha, G.A., Wejden, B., Været, L., and Simonsen, M.B., 2005. Groundwater-dependent Ecology of the Shoreline of the Subtropical Lake St Lucia Estuary. Environmental Geology. 49, Pages 586–600

Thornhill, M., and Van Vuuren, D., (Ed.) 2009. Status Quo Report: Environmental Management Framework for the Richards Bay Port Expansion Area and Industrial Development Zone. Report produced for the Department of Agriculture, Environmental Affairs and Rural Development. Report No. TX2009/C007-14, Pietermaritzburg, South Africa.

Torsvik, H.T., and Cocks, L.R.M., 2013. Gondwana from Top to Base in time. Elsevier, Gondwana Research 24, pages 999 – 1030.

Van Zijl, J. S. V., 1985. A Practical Manual on the Resistivity Method (Revised Edition), Geophysical Division, National Physical Research Laboratory, CISR, Pretoria, South Africa.

Wang, F. H., and Anderson, P. M., 1995. Introduction to Groundwater Modeling Finite Element and Finite Difference Methods. Academic Press Limited, 24 – 28 Oral Road, London, NWI 7Dk.

Watkeys, M.K., Mason, T.R., and Godman, P.S., 1993. The Role of Geology in the development of Maputaland, South Africa. Journal of African Earth Science 16(1/2), pages 205 – 225.

Weitz, J., Demlie, M., 2013. Conceptual modelling of groundwater–surface water interactions in the Lake Sibayi Catchment, Eastern South Africa. Journal of African Earth Sciences. http://dx.doi.org/10.1016/j.jafrearsci.2013.11.018.

Worthington, P. F., 1978. Groundwater Conditions of Zululand Coastal Plains around Richards Bay. CSIR Geophysics Division Research Report No. 182, pages 200 – 210.

Worthington, P.F., 1993. The Uses and Abuses of Archie Equations: 1. The Formation Factor – Porosity Relationship. Journal of Applied geophysics 30, pages 215 – 228.

Wright, C.I., Miller, W.R., and Cooper, J.A.G., 2000. The late Cenozoic evolution of coastal water bodies in Northern KwaZulu-Natal, South Africa. Marine Geology 167, pages 207–229

Wright, C.I., and Mason, T.R., 1993. Management and sediment dynamics of the St. Lucia Estuary mouth, Zululand, South Africa Environmental Geology 22, pages 227 241.

Zorhdy, A.A.R., Eaton G.P., and Mabey, D.R., 1974b. Application of Surface Geophysics to Ground-Water Investigation, Techniques of Water Resources Investigation. US Geological Survey, Chapter DI, Page 116.

APPENDIX 1

SUMMARY TABLES FOR THE VES RESULTS

Table 15: Summary of VES 01

Layer	Resistivity (Ωm)	Thickness (m)	Depth (m)	Lithology	Age	Formation	Hydrostratigraphy
1	6195	3	3	Medium to coarse grained sand	Pleistocene	Kwambonambi Formation	Dry sand
2	859	6	9	Medium to coarse grained sand	Pleistocene	Kwambonambi Formation	Unconfined aquifer
3	198	36	45	Fine to medium grained sand	Pleistocene	Kosi Bay Formation	Aquiclude
4	14	43	87	Calcrete/con-glomerate	Miocene to Pliocene	Uloa/Umkwelane Formations	Semi confined aquifer
5	1442	∞	∞	Siltstone	Cretaceous		Aquitard

Table 16: Summary of VES 06

Layer	Resistivity (Ωm)	Thickness (m)	Depth (m)	Lithology	Age	Formation	Hydrostratigraphy
1	6989	3	3	Medium to coarse grained sand	Pleistocene	Kwambonambi Formation	Dry sand
2	971	6	9	Medium to coarse grained sand	Pleistocene	Kwambonambi Formation	Unconfined aquifer
3	194	35	45	Fine to medium grained sand	Pleistocene	Kosi Bay Formation	Aquiclude
4	14	42	87	Calcrete/con-glomerate	Miocene to Pliocene	Uloa/Umkwelane Formations	Semi confined aquifer
5	1330	∞	∞	Siltstone	Cretaceous		Aquitard

Table 17: Summary of VES 08

Layer	Resistivity (Ωm)	Thickness (m)	Depth (m)	Lithology	Age	Formation	Hydrostratigraphy
1	3502	5	5	Medium to coarse grained sand	Pleistocene	Kwambonambi Formation	Dry sand
2	1238	4	9	Medium to coarse grained sand	Pleistocene	Kwambonambi Formation	Dry Sand
3	159	34	43	Fine to medium grained sand	Pleistocene	Kosi Bay Formation	Aquiclude
4	48	25	68	Calcrete/con-glomerate	Miocene to Pliocene	Uloa/Umkwelane Formations	Semi confined aquifer
5	1433	∞	∞	Siltstone	Cretaceous		Aquitard

Table 18: Summary of VES 09

Layer	Resistivity (Ωm)	Thickness (m)	Depth (m)	Lithology	Age	Formation	Hydrostratigraphy
1	3641	9	9	Medium to coarse grained sand	Pleistocene	Kwambonambi Formation	Dry sand
2	1214	4	13	Medium to coarse grained sand	Pleistocene	Kwambonambi Formation	Unconfined aquifer
3	147	29	42	Fine to medium grained sand	Pleistocene	Kosi Bay Formation	Aquiclude
4	20	18	59	Calcrete/con-glomerate	Miocene to Pliocene	Uloa/Umkwelane Formations	Semi confined aquifer
5	3374	∞	∞	Siltstone	Cretaceous		Aquitard

Table 19: Summary of VES 10

Layer	Resistivity (Ωm)	Thickness (m)	Depth (m)	Lithology	Age	Formation	Hydrostratigraphy
1	3298	7	7	Medium to coarse grained sand	Pleistocene	Kwambonambi Formation	Dry sand
2	738	20	27	Medium to coarse grained sand	Pleistocene	Kwambonambi Formation	Unconfined aquifer
3	115	12	39	Sandy silt with clay	Pleistocene	Kosi Bay Formation	Aquiclude
4	28	25	64	Calcrete/con-glomerate	Miocene to Pliocene	Uloa/Umkwelane Formations	Semi confinec aquifer
5	7225	∞	∞	Siltstone	Cretaceous		Aquitard

Table 20: Summary of VES 11

Layer	Resistivity (Ωm)	Thickness (m)	Depth (m)	Lithology	Age	Formation	Hydrostratigraphy
1	6403	5	5	Medium to coarse grained sand	Pleistocene	Kwambonambi Formation	Dry sand
2	850	11	16	Medium to coarse grained sand	Pleistocene	Kwambonambi Formation	Unconfined aquifer
3	133	36	52	Fine to medium grained sand	Pleistocene	Kosi Bay Formation	Aquiclude
4	25	56	108	Calcrete/con-glomerate	Miocene to Pliocene	Uloa/Umkwelane Formations	Semi confined aquifer
5	3583	∞	∞	Siltstone	Cretaceous		Aquitard

Table 21: Summary of VES 12

Layer	Resistivity (Ωm)	Thickness (m)	Depth (m)	Lithology	Age	Formation	Hydrostratigraphy
1	7915	4	4	Medium to coarse grained sand	Pleistocene	Kwambonambi Formation	Dry sand
2	859	9	13	Medium to coarse grained sand	Pleistocene	Kwambonambi Formation	Unconfined aquifer
3	126	25	39	Fine to medium grained sand	Pleistocene	Kosi Bay Formation	Aquiclude
4	11	28	67	Calcrete/con-glomerate	Miocene to Pliocene	Uloa/Umkwelane Formations	Semi confined aquifer
5	3688	∞	∞	Siltstone	Cretaceous		Aquitard

Table 22: Summary of VES 13

Layer	Resistivity (Ωm)	Thickness (m)	Depth (m)	Lithology	Age	Formation	Hydrostratigraphy
1	10115	2	2	Medium to coarse grained sand	Pleistocene	Kwambonambi Formation	Dry sand
2	1334	8	9	Medium to coarse grained sand	Pleistocene	Kwambonambi Formation	Unconfined aquifer
3	99	32	41	Sandy silt with clay	Pleistocene	Kosi Bay Formation	Aquiclude
4	12	24	65	Calcrete/con-glomerate	Miocene to Pliocene	Uloa/Umkwelane Formations	Semi confined aquifer
5	6216	∞	∞	Siltstone	Cretaceous		Aquitard

Table 23: Summary of VES 14

Layer	Resistivity (Ωm)	Thickness (m)	Depth (m)	Lithology	Age	Formation	Hydrostratigraphy
1	4687	3	3	Medium to coarse grained sand	Pleistocene	Kwambonambi Formation	Dry sand
2	852	3	5	Medium to coarse grained sand	Pleistocene	Kwambonambi Formation	Unconfined aquifer
3	82	23	29	Sandy silt with clay	Pleistocene	Kosi Bay Formation	Aquiclude
4	21	29	58	Calcrete/con-glomerate	Miocene to Pliocene	Uloa/Umkwelane Formations	Semi confined aquifer
5	10910	∞	∞	Siltstone	Cretaceous		Aquitard

Table 24: Summary of VES 16

Layer	Resistivity (Ωm)	Thickness (m)	Depth (m)	Lithology	Age	Formation	Hydrostratigraphy
1	6195	3	3	Medium to coarse grained sand	Pleistocene	Kwambonambi Formation	Dry sand
2	859	6	9	Medium to coarse grained sand	Pleistocene	Kwambonambi Formation	Unconfined aquifer
3	198	36	45	Fine to medium grained sand	Pleistocene	Kosi Bay Formation	Aquiclude
4	14	43	87	Calcrete/con-glomerate	Miocene to Pliocene	Uloa/Umkwelane Formations	Semi confined aquifer
5	1442	∞	∞	Siltstone	Cretaceous		Aquitard

Table 25: Summary of VES 17

Layer	Resistivity (Ωm)	Thickness (m)	Depth (m)	Lithology	Age	Formation	Hydrostratigraphy
1	2941	2	2	Medium to coarse grained sand	Pleistocene	Kwambonambi Formation	Dry sand
2	724	10	12	Medium to coarse grained sand	Pleistocene	Kwambonambi Formation	Unconfined aquifer
3	112	38	50	Sandy silt with clay	Pleistocene	Kosi Bay Formation	Aquiclude
4	43	40	91	Calcrete/con-glomerate	Miocene to Pliocene	Uloa/Umkwelane Formations	Semi confined aquifer
5	6688	∞	∞	Siltstone	Cretaceous		Aquitard

Table 26: Summary of VES 18

Layer	Resistivity (Ωm)	Thickness (m)	Depth (m)	Lithology	Age	Formation	Hydrostratigraphy
1	7441	2	2	Medium to coarse grained sand	Pleistocene	Kwambonambi Formation	Dry sand
2	3140	10	12	Medium to coarse grained sand	Pleistocene	Kwambonambi Formation	Unconfined aquifer
3	178	36	47	Fine to medium grained sand	Pleistocene	Kosi Bay Formation	Aquiclude
4	20	33	80	Calcrete/con-glomerate	Miocene to Pliocene	Uloa/Umkwelane Formations	Semi confined aquifer
5	4139	∞	∞	Siltstone	Cretaceous		Aquitard

Table 27: Summary of VES 21

Layer	Resistivity (Ωm)	Thickness (m)	Depth (m)	Lithology	Age	Formation	Hydrostratigraphy
1	8141	4	4	Medium to coarse grained sand	Pleistocene	Kwambonambi Formation	Dry sand
2	510	15	19	Medium to coarse grained sand	Pleistocene	Kwambonambi Formation	Unconfined aquifer
3	97	19	39	Sandy silt with clay	Pleistocene	Kosi Bay Formation	Aquiclude
4	21	59	97	Calcrete/con-glomerate	Miocene to Pliocene	Uloa/Umkwelane Formations	Semi confined aquifer
5	6285	∞	∞	Siltstone	Cretaceous		Aquitard

Table 28: Summary of VES 22

Layer	Resistivity (Ωm)	Thickness (m)	Depth (m)	Lithology	Age	Formation	Hydrostratigraphy
1	7777	5	5	Medium to coarse grained sand	Pleistocene	Kwambonambi Formation	Dry sand
2	386	13	19	Medium to coarse grained sand	Pleistocene	Kwambonambi Formation	Unconfined aquifer
3	82	34	52	Sandy silt with clay	Pleistocene	Kosi Bay Formation	Aquiclude
4	46	40	92	Calcrete/con-glomerate	Miocene to Pliocene	Uloa/Umkwelane Formations	Semi confined aquifer
5	9116	∞	∞	Siltstone	Cretaceous		Aquitard

Table 29: Summary of VES 23

Layer	Resistivity (Ωm)	Thickness (m)	Depth (m)	Lithology	Age	Formation	Hydrostratigraphy
1	6005	4	4	Medium to coarse grained sand	Pleistocene	Kwambonambi Formation	Dry sand
2	665	4	8	Medium to coarse grained sand	Pleistocene	Kwambonambi Formation	Unconfined aquifer
3	85	43	50	Sandy silt with clay	Pleistocene	Kosi Bay Formation	Aquiclude
4	39	28	78	Calcrete/con-glomerate	Miocene to Pliocene	Uloa/Umkwelane Formations	Semi confined aquifer
5	1060	∞	∞	siltstone	Cretaceous		Aquitard

Table 30: Summary of VES 24

Layer	Resistivity (Ωm)	Thickness (m)	Depth (m)	Lithology	Age	Formation	Hydrostratigraphy
1	220	4	4	Medium to coarse grained sand	Pleistocene	Kwambonambi Formation	Unconfined aquifer
2	94	24	28	Sandy silt with clay	Pleistocene	Kosi Bay Formation	Aquiclude
3	13	23	50	Calcrete/con-glomerate	Miocene to Pliocene	Uloa/Umkwelane Formations	Semi confined aquifer
4	1285	∞	∞	Siltstone	Cretaceous		Aquitard

Table 31: Summary of VES 25

Layer	Resistivity (Ωm)	Thickness (m)	Depth (m)	Lithology	Age	Formation	Hydrostratigraphy
1	8213	3	3	Medium to coarse grained sand	Pleistocene	Kwambonambi Formation	Dry sand
2	189	31	33	Fine to medium grained sand	Pleistocene	Kosi Bay Formation	Unconfined aquifer
3	72	52	34	Sandy silt with clay	Pleistocene	Kosi bay Formation	Aquiclude
4	28	34	86	Calcrete/con-glomerate	Miocene to Pliocene	Uloa/Umkwelane Formations	Semi confined aquifer
5	17292	∞	∞	Siltstone	Cretaceous		Aquitard

Table 32: Summary of VES 26

Layer	Resistivity (Ωm)	Thickness (m)	Depth (m)	Lithology	Age	Formation	Hydrostratigraphy
1	4188	4	4	Medium to coarse grained sand	Pleistocene	Kwambonambi Formation	Dry sand
2	1461	11	15	Medium to coarse grained sand	Pleistocene	Kwambonambi Formation	Unconfined aquifer
3	76	33	48	Sandy silt with clay	Pleistocene	Kosi Bay Formation	Aquiclude
4	37	40	88	Calcrete/con-glomerate	Miocene to Pliocene	Uloa/Umkwelane Formations	Semi confined aquifer
5	3345	∞	∞	Siltstone	Cretaceous		Aquitard

Table 33: Summary of VES 29

Layer	Resistivity (Ωm)	Thickness (m)	Depth (m)	Lithology	Age	Formation	Hydrostratigraphy
1	7035	3	3	Medium to coarse grained sand	Pleistocene	Kwambonambi Formation	Dry sand
2	442	3	6	Medium to coarse grained sand	Pleistocene	Kwambonambi Formation	Unconfined aquifer
3	94	49	55	Sandy silt with clay	Pleistocene	Kosi Bay Formation	Aquiclude
4	38	53	108	Calcrete/con-glomerate	Miocene to Pliocene	Uloa/Umkwelane Formations	Semi confined aquifer
5	1526	∞	∞	Siltstone	Cretaceous		Aquitard

Table 34: Summary of VES 30

Layer	Resistivity (Ωm)	Thickness (m)	Depth (m)	Lithology	Age	Formation	Hydrostratigraphy
1	15543	3	3	Medium to coarse grained sand	Pleistocene	Kwambonambi Formation	Dry sand
2	142	21	24	Fine to Medium grained sand	Pleistocene	Kosi Bay Formation	Aquiclude
3	13	29	53	Calcrete/con-glomerate	Miocene to Pliocene	Uloa/Umkwelane Formations	Semi confined aquifer
4	2397	∞	∞	Siltstone	Cretaceous		Aquitard

Table 35: VES Data Sheet

SCHLUMBERGER ARRAY FIELD RECRDING SHEET													
Client:		Department of Hydrology, University of Zululand				Project No:		SOD					
Project Name:		M. Sc. Research				Remarks:							
Ref. No:			Traverse Co-ordinates:		End 1:						Time		
Date:					End 2:						Start:		
Travers Direction:			Point Co-ordinates:								End:		
Electrode Spacing					Geometric Factor k	Field Recorded Result							
AB	MN	OA OB	ON OM	Check MN<AB/5		ΔV (mV)	I (mA)	Rho (Ωm)	Standard Deviation	No of Cycles	Base Reading V	Base Reading I	
2	0.5												
3	0.5												
4	0.5												
5	0.5												
10	0.5												
15	0.5												
20	0.5												
10	2												
15	2												
20	2												
25	2												
30	2												
40	2												
25	5												
30	5												
40	5												
50	5												
60	5												
80	5												
50	10												
60	10												
80	10												
120	10												
160	10												
200	10												

APPENDIX 2

CURVES AND MODEL FOR 20 VES RESULT

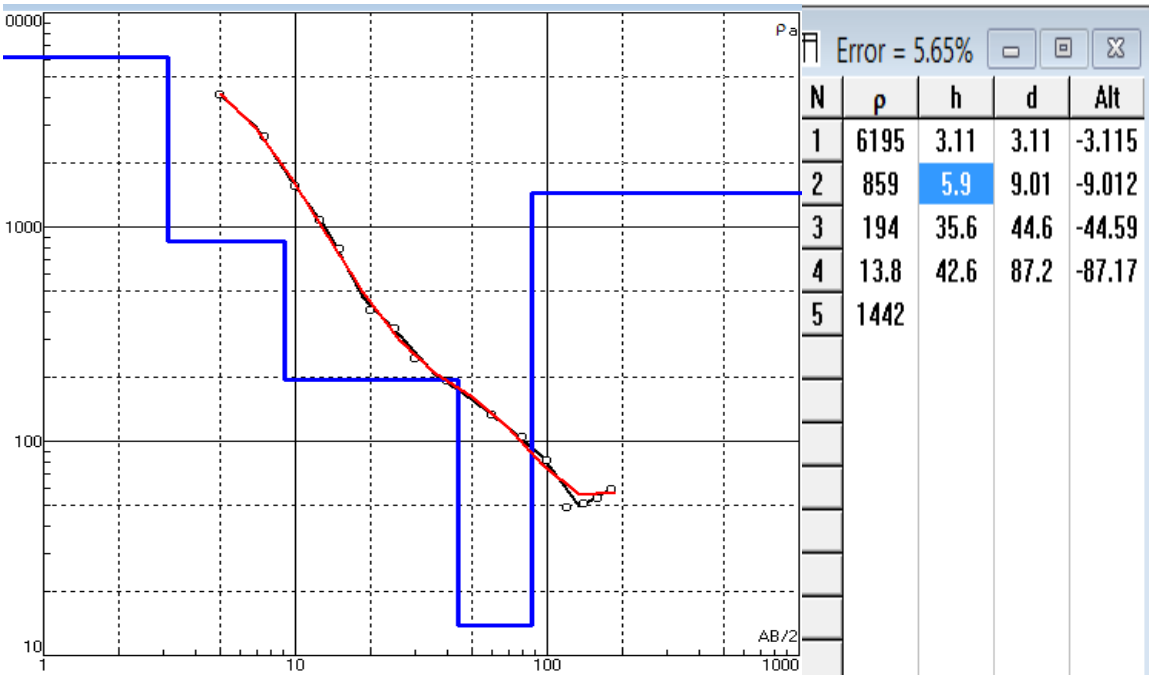

N	ρ	h	d	Alt
1	6195	3.11	3.11	-3.115
2	859	5.9	9.01	-9.012
3	194	35.6	44.6	-44.59
4	13.8	42.6	87.2	-87.17
5	1442			

Figure 33: Curve and Model for VES 01

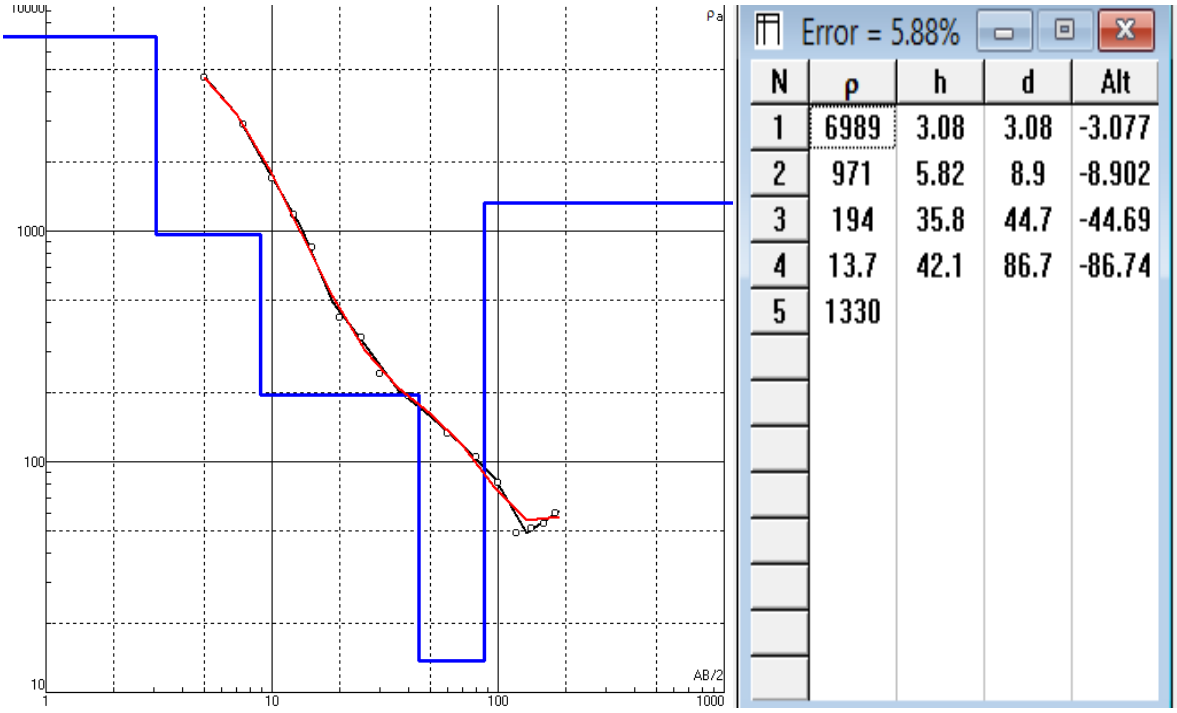

Figure 34: Curve and Model for VES 06

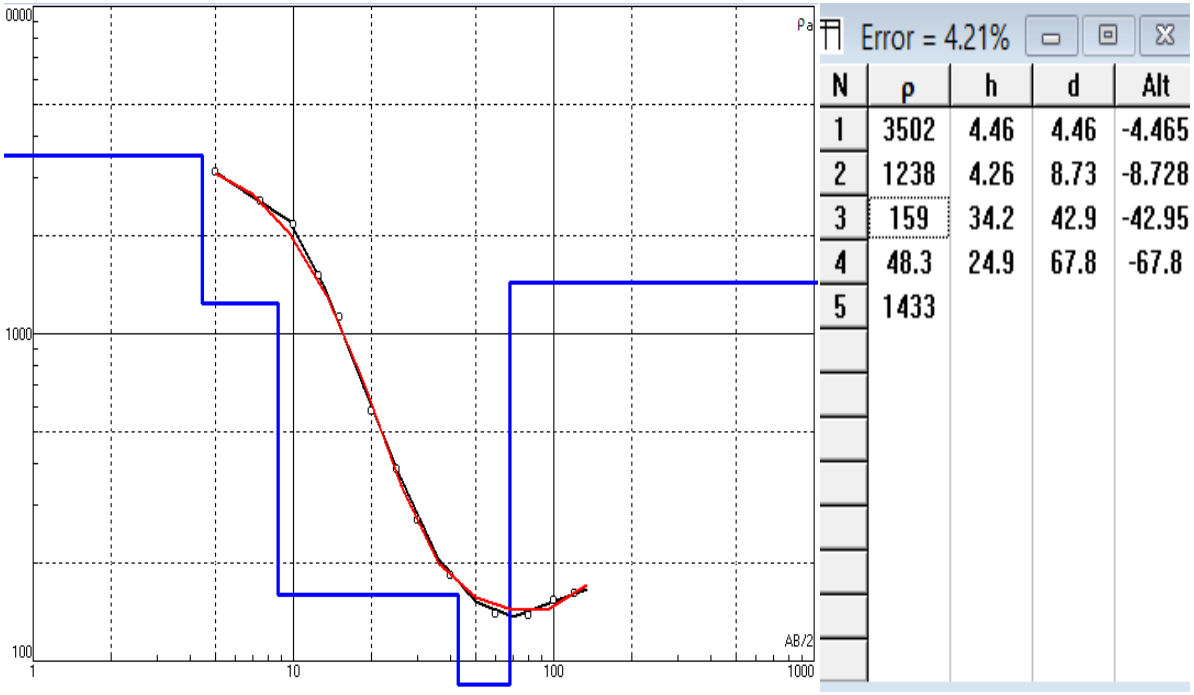

Figure 35: Curve and Model for VES 08

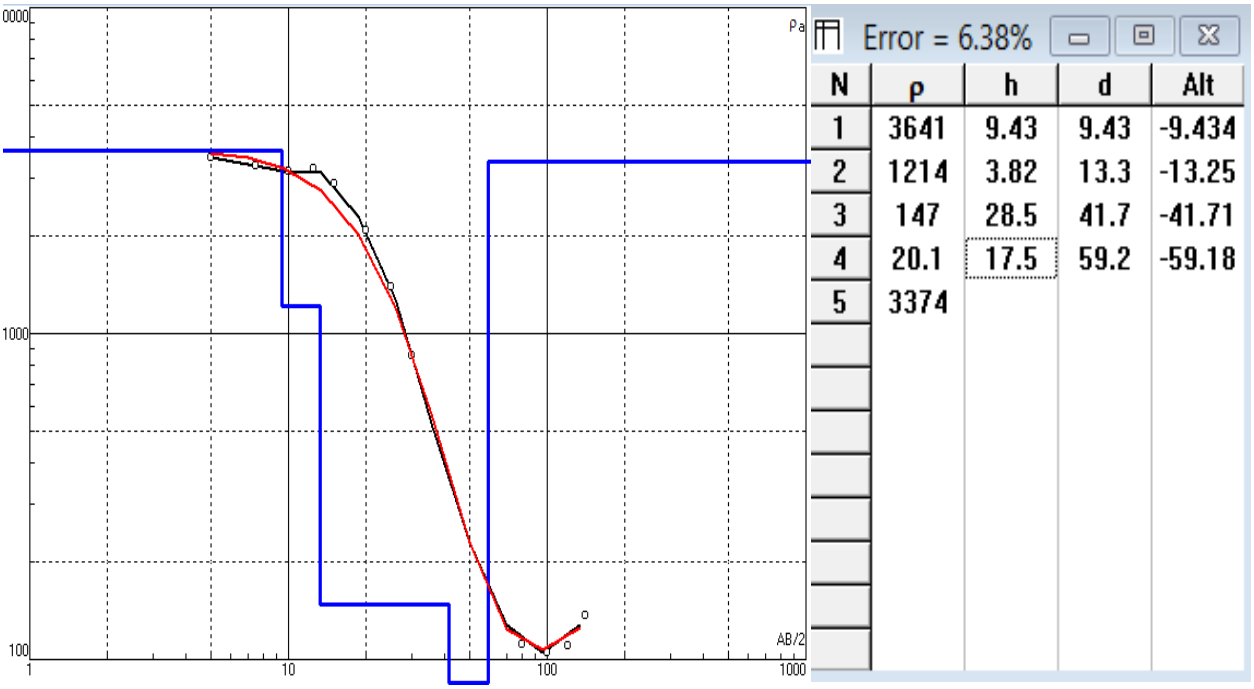

N	ρ	h	d	Alt
1	3641	9.43	9.43	-9.434
2	1214	3.82	13.3	-13.25
3	147	28.5	41.7	-41.71
4	20.1	17.5	59.2	-59.18
5	3374			

Figure 36: Curve and Model for VES 09

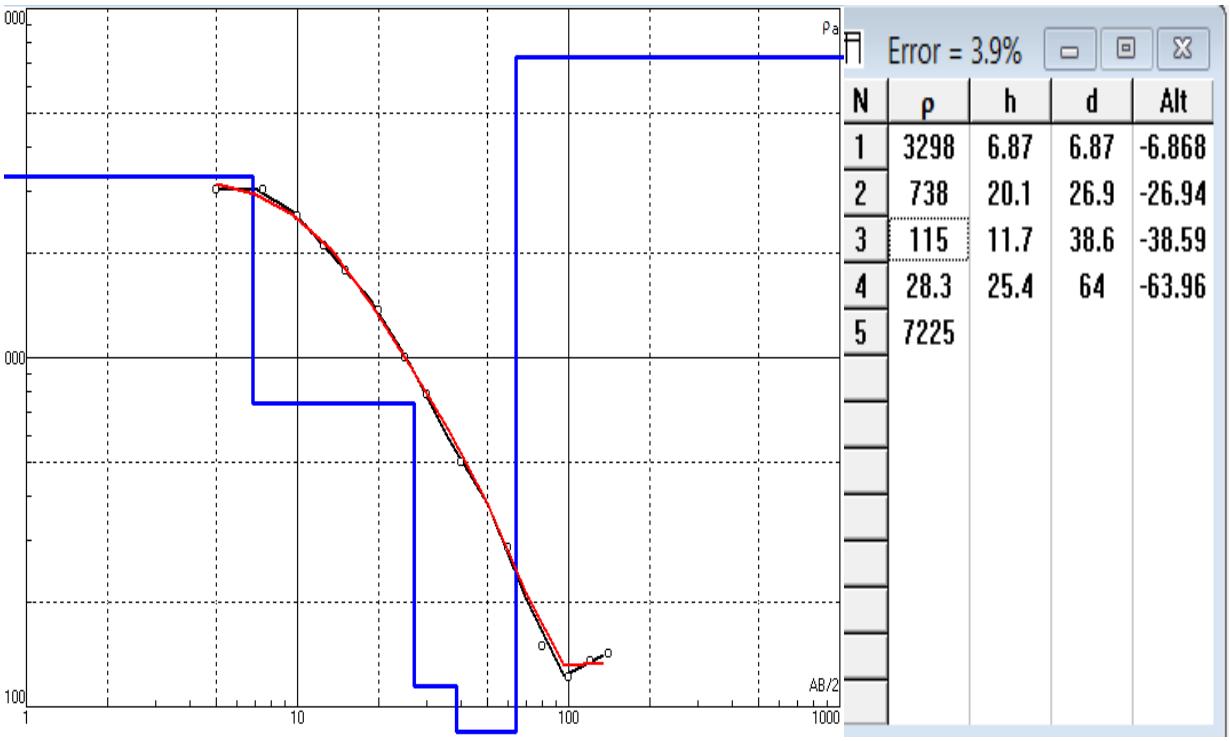

N	ρ	h	d	Alt
1	3298	6.87	6.87	-6.868
2	738	20.1	26.9	-26.94
3	115	11.7	38.6	-38.59
4	28.3	25.4	64	-63.96
5	7225			

Figure 37: Curve and Model for VES 10

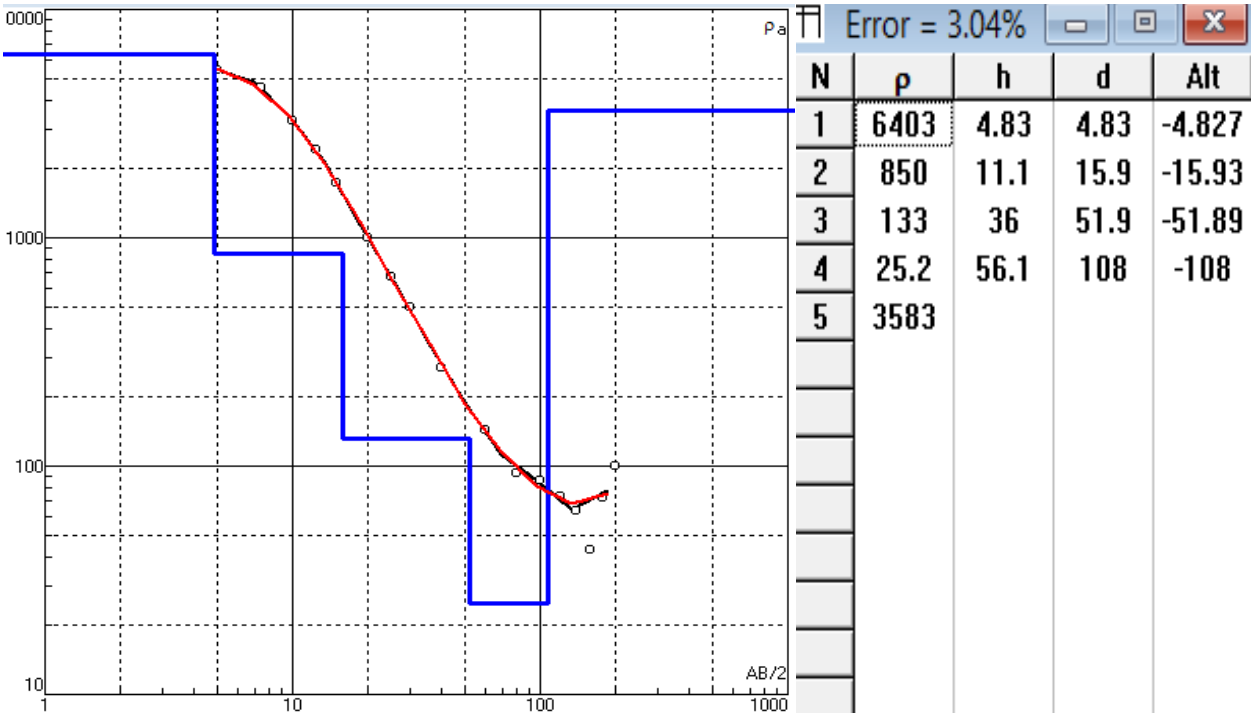

Figure 38: Curve and Model for VES 11

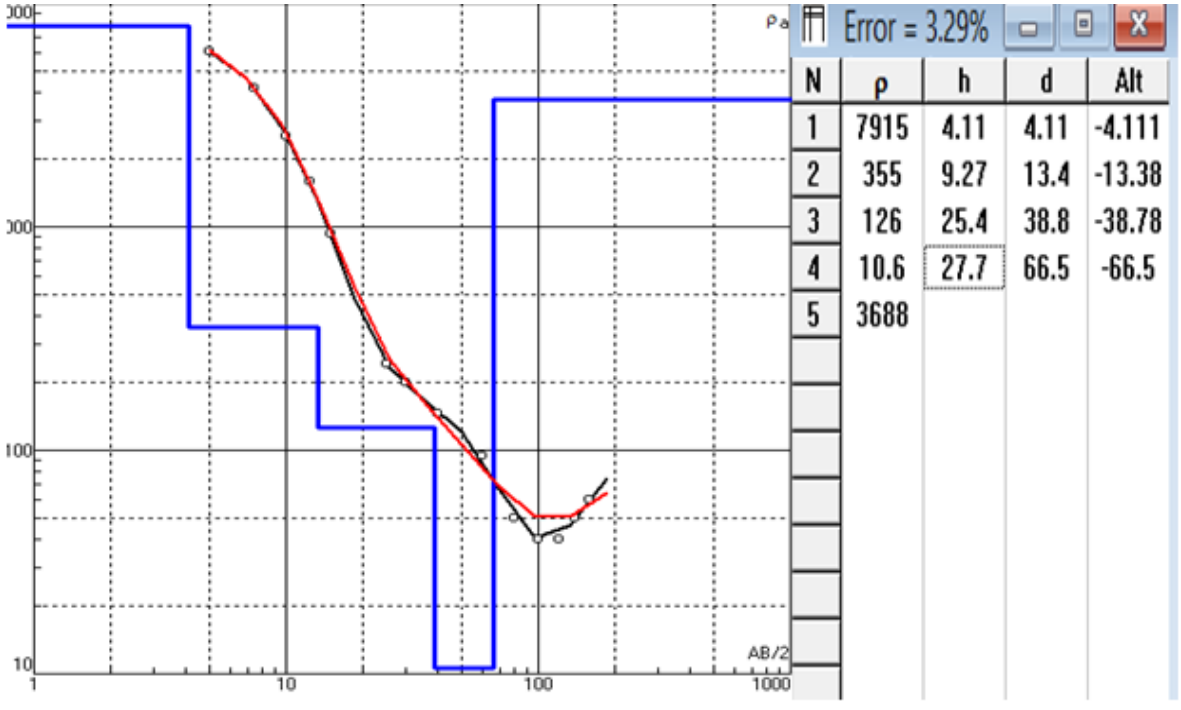

Figure 39: Curve and Model for VES 12

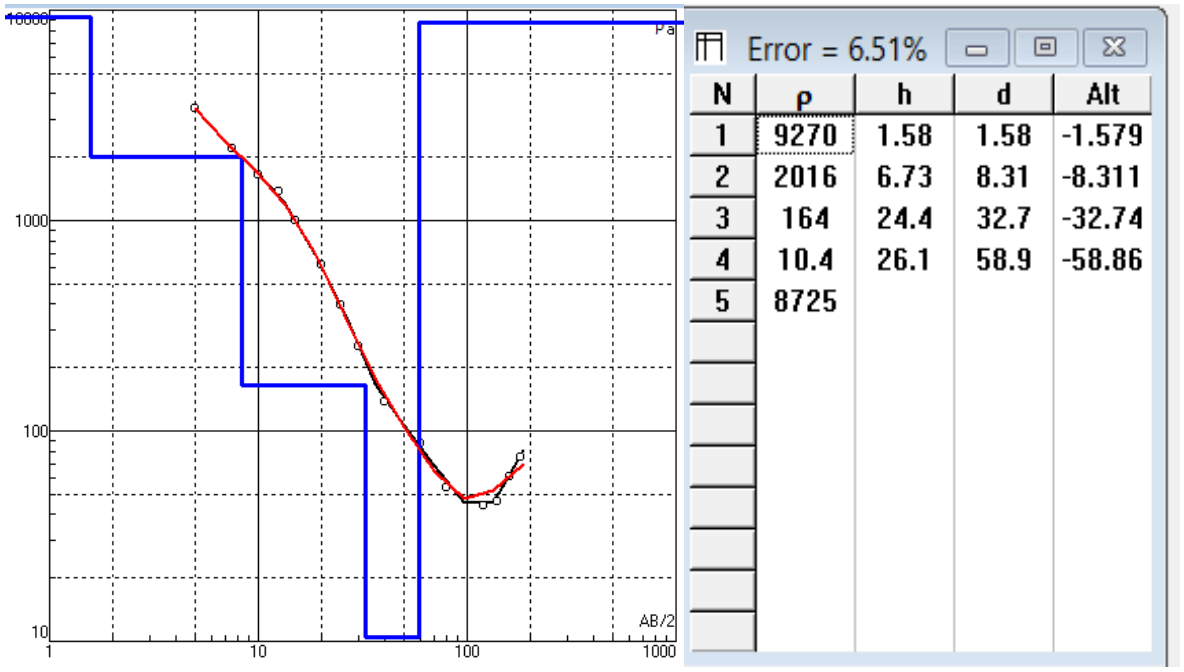

N	ρ	h	d	Alt
1	9270	1.58	1.58	-1.579
2	2016	6.73	8.31	-8.311
3	164	24.4	32.7	-32.74
4	10.4	26.1	58.9	-58.86
5	8725			

Figure 40: Curve and Model for VES 13

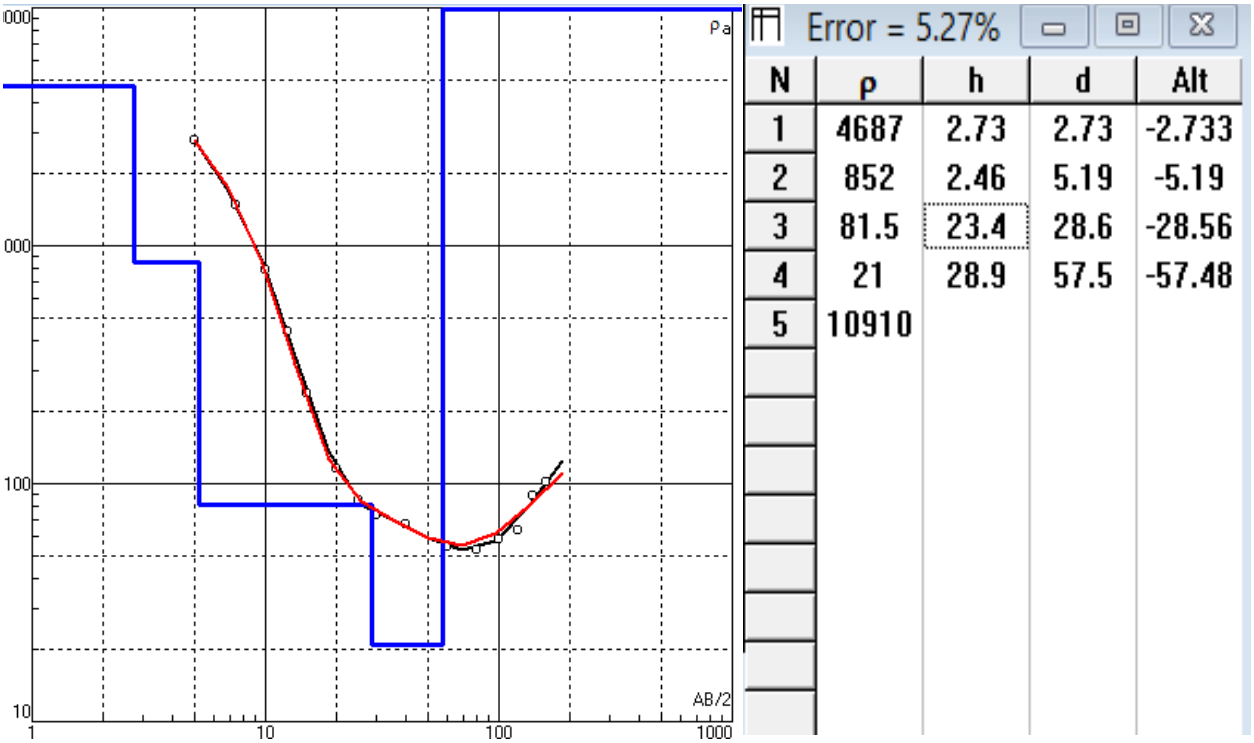

N	ρ	h	d	Alt
1	4687	2.73	2.73	-2.733
2	852	2.46	5.19	-5.19
3	81.5	23.4	28.6	-28.56
4	21	28.9	57.5	-57.48
5	10910			

Figure 41: Curve and Model for VES 14

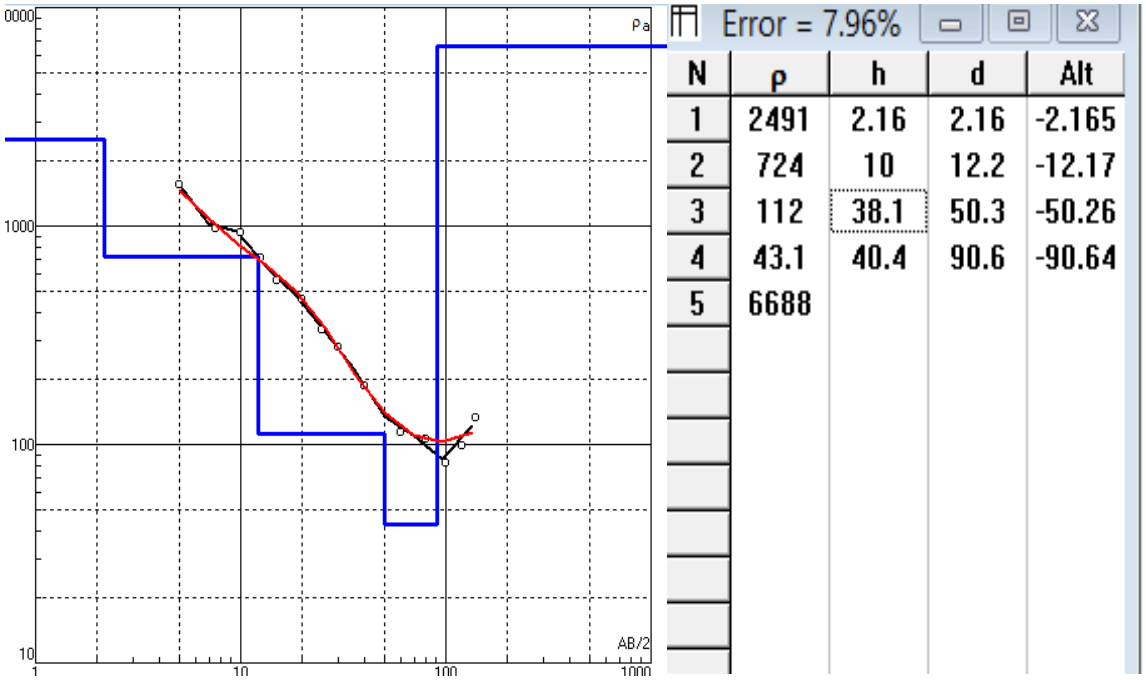

Figure 42: Curve and Model for VES 17

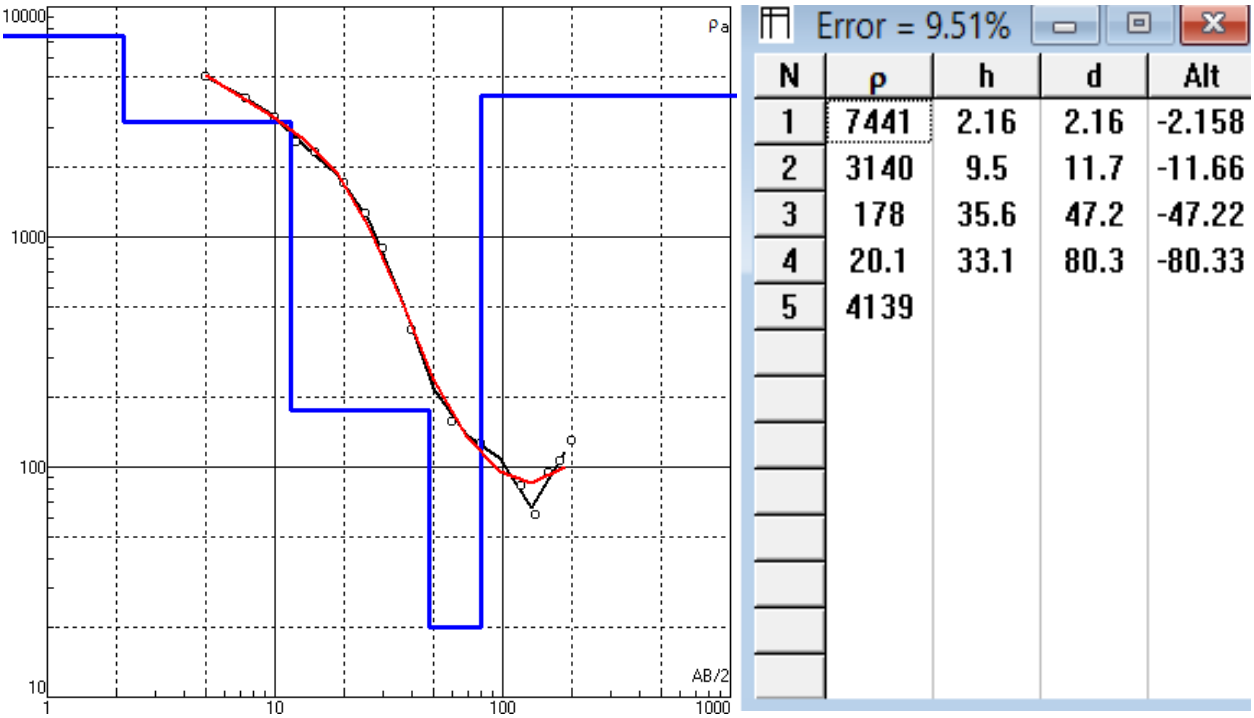

Figure 43: Curve and Model for VES 18

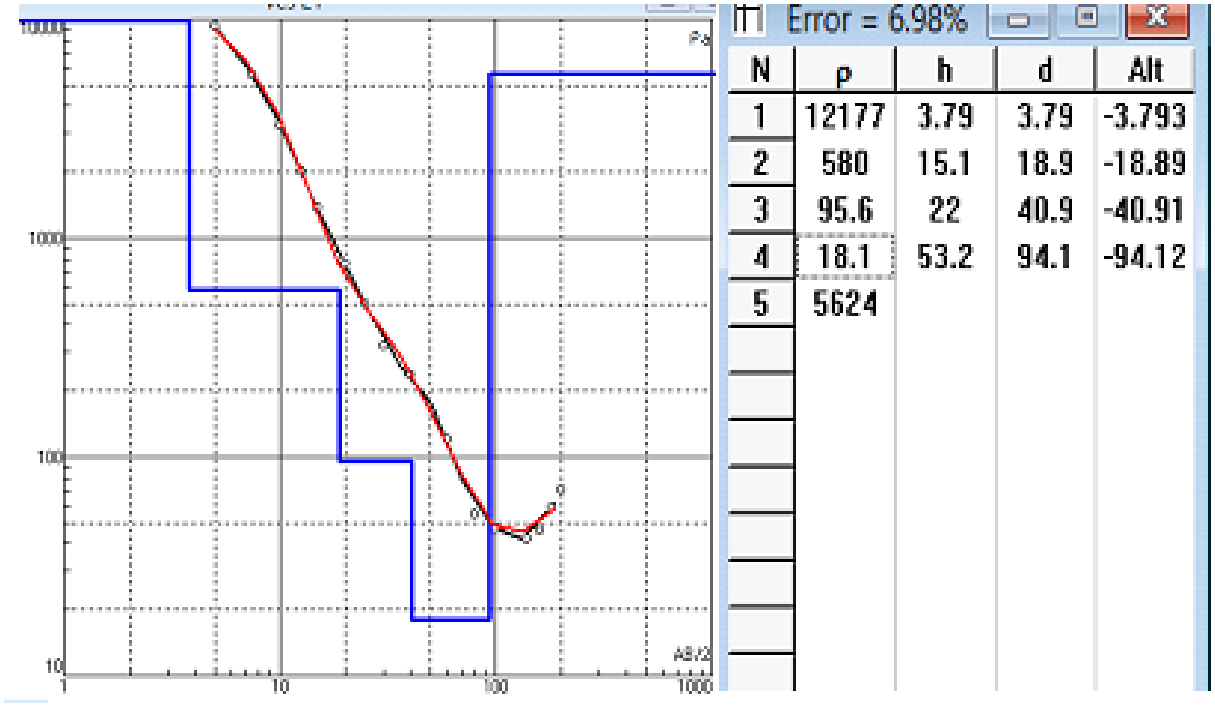

Figure 44: Curve and Model for VES 21

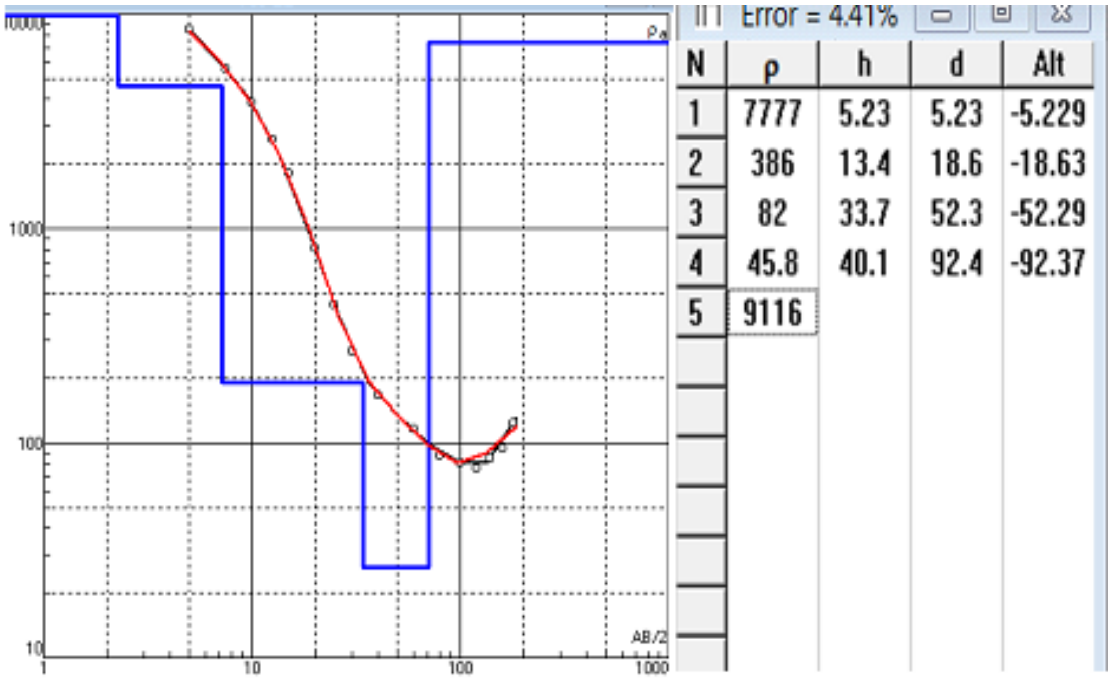

Figure 45: Curve and Model for VES 22

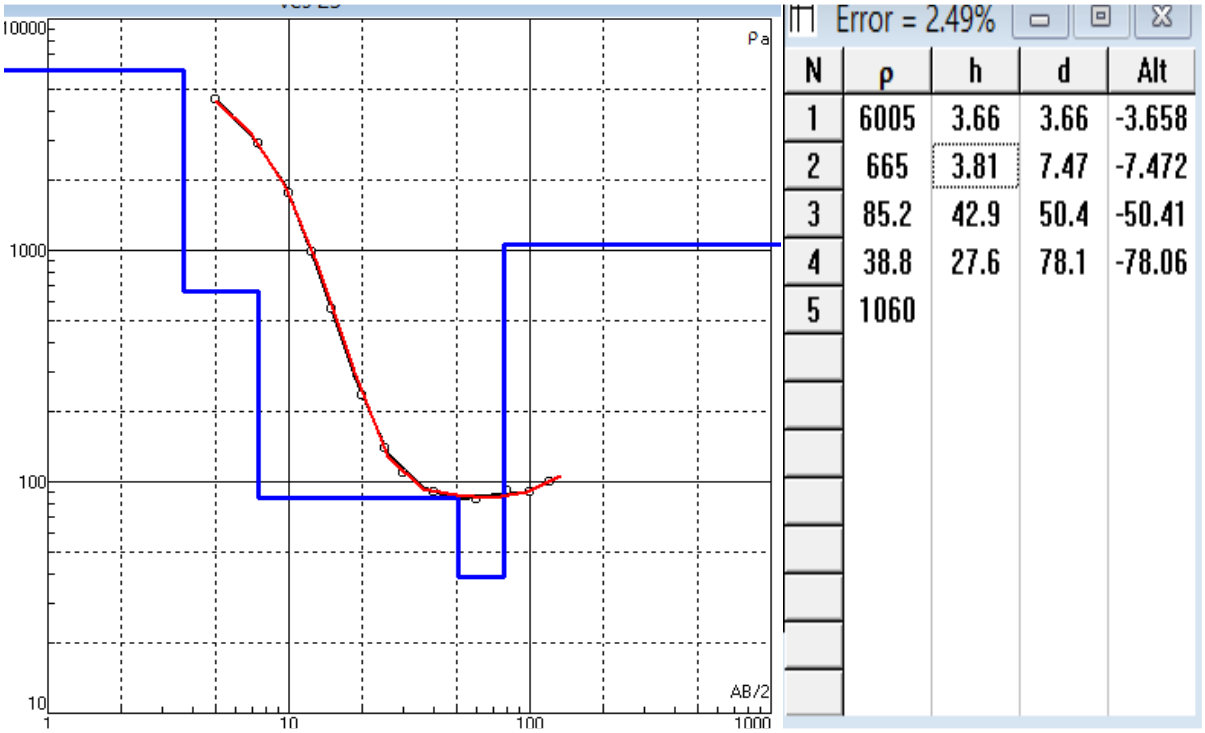

Figure 46: Curve and Model for VES 23

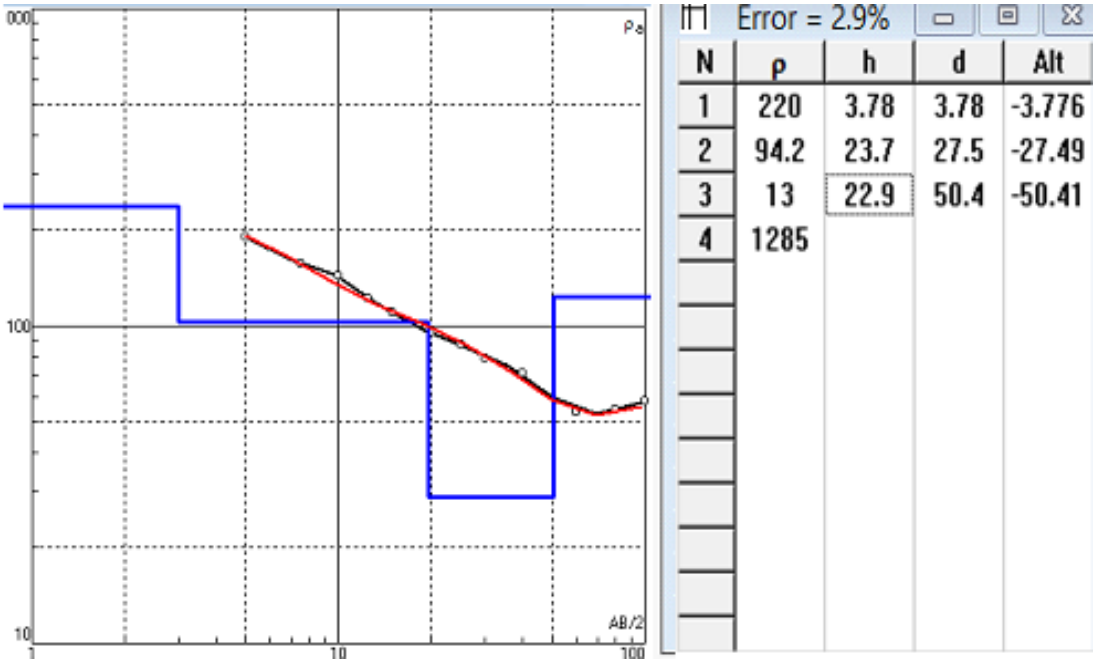

Figure 47: Curve and Model for VES 24

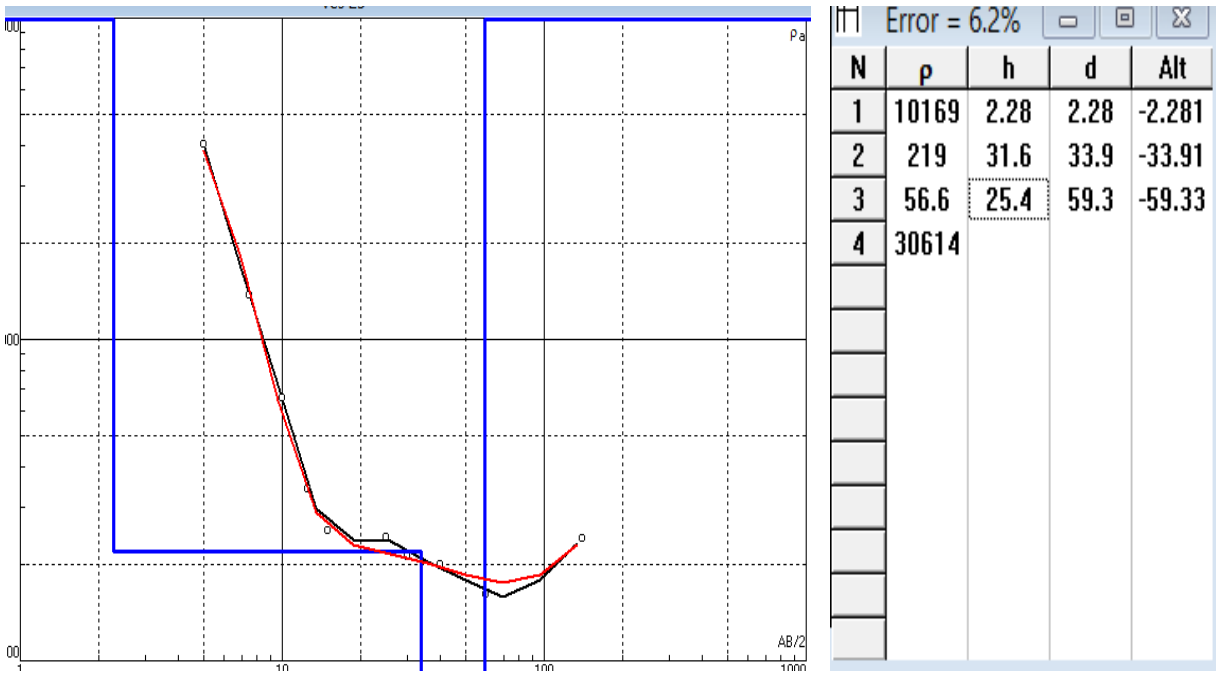

N	ρ	h	d	Alt
1	10169	2.28	2.28	-2.281
2	219	31.6	33.9	-33.91
3	56.6	25.4	59.3	-59.33
4	30614			

Figure 48: Curve and Model for VES 25

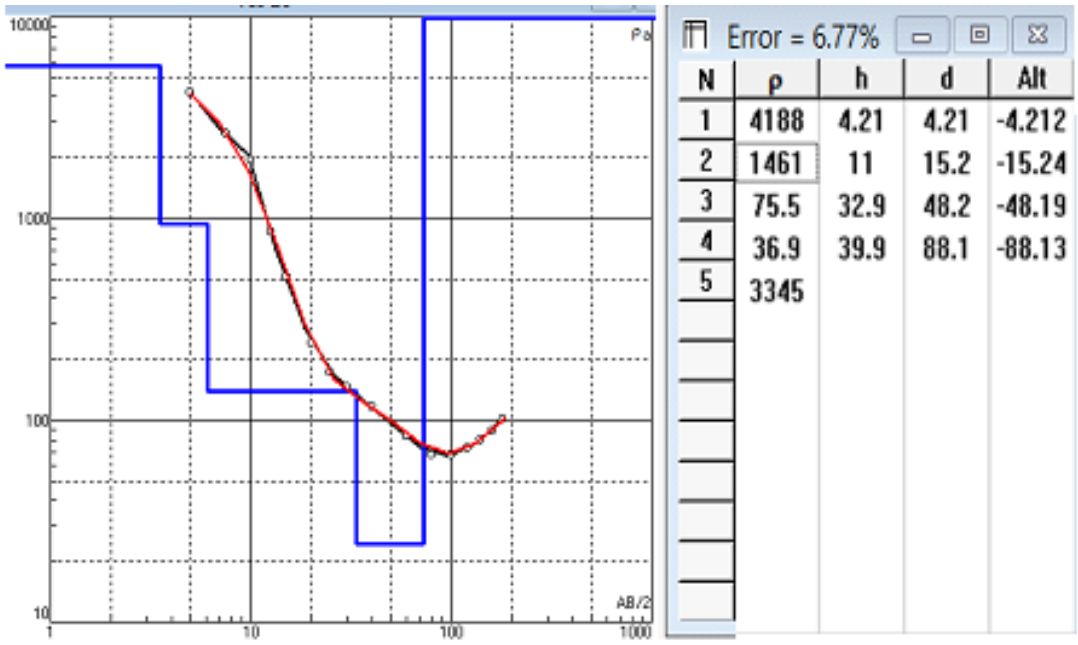

N	ρ	h	d	Alt
1	4188	4.21	4.21	-4.212
2	1461	11	15.2	-15.24
3	75.5	32.9	48.2	-48.19
4	36.9	39.9	88.1	-88.13
5	3345			

Figure 49: Curve and Model for VES 26

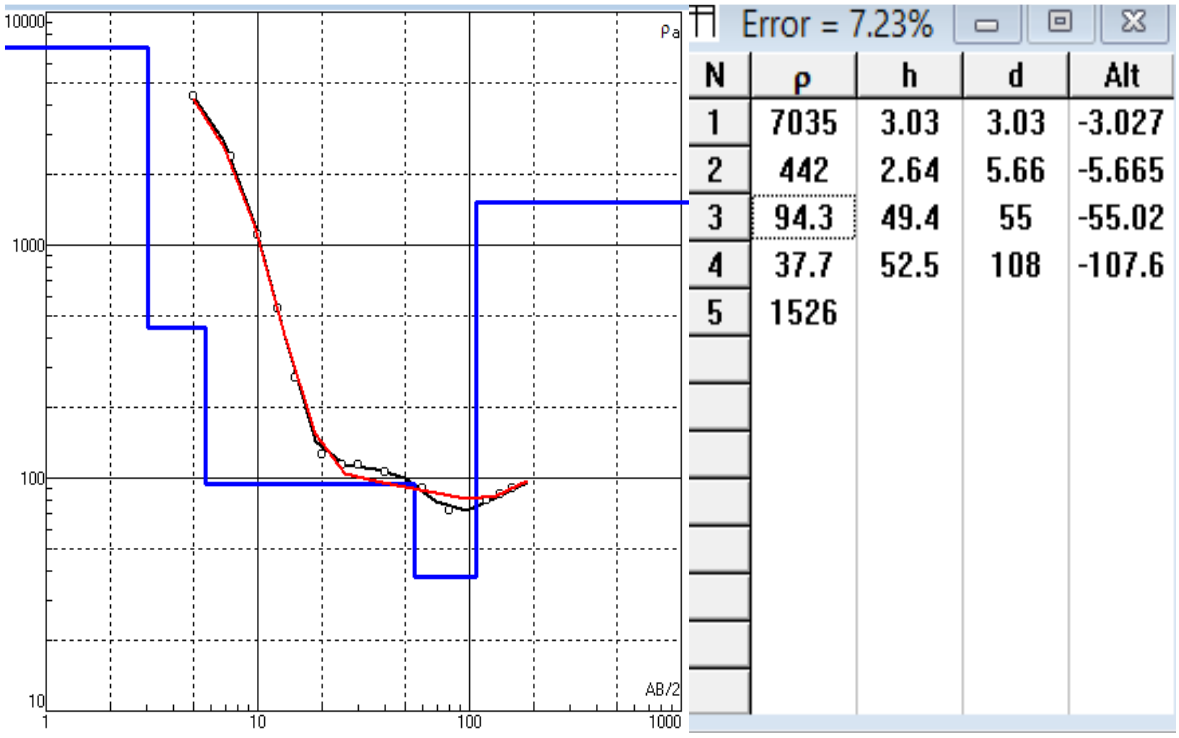

N	ρ	h	d	Alt
1	7035	3.03	3.03	-3.027
2	442	2.64	5.66	-5.665
3	94.3	49.4	55	-55.02
4	37.7	52.5	108	-107.6
5	1526			

Figure 50: Curve and Model for VES 29

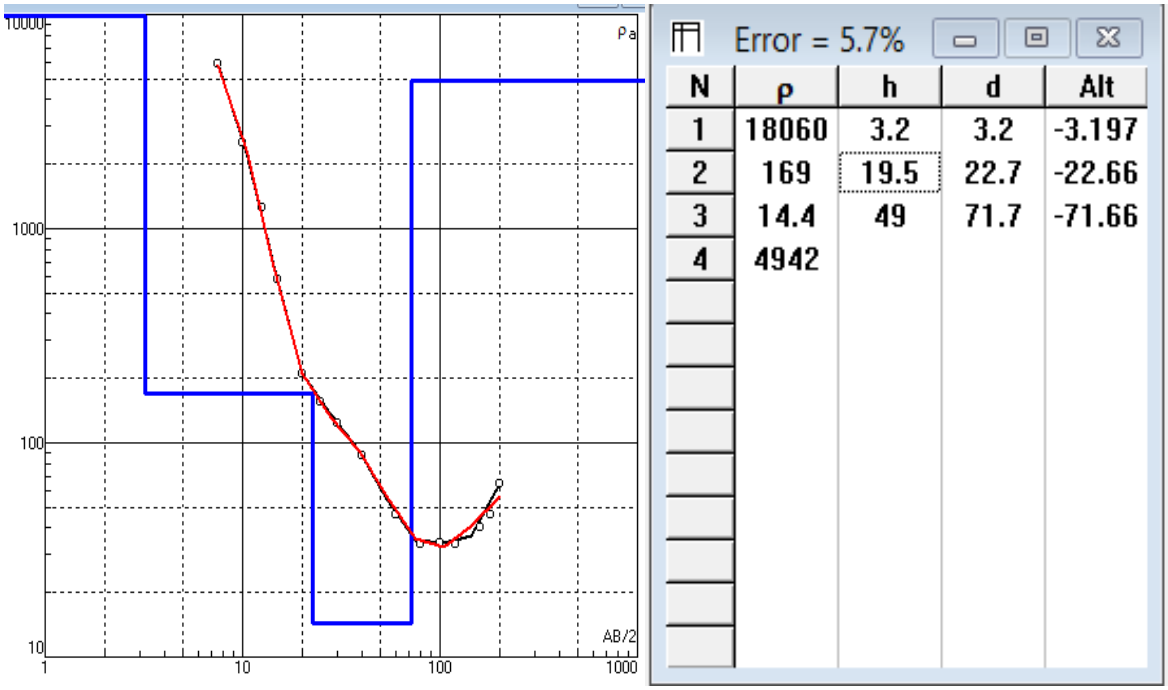

N	ρ	h	d	Alt
1	18060	3.2	3.2	-3.197
2	169	19.5	22.7	-22.66
3	14.4	49	71.7	-71.66
4	4942			

Figure 51: Curve and Model for VES 30